

**UNIVERSIDADE DE SÃO PAULO
INSTITUTO DE GEOCIÊNCIAS**

**EVOLUÇÃO QUÍMICA DO MANTO LITOSFÉRICO SUBCONTINENTAL NO NORDESTE
DA PROVÍNCIA BORBOREMA COM BASE EM GEQUÍMICA ELEMENTAR E ISOTÓPICA**

Emmanuel Donald Ngonge

Orientadora

Prof^a. Dr^a. Maria Helena Bezerra Maia de Hollanda

TESE DE DOUTORAMENTO

Programa de Pós-graduação em Geoquímica e Geotectônica

SÃO PAULO

2015

AGRADECIMENTOS

Palavras me faltam para agradecer à Professora Maria Helena B. Maia de Hollanda. Foi muito bom, bom demais, e ótimo trabalhar junto a ela neste projeto de Doutorado. Ela deu toda sua energia, tempo, mente e paciência para alcançarmos os resultados apresentados neste documento.

Agradeço ao Professor Carlos José Archanjo pelo apoio, amizade e contribuição indireta à algumas etapas deste projeto, especialmente numa excursão de campo (agosto de 2013) que fizemos juntos na região de Lajes, Rio Grande do Norte, para coleta de xenólitos peridotíticos. Foi uma boa experiência.

Agradeço à Coordenação de Aperfeiçoamento de Pessoal de Nível Superior (CAPES) pela bolsa concedida, a qual me deu condições financeiras para fazer o curso de doutorado.

Agradeço ao CNPq (Proj. 473.638/2011-8) pelo financiamento das análises de química mineral, geoquímica e isotópicas (Re-Os) realizadas no âmbito deste projeto. Agradeço igualmente ao CPGeo que propiciou a realização de algumas das análises Sr-Nd-Pb aqui apresentadas, e ao Programa de Pesquisa em Geoquímica e Geotectônica pelo financiamento do meu deslocamento aéreo para os Estados Unidos da América (Maryland) onde tive a oportunidade de trabalhar com o Dr. Richard Walker para a obtenção dos dados Re-Os em xenólitos. A esse pesquisador agradeço por me receber, me ensinar e, sobretudo, pelo interesse no meu projeto e pelo convite feito às futuras colaborações.

Agradeço ao Instituto de Geociências da USP, na pessoa do atual diretor, por fornecer a nós, estudantes, a excelente infra-estrutura de pesquisa na forma de laboratórios, biblioteca e pessoal técnico e acadêmico qualificado. Estou grato por ter feito parte dessa comunidade.

Agradeço muitos aos professores com quem pude ter maior contato nesse período da pós-graduação, com quem aprendi muito: Colombo C. G. Tassinari, Oswaldo Junior, Ginaldo Campanha, Rômulo Machado, Rogério Azzone, Marcos Egydio da Silva, Jorge Bittencourt e o Valdecir Janasi, e tantos outros.

Agradeço meus colegas pos-graduandos do Bloco D, em especialmente a Geanne Carolina Cavalcante e Natali Barbosa, as quais me ajudaram com a correção do português deste documento.

Agradeço muito à minha querida esposa Elizabeth e a meus filhos, pela paciência comigo, muitas vezes tão ocupado em meu trabalho de pesquisa.

MY GOD IS SO GOOD TO ME!

RESUMO

Essa tese de Doutorado tem por objetivo apresentar uma discussão sobre a evolução do manto litosférico subcontinental na região nordeste da Província Borborema, desde o Mesozóico até Cenozóico. Para isso foram obtidos dados de geoquímica elementar e isotópica de dois importantes eventos magmáticos expostos na região: (i) o enxame de diques toleíticos Ceará-Mirim (Cretáceo Inferior) e (ii) o vulcanismo alcalino Macau representado por *plugs*, *necks* e lavas com idades distribuídas desde o Oligoceno ao Mioceno.

O enxame de diques de Ceará Mirim é composto de (i) olivina toleítos de alto-Ti, (ii) toleítos evoluídos de alto-Ti ($\text{TiO}_2 > 1,5 \text{ wt.\%}$; $\text{Ti/Y} > 360$), e (iii) toleítos de baixo-Ti ($\text{TiO}_2 < 1,5 \text{ wt\%}$; $\text{Ti/Y} < 360$), todos com forte enriquecimento em elementos incompatíveis relativo ao manto primitivo. Os olivina toleitos exibem teores em Nb-Ta semelhante àqueles de magmas do tipo OIB. Ao contrário, os toleitos evoluídos de alto-Ti e os toleítos a baixo-Ti mostram anomalias negativas em Nb-Ta, as quais são mais pronunciadas nos basaltos de baixo-Ti. Os olivina toleítos mostram razões iniciais $^{87}\text{Sr}/^{86}\text{Sr}$ uniformes (0,7034–0,7037), enquanto que as composições isotópicas de Nd e Pb são variáveis, parte delas moderadamente radiogênicas (0,512518–0,512699; 19,13–19,25). As composições isotópicas de Pb sugerem a contribuição de um componente FOZO na gênese desses olivina toleitos. Os outros toleítos apresentam valores muito mais variáveis, com $^{87}\text{Sr}/^{86}\text{Sr}$ radiogênicas (em comparação ao $\text{BSE}_{t=127}$) e valores subcondrícticos para Nd ($< 0,512442$ ou $\varepsilon_{\text{Nd}} < -0,6$). Quando combinadas com razões $^{206}\text{Pb}/^{204}\text{Pb}$ entre 17,08 e 18,41, os toleitos evoluídos de alto-Ti e os toleitos de baixo-Ti mostram afinidade com o componente EMI, sendo as características enriquecidas dos toleitos de baixo-Ti mais acentuadas devido a contaminação crustal durante ascensão. As similaridades com EMI, as anomalias de Nb e idades modelo $T_{\text{DM}} > 1 \text{ Ga}$, são evidências compostionais para atribuir a origem dos toleítos evoluídos de alto e baixo-Ti à fusão do manto litosférico subcontinental proterozóico, metasomatizado por um componente de subducção. Os dados de termometria aliados aos padrões fracionados de elementos terras raras indicam que a fusão deve ter ocorrido a ~60 km, na região de transição granada-espinélio assumindo uma litosfera afinada durante o Cretáceo. Os olivina toleitos, por sua vez, teriam fundido em profundidades de ~75 km a partir da astenosfera tipo-FOZO, passivamente soerguida em decorrência de afinamento litosférico relacionado a esforços distensivos durante o Cretáceo.

O vulcanismo cenozóico Macau é representado por alcali-basaltos, basanitos e nefelinitos. Basaltos toleíticos são menos comuns. Em geral, os basaltos Macau guardam alguma semelhança com os olivina toleitos cretáceos. São enriquecidos em elementos incompatíveis e

em Nb-Ta, mas com características mais primitivas como $10 < \text{MgO} < 15 \text{ wt.\%}$ e $200 < \text{Ni} < 500 \text{ ppm}$. Todos experimentaram fracionamento de olivina e clinopiroxênio, enquanto plagioclásio contribuiu em menor importância. O modelamento feito a partir de razões entre elementos terras raras combinado a dados termométricos indicam que os basanitos e alcali-basaltos teriam fundido a partir de lherzolitos a profundidade entre 80–90 km, na região de transição espinélio-granada, enquanto que os nefelinitos seriam produto da fusão ($<0,1\%$) mais profunda, a ~ 120 km de profundidade ($\sim 1470^\circ\text{C}$). As composições isotópicas Sr-Nd-Pb são semelhantes a magmas OIB gerados pela mistura de dois reservatórios, modelados como FOZO e EM. A identificação de FOZO no Cenozóico da Província Borborema aliada à ausência de um cenário tectônico compatível com afinamento litosférico/ascensão passiva da astenosfera e/ou presença de plumas, nos leva a propor que a astenosfera tipo-FOZO teria se re-equilibrado termalmente com o manto litosférico subcontinental desde o Cretáceo. Ao contrário, o componente EM nos basaltos Macau não pode ser correlacionado ao mesmo manto litosférico enriquecido identificado nos toleitos. Embora ainda não muito clara, sua origem é por ora atribuída a metassomatismo potássico provavelmente relacionado ao impacto da pluma de Fernando de Noronha sob o continente. As similaridades isotópicas entre esses basaltos oceânicos e os basaltos continentais sugerem que alguma ligação genética deve ser considerada.

Por fim, composições isotópicas de Os e idades modelo T_{RD} obtidos de xenólitos peridotíticos nos basaltos cenozóicos, registram a recorrência de múltiplos eventos de extração de magmas (1,3 a 0,1 Ga) e metassomatismo, confirmando a evolução química complexa experimentada pelo manto litosférico subcontinental no extremo nordeste da Província Borborema.

Palavras-chaves: magmatismo toleítico, magmatismo alcalino intraplaca, manto litosférico subcontinental, componente FOZO

ABSTRACT

The objective of this doctoral thesis is to present a discussion on the evolution of the subcontinental lithospheric mantle in the northeast of the Borborema Province from the Mesozoic to the Cenozoic. For this reason, element and isotope geochemical data were obtained from two important magmatic events in the region: (i) the Lower Cretaceous Ceará-Mirim dyke swarm and (ii) the Macau alkaline volcanism characterized by plugs, necks and flows of Oligocene to Miocene ages.

The Ceará-Mirim dyke swarm is composed of (i) high-Ti olivine tholeiites, (ii) evolved high-Ti tholeiites ($\text{TiO}_2 > 1.5 \text{ wt.\%}$; $\text{Ti/Y} > 360$), and (iii) low-Ti tholeiites ($\text{TiO}_2 < 1.5 \text{ wt.\%}$; $\text{Ti/Y} < 360$), all exhibiting strong enrichment in incompatible elements relative to the primitive mantle. The Nb-Ta abundance in the olivine tholeiites is of OIB affinity, while the evolved high-Ti and the low-Ti tholeiites demonstrate Nb-Ta negative anomalies, more accentuated in the low-Ti basalts. Initial $^{87}\text{Sr}/^{86}\text{Sr}$ ratios in the olivine tholeiites are less variable (0.7034–0.7037), but have variable Nd and Pb isotopic compositions with some moderately radiogenic (0.512518–0.512699; 19.13–19.25). The Pb isotopic compositions suggest the contribution of a FOZO component in the genesis of the olivine tholeiites. The other tholeiites exhibit more variable values, with radiogenic $^{87}\text{Sr}/^{86}\text{Sr}$ (relative to $\text{BSE}_{t=127}$) and subchondritic Nd (< 0.512442 or $\epsilon\text{Nd} < -0.6$). When combined with the $^{206}\text{Pb}/^{204}\text{Pb}$ ratios of 17.08 to 18.41, the evolved high-Ti tholeiites demonstrate EM1 affinity, with the enriched nature of the low-Ti tholeiites more enhanced due to crustal assimilation during ascent. The similarities with EM1, the Nb anomaly and the T_{DM} model age $> 1 \text{ Ga}$, are compositional evidence that suggest the magmas of the evolved high-Ti and low-Ti tholeiites were generated from the melting of the Proterozoic subcontinental lithospheric mantle, metasomatized by a subduction component. A combination of the inferred temperature data with the fractionated rare earth element patterns indicate that melting might have occurred at $\sim 60 \text{ km}$, at the garnet-spinel lherzolites transition zone in a thinned lithosphere during the Cretaceous. On the other hand, the olivine tholeiite magma might have been generated at $\sim 75 \text{ km}$ depth, in a FOZO-type asthenosphere that passively welled up due to the lithospheric extension and thinning in the Cretaceous.

The Macau volcanism is composed of alkali basalts, basanites and nephelinites, and rare tholeiitic basalts. Generally, the Macau basalts and the Cretaceous olivine tholeiites share some similarities. They are enriched in incompatible elements and in Nb-Ta, but with more primitive characteristics like $10 < \text{MgO} < 15 \text{ wt.\%}$ and $200 < \text{Ni} < 500 \text{ ppm}$. All experienced fractionation of olivine and clinopyroxene, but less important for plagioclase. Rare earth element modeling and

inferred temperature data indicate that the basanitic and the alkaline basaltic magmas melted from lherzolites at 80-90 km depth, at the spinel-garnet transition, while the nephelinic magmas were generated from melting (<0.1%) at deeper levels, at ~120 km of depth (~1470°C). The Sr-Nd-Pb isotopic compositions have affinity to OIB magmas generated from the mixing of two reservoirs, modeled as FOZO and EM. The identification of FOZO in the Borborema Province in the Cenozoic with the absence of a compatible tectonic scenario such as lithospheric thinning/pассив asthenospheric upwelling and/or the presence of plumes, make us to propose that a FOZO-type asthenosphere might have thermally re-equilibrated as a subcontinental lithospheric mantle since the Cretaceous. On the other hand, the EM component in the Macau basalts cannot be linked to the same enriched lithospheric mantle identified with the tholeiites. However, their origin, though not very clear, is attributed to potassic metasomatism probably linked to the impact of the Fernando de Noronha plume on the continent. The similarities in isotopic signatures between the oceanic and continental basalts suggest a genetic link between both.

Lastly, the Os isotopic compositions and T_{RD} model ages constrained from the peridotite xenoliths in the Cenozoic basalts, record the occurrence of multiple magma extraction (1.3 to 0.1 Ga) and metasomatism events, confirming a complex chemical evolution in the subcontinental lithosphere in the far northeast of the Borborema Province.

Keywords: tholeiitic magmatism, intraplate alkali magmatism, subcontinental lithospheric mantle, FOZO component

SUMÁRIO

CAPÍTULO 1	
INTRODUÇÃO	12
1.1 ASPECTOS GERAIS	12
1.2 CONHECIMENTO GEOLÓGICO PRÉVIO	14
1.3 ENXAME DE DIQUES CEARÁ-MIRIM	14
1.3.1 VULCANISMO MACAU	16
1.3.2 OBJETIVOS E JUSTIFICATIVA	18
CAPÍTULO 2	20
REVISÃO CONCEITUAL	20
2.1 MANTO SUPERIOR ASTENOSFÉRICO-LITOSFÉRICO	20
2.2 RESERVATÓRIOS MAGMÁTICOS	21
CAPÍTULO 3	31
PETROLOGY OF CONTINENTAL THOLEIITIC MAGMAS FORMING A 350 KM-LONG MESOZOIC DYKE SWARM IN NE BRAZIL: CONSTRAINTS OF GEOCHEMICAL AND ISOTOPIC DATA	32
3.1 INTRODUCTION	32
3.2 GEOLOGICAL BACKGROUND	34
3.3 ANALYTICAL PROCEDURES	35
3.4 RESULTS	38
3.4.1 $^{40}\text{Ar}/^{39}\text{Ar}$ GEOCHRONOLOGY	38
3.4.2 PETROGRAPHY AND MINERAL CHEMISTRY	38
3.4.3 MAJOR AND TRACE ELEMENT COMPOSITIONS	40
3.4.4 SR-Nd-Pb ISOTOPIC COMPOSITIONS	46
3.5 DISCUSSION ON THE PETROGENETIC PROCESSES	49
3.5.1 MAGMA GENERATION	49
3.5.2 EVALUATION OF LOW-PRESSURE CRUSTAL CONTAMINATION	51
3.5.3 MANTLE SOURCE COMPONENTS	53
3.6 GEODYNAMIC CONSIDERATIONS	59
3.7 CONCLUSIONS	61
ACKNOWLEDGMENTS	62
REFERENCES	63
CAPÍTULO 4	68
PETROGENESIS OF ALKALINE ROCKS OF THE MACAU VOLCANIC FIELD, NORTHEASTERN BRAZIL	69
INTRODUCTION	69
4.1 GEOLOGICAL OVERVIEW	70
4.2 SAMPLING STRATEGY	73
4.3 RESULTS	74
4.4 PETROGRAPHY AND MINERAL CHEMISTRY	74
4.4.1 MAJOR AND TRACE ELEMENT GEOCHEMISTRY	75
4.4.2 SR-Nd-Pb ISOTOPE COMPOSITIONS	82
4.4.3 DISCUSSION	83
4.5 FRACTIONAL CRYSTALLIZATION AND CRUSTAL ASSIMILATION	83
4.5.1 ESTIMATION OF MELTING DEGREE AND MELT FRACTION	86
4.5.2 THE ISOTOPE RESERVOIRS PROPOSED FOR THE MVF MAGMAS	89
4.5.3 INSIGHTS ON THE CHEMICAL EVOLUTION OF THE SUBCONTINENTAL	91

	LITHOSPHERIC MANTLE IN THE NORTHEASTERN BORBOREMA PROVINCE	
4.5.4	CONCLUSION	94
4.6	ACKNOWLEDGMENTS	95
	REFERENCES	96
 CAPÍTULO 5		
	GEOQUÍMICA ISOTÓPICA RE-OS DE XENÓLITOS PERIDOTÍTICOS	100
	INTRODUÇÃO	100
5.1	PROCEDIMENTO ANALÍTICO PARA OBTENÇÃP DE DADOS RE-OS E ELEMENTOS DO GRUPO DA PLATINA	101
5.2	DIGESTÃO ÁCIDA DE AMOSTRAS	101
5.2.1	PREPARAÇÃO DA FRAÇÃO OS	102
5.2.2	PREPARAÇÃO DA FRAÇÃO RE	102
5.2.3	RESULTADOS	103
5.3	COMENTÁRIOS GERAIS SOBRE QUÍMICA MINERAL E GEOQUÍMICA DE ROCHA TOTAL	103
5.3.1	DADOS ISOTÓPICOS RE-OS E CONCENTRAÇÕES DE PGE	107
5.4.	COMENTÁRIOS PRELIMINARES SOBRE IDADES DE EVENTOS DE EXTRAÇÃO DE MANGMAS E METASSOMATISMO NO MANTO LITOSFÉRICO SUBCONTINENTAL	109
 CAPÍTULO 6		
	CONSIDERAÇÕES FINAIS	111
	REFERÊNCIAS	111
		115

LISTA DE FIGURAS

CAPÍTULO 1		
Fig.1.1	Mapa esquemático da porção NE da Província Borborema mostrando o limite meridional da Bacia Potiguar (em cinza, na parte superior da figura) e a localização do enxame de diques Rio Ceará-Mirim e os basaltos de Macau	15
CAPÍTULO 3		
Fig. 3.1	(a) Schematic illustration of the West Gondwana with focus on the main Neoproterozoic cratonic areas – Amazonian, São Francisco-Congo, West African and Kalahari. The study area is shown in the box	33
Fig.3.2	(a) $^{40}\text{Ar}/^{39}\text{Ar}$ step-heating diagram for two multigrain replicates (#0480-01 and -03) of the tholeiite CM-12.	38
Fig.3.3	Ca-Mg-Fe ternary plot used for the classification of pyroxenes analyzed for the CMDS tholeiites.	40
Fig.3.4	Major element classification for the CMDS tholeiites based on (a) TAS and (b) SiO_2 versus $\text{Fe}_2\text{O}_{3T}/\text{MgO}$ diagrams.	41
Fig.3.5	(a) Mg versus Ti oxides and (b) Ti/Y versus Ti/Zr plots for discrimination between high- and low-Ti magmas.	44
Fig.3.6	Variation diagrams of major elements against MgO.	45
Fig.3.7	Profiles for average abundances of (a) chondrite-normalized REE and (b) PM-normalized incompatible element patterns.	46
Fig.3.8	Initial (a) $^{87}\text{Sr}/^{86}\text{Sr}$ versus $^{143}\text{Nd}/^{144}\text{Nd}$, (b) $^{206}\text{Pb}/^{204}\text{Pb}$ versus $^{207}\text{Pb}/^{204}\text{Pb}$ and (c) $^{206}\text{Pb}/^{204}\text{Pb}$ versus $^{208}\text{Pb}/^{204}\text{Pb}$ plots showing the distribution of the CMDS isotopic compositions.	48
Fig.3.9	Model of mixing curves between spinel (in blue) and garnet (in red) lherzolite melts using normalized-Dy/Yb and La/Yb ratios to estimate rates of partial melting and magma sources for the CMDS tholeiitic magmas.	51
Fig.3.10	(a) Initial $^{87}\text{Sr}/^{86}\text{Sr}$ versus K_2O and (b) $^{87}\text{Sr}/^{86}\text{Sr}$ versus $1/\text{Sr} \times 1,000$ plots used to evaluate low-pressure crustal contamination levels in the CMDS tholeiitic magmas.	53

Fig.3.11	Incompatible element profiles for (a) olivine tholeiites, (b) high-Ti evolved tholeiites and (c) low-Ti tholeiites.	55
Fig.3.12	Isotopic companion plots used to differentiate FOZO and HIMU components and to compare their Pb and Nd signatures with those of the CMDS tholeiitic groups.	58
CAPÍTULO 4		
Fig.4.1	(a) Schematic illustration of the West Gondwana with focus on the main Neoproterozoic cratonic areas – Amazonian, São Francisco-Congo, West African and Kalahari. The study area is shown in the box	72
Fig.4.2	Major element classification for the MVF lavas based on (a) TAS and (b) Na ₂ O versus K ₂ O diagrams.	78
Fig.4.3	Variation diagrams of major elements against MgO.	80
Fig.4.4	Profiles for the average abundances of (a) chondrite-normalized REE and (b) PM-normalized incompatible element patterns.	81
Fig.4.5	Isotopic companion plots used to compare the Sr, Nd and Pb signatures of the four MVF lava groups to the distinct mantle endmembers – HIMU, FOZO and EM (I and II).	84
Fig.4.6	Plots of ratios between incompatible trace elements (and oxide – P ₂ O ₅) against SiO ₂ to qualitatively evaluate the extent of crustal contamination.	86
Fig.4.7	(a) Correlation between the normalized-La/Sm and Tb/Yb ratios showing that the MVF compositions are compatible with the melting of garnet-bearing mantle sources.	87
Fig.4.8	Correlation between (a) normalized-K/Nb and K/La and (b) Rb/Sr and ⁸⁷ Sr/ ⁸⁶ Sr ratios suggesting the preferential presence of amphibole	89
CAPÍTULO 5		
Fig.5.1	Óxidos vs MgO rocha total dos xenólitos de peridotitos de MVF e FN	105

LISTA DE TABELAS

CAPÍTULO 3		
Table 3.1	Table 1. 40Ar/39Ar data obtained for the tholeiite CM-12	36
		36
Table 3.2	Table 3.2. Geochemical data for the Ceará-Mirim dykes	42
Table 3.3	Sr, Nd and Pb isotopic compositions of the CMDS tholeiites	47
CAPÍTULO 4		
Table 4.1	Average mineral chemistry of olivine, pyroxene and plagioclase of the MVF basalts	75
Table 4.2	Major and minor element chemistry for the MVF basalts	78
Table 4.3	Sr, Nd and Pb isotopic compositions of the MVF basalts	82
CAPÍTULO 5		
Tabela 5.1	Dados de geoquímica elementar e isótopos Re-Os para os xenólitos peridotíticos	104
APPENDIX	Mineral chemistry of the CMDS tholeiites	118
ANEXO	Olivine compositions of the continental and oceanic xenoliths of NE Brazil	121

CAPÍTULO 1

INTRODUÇÃO

1.1 ASPECTOS GERAIS

Do sul ao norte da Placa Sul-Americana oriental há várias ocorrências de magmatismo basáltico de natureza toleítica de idade Cretácea (p.ex., Almeida, 1986; Almeida e Carneiro, 1989) representado por:(1) Enxames de Diques da Serra do Mar (Comin-Chiaromonti et al., 1983; Regelous, 1993; Garda, 1995; Valente et al., 1998, 1999; Guedes et al., 1999; Lobo et al., 1999) e de Ponta Grossa (Piccirillo et al., 1990), (2) derrames basálticos internos às bacias *rift* (Fodor e Vetter, 1984; Fodor et al., 1983, 1984; Mizusaki et al., 1992; Almeida et al., 1996; Caineli e Mohriak, 1999; Thomaz Filho et al., 2000; Mohriak et al., 2002), e (3) derrame basáltico da Província Paraná-Etendeka (p.ex., Piccirillo e Melfi, 1988). Ainda, no extremo nordeste da Província Borborema são reconhecidos (4) o Enxame de Diques Ceará-Mirim (Bellieni et al., 1992; Hollanda et al., 2006) e (5) as soleiras e diques do magmatismo Sardinha, expostos na Bacia do Parnaíba (Bellieni et al., 1990; Fodor et al., 1990; Baksi and Archibald, 1997), e sob o Cráton Amazônico, (6) ocorrências do vulcanismo Penacateua (segundo um relatório de IBAMA (licenciamento.ibama.gov.br), são diques e soleiros jurássicos na vizinhança da cidade de Altamira). Todos esses eventos têm sido interpretados como produtos de esforços tectônicos e/ou atividade de plumas relacionadas à abertura diacrônica do Oceano Atlântico, durante o Cretáceo. No Cenozóico, a atividade epirogenética esteve especialmente restrita à margem nordeste do Brasil, tendo como produtos os episódios vulcânicos Macau e Mecejana, cuja origem tem sido atribuída (e também questionada) a efeitos da passagem do *hot spot* de Fernando de Noronha sob o continente. Independente da idade, todos esses eventos magmáticos e produtos relacionados estão muito claramente caracterizados na literatura a partir de dados geoquímicos e isotópicos (ver referências acima citadas), desde os magmas toleitos de alto- e baixo-Ti dominantes no Cretáceo, até os magmas alcalinos que se distribuem desde o Cretáceo Superior (a Província Alcalina de Goiás) até o Oligoceno-Mioceno (vulcanismo Macau). Estudar os aspectos petrogenéticos desses vários eventos magmáticos é de inegável relevância para reconhecer a natureza química do manto litosférico subcontinental, e é nessa linha que a presente tese pretende contribuir. Os alvos para essa abordagem são o enxame de diques Ceará-Mirim e o

vulcanismo Macau, ambos expostos no extremo nordeste da Província Borborema, no domínio continental do Atlântico equatorial. O vulcanismo Macau consiste na atividade epirogenética mais jovem registradano escudo precambriano brasileiro, e tem a particularidade de hospedar xenólitos peridotíticos que, como tal, trazem informação direta e valiosa sobre a história química do manto, muitas vezes inacessível a partir dos magmas basálticos.

Essa tese de doutorado reúne um conjunto significativo de dados geoquímicos de elementos maiores e traços incluindo aqueles: de comportamento incompatível durante a fusão parcial, de afinidade siderófila e os terras raras conhecidos, repsectivamente, pelos acrônimos em inglês LILE (*large ion lithophile elements*), HFSE (*high field strength elements*), HSE (*high siderophile elements*) e REE (*rare earth elements*). Somam-se aos dados geoquímicos um conjunto igualmente expressivo de dados isotópicos Sr, Nd, Pb e Os, usados em combinação para caracterizaro quimismo dos magmas máficos relacionados ao vulcanismo fissural Ceará-Mirim e ao vulcanismo Macau, suas fontes no manto e processos relacionados à sua evolução desde a fonte até alojamento e cristalização na crosta. O enxame de diques Ceará-Mirim é basicamente constituído por diabásios toleíticos cuja intrusão está temporalmente associada à evolução do *rift* Potiguar durante a abertura do Atlântico Equatorial (p.ex., Matos, 1992, 2000). Dentre os poucos trabalhos científicos publicados na literatura sobre os diques Ceará-Mirim destacamos: (1) Bellieni et al. (1992), que inclui dados litogeoquímicos-isotópicos (Sr-Nd) e a assinatura paleomagnética do enxame, posicionando-os principalmente no Cretáceo; (2) Archanjo et al. (2000, 2002), que apresenta o modelo da trama magnética-magmática dos diques identificando, a partir do padrão de linhações magnéticas e orientações preferenciais de minerais magmáticos, as prováveis zonas de alimentação do enxame na intersecção com o alinhamento N-S definido pelos edifícios vulcânicos do Macau, e (3) Hollanda et al. (2006), que reúne dados geoquímicos e isotópicos (Sr-Nd-Pb) a partir de uma amostragem mais ampla que aquela apresentada por Bellieni e co-autores para discutir as prováveis fontes mantélicas para os magmas toleíticos. É no trabalho de Hollanda e colaboradores que surge a primeira indicação para participação de um componente radiogênico em Pb como fonte desses magmas, preliminarmente interpretado como sendo o reservatório HIMU. Apesar dessas contribuições, o acervo geocronológico sobre os diques Ceará-Mirim ainda é insuficiente, principalmente baseado em dados K-Ar agrupados no intervalo entre 135 e 110 Ma (Bellieni et al., 1992; Oliveira, 1992; Mizusaki et al., 2002).

O vulcanismo Macau é constituído por basaltos alcalinos que ocorrem na forma de plugs, necks, soleiras e poucos diques distribuídos segundo um alinhamento N-S com extensão de aproximadamente 300 km. Sial (1981) publicou os primeiros dados geoquímicos e de química

mineral das lavas Macau, os quais foram complementados e refinados nos trabalhos subsequentes de Fodor et al. (1998) e nas teses não publicadas de M.H.B.M. Hollanda (2002) e F.V. Silveira(2006). A primeira abordou principalmente a utilização de dados isotópicos para caracterização da natureza das fontes, a segunda enfatizando aspectos cartográficos, petrográficos e geocronológicos $^{40}\text{Ar}/^{39}\text{Ar}$ posicionando, em definitivo, o vulcanismo Macau entre 52 e 7 Ma. Parte das idades obtidas por Silveira foram publicadas em Knesel et al.(2011), aquelas referentes aos representantes mais jovens. Com base nas idades obtidas, Knesel e colaboradores discutem e rejeitam qualquer associação genética e temporal do vulcanismo Macau com o *hot spot* de Fernando de Noronha, como proposto nos trabalhos de Fodor et al. (1998, 2002) e Rivalenti et al. (2000) a partir de similaridades químicas entre as lavas no continente e aquelas oceânicas, bem como no quimismo dos xenólitos.

A presente tese está organizada na forma de seis capítulos, sendo três introdutórios que versam sobre os objetivos/justificativas, conhecimento geológico já existente sobre os alvos deste estudo e métodos usados para obtenção dos dados aqui apresentados. Os resultados compõem os três capítulos principais que discutem, separadamente, a petrogênese e a natureza das fontes no manto dos magmas toleíticos que constituem o Enxame de Diques Ceará-Mirim (Capítulo 4) e dos magmas alcalinos representantes do vulcanismo Macau (Capítulo 5). Ambos estão organizados no formato de artigos científicos, submetidos aos periódicos *Lithos* e *Journal of Volcanology and Geothermal Research*, respectivamente. O Capítulo 6 reúne os dados Re-Os obtidos para os xenólitos hospedados nas lavas Macau, os quais foram obtidos através de uma parceria com a University of Maryland, através do Dr. Richard Walker. Ao final deste último capítulo, é apresentada uma conclusão geral de todos os resultados obtidos no âmbito deste doutorado.

1.2. SÍNTESE DO CONHECIMENTO GEOLÓGICO PRÉVIO

1.2.1 O ENXAME DE DIQUES CEARÁ-MIRIM

O enxame de diques Ceará-Mirim distribui-se ao longo de aproximadamente 350 km, acompanhando o vale do Rio Ceará-Mirim, segundo uma direção predominantemente E-W. Os diques intrudem preferencialmente o embasamento precambriano na porção que atualmente corresponde ao limite meridional da Bacia Potiguar; mas a oeste, o enxame passa para uma orientação NE-SW, paralela ao eixo do *rift* Potiguar (Fig. 1.1a). Em reconstruções pré-deriva, o enxame representaria a contrapartida brasileira do evento magmático mais antigo associado ao

rift Benue (SE-Nigéria a N-Camarões). Os intervalos de idades K-Ar e $^{40}\text{Ar}/^{39}\text{Ar}$ conhecidas são coincidentes: c. 135-110 Ma para o Ceará-Mirim (K-Ar: Horn et al., 1988; Bellieni et al., 1992; Oliveira, 1992, e $^{40}\text{Ar}/^{39}\text{Ar}$: Smith et al., 2001; Araújo et al., 2001; Mizusaki et al., 2002) e c. 147-106 Ma para o magmatismo no setor setentrional do *rift* Benue (Maluski et al., 1995). A superposição cronológica levou Marzoli et al. (2000) a considerar esses dois eventos magmáticos como pertencentes a um único, de escala continental, nucleado na região equatorial do Oceano Atlântico (*Equatorial Circum-Atlantic - EQA*).

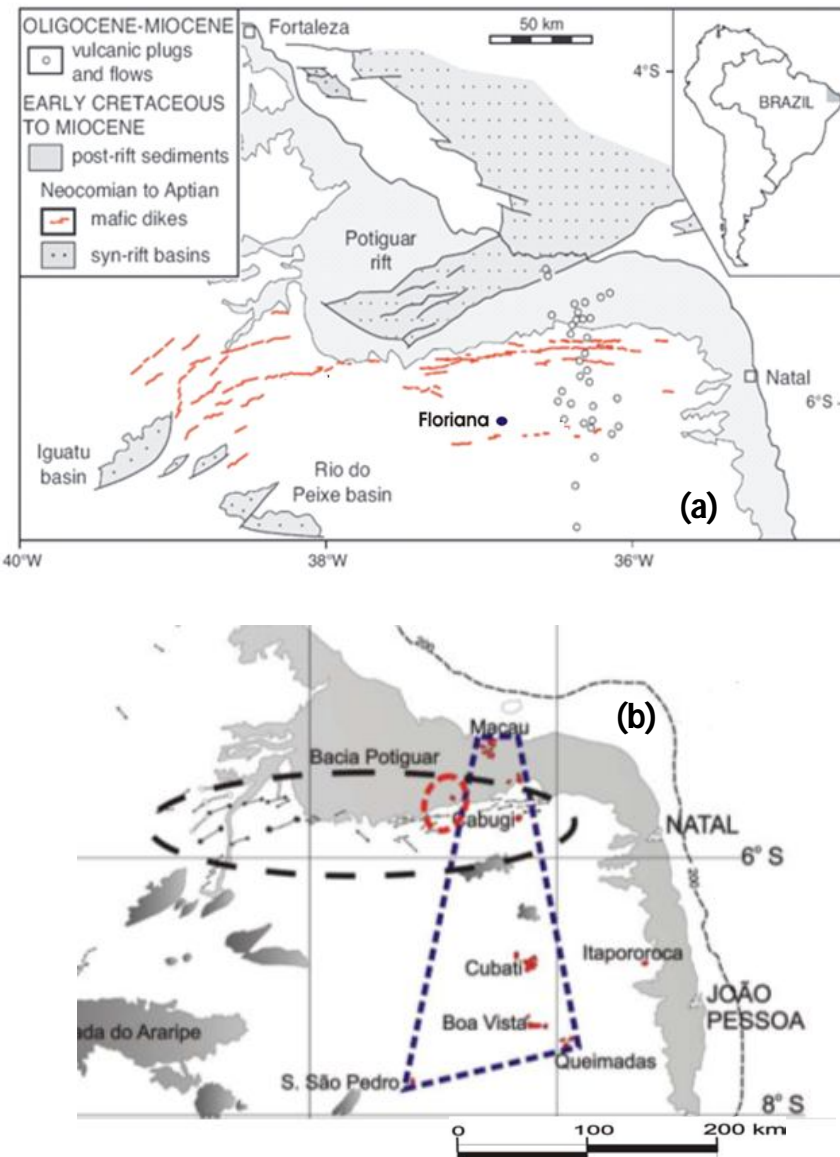


FIGURA 1.1. (a) Mapa esquemático da porção NE da Província Borborema mostrando o limite meridional da Bacia Potiguar (em cinza, na parte superior da figura) e a localização do enxame de diques Rio Ceará-Mirim e os basaltos de Macau (Vulcanic plugs and flows no mapa). A leste e oeste da cidade de Florânia ocorre um sub-enxame de diques “alcalinos” relacionados ao enxame principal; (b) demonstra a extensão dos basaltos de Macau definida pelo polígono de São Pedro a Macau (de Silveira, 2006). Os afloramentos são em vermelho.

Os diques são corpos verticais variando de 1-150 metros de largura e 3-4 km de comprimento, com distribuição linear ao longo da atual borda sul da Bacia Potiguar. Inclui essencialmente diabásios toleíticos ($\text{SiO}_2 = \sim 53\text{-}50\%$, $\text{MgO} = \sim 4\%$ e álcalis total = $\sim 6\text{-}4\%$), com: (i) alto- a baixo-Ti, (ii) forte a moderado enriquecimento em LILE e HFSE, (iii) razões altas de $^{87}\text{Sr}/^{86}\text{Sr}$ (0,70713–0,70473) associadas a baixas razões de $^{143}\text{Nd}/^{144}\text{Nd}$ (0,512494–0,512000) e $^{206}\text{Pb}/^{204}\text{Pb}$ (18,77–18,34) (Bellieni et al., 1992; Hollanda et al., 2006).

Esse padrão geoquímico-isotópico, juntamente com idades-modelo Sm-Nd entre 1,0-1,5 Ga, sugerem que os magmas toleíticos evoluíram a partir de um manto litosférico antigo, tipo EM (Hollanda et al., 2006). Um conjunto menor de diques E-W ocorre mais a sul do enxame principal diferindo em composição por apresentarem olivina modal e afinidade alcalina, correspondendo ao sub-enxame V de Bellieni et al. (1992). Apesar de sua aparente correlação com o enxame principal, toleítico, as características geoquímicas e isotópicas desses diques são ainda pouco conhecidas. Análises da trama magnética dos diques Ceará-Mirim mostraram variação no mergulho da lineação passando de um padrão sub-vertical, na porção centro-oriental do enxame, para um padrão horizontal na extremidade ocidental (Archanjo et al., 2000, 2002). Esse comportamento sugere que a zona de alimentação do enxame estaria localizada na sua porção central, atualmente abaixo dos arenitos terciários da Serra de Santana, próximo à cidade de Florânia.

1.2.2 O VULCANISMO MACAU

O vulcanismo Macau ocorre na forma de *plugs* e *necks* de dimensões variadas que intrudem o embasamento precambriano, e soleiras intercaladas nos sedimentos da Bacia Potiguar. Em conjunto, as inúmeras ocorrências cartografadas do vulcanismo Macau estão circunscritas em um polígono com orientação geral N-S, e comprimento de aproximadamente 300 km entre as cidades de Macau (RN) e Serra de São Pedro (PE) (Fig. 1.1b). Constituem predominantemente rochas alcalinas (Ne normativa; $\text{Na}+\text{K} > 3,5\%$) incluindo olivina basaltos, basanitos, ankaramitos e nefelinitos (Sial et al., 1981; Fodor et al., 1998; Hollanda, 2002; Silveira, 2006; Knesel et al., 2011). Toleíticos transicionais são reconhecidos subordinadamente (Silveira, 2006). De acordo com Fodor et al. (1998) e Hollanda (2002) as composições isotópicas Sr-Nd das lavas Macau são consistentes com magmas tipo OIB, representando misturas de componentes astenosférico e litosférico. Suas características resumem-se a: (i) forte enriquecimento em LILE (Rb, Sr, K, Ba), terras raras leves e HFSE (Nb, Ta, Ti), associado a (ii) razões isotópicas $^{87}\text{Sr}/^{86}\text{Sr}$ e $^{143}\text{Nd}/^{144}\text{Nd}$ fortemente variáveis entre 0,7038–0,7051 e 0,51266–

0,51280, respectivamente. As razões $^{206}\text{Pb}/^{204}\text{Pb}$ determinadas em algumas poucas amostras variam entre 18,52 e 19,35. O componente astenosférico foi interpretado como líquidos (*melts*) de natureza HIMU+DM interagindo com um manto litosférico que se aproxima de composições tipo EM. Essa interpretação é endossada pela assinatura geoquímica de piroxênios de xenólitos peridotíticos inclusos em basaltos do Pico do Cabugi que indicam natureza de manto litosférico com forte afinidade EMI (Rivalenti et al., 2000).

Os dados geocronológicos $^{40}\text{Ar}/^{39}\text{Ar}$ de Silveira (2006) e Knesel et al. (2011) demonstram idades que se distribuem em um intervalo de aproximadamente 45 milhões de anos, desde o Eoceno (*c.* 52 Ma) até o Mioceno (*c.* 7 Ma). Nesse conjunto dois picos de idades têm destaque: em 8 ± 2 Ma e outro em $25,5 \pm 2$ Ma. A superposição das idades mais jovens do vulcanismo Macau com as idades definidas para as rochas da Ilha de Fernando de Noronha (K/Ar: Cordani, 1967; $^{40}\text{Ar}/^{39}\text{Ar}$: Cordani et al., 2004; Buikin et al., 2009), bem como alguns aspectos geoquímicos-isotópicos similares, tem levado alguns autores a concluir em defesa da associação genética entre os produtos desses dois eventos magmáticos (Fodor et al., 1998, 2002). Essa interpretação não encontra suporte na distribuição dos dados geocronológicos $^{40}\text{Ar}/^{39}\text{Ar}$, incompatível com deslocamento para oeste da placa sul-americana sobre o *hot spot* de Fernando de Noronha (Knesel et al., 2011).

A ocorrência extensiva de xenólitos ultramáficos é observada nos basaltos Macau. São predominantemente peridotitos (Sial et al., 1981; Fodor et al., 1998, 2002; Rivalenti et al., 2000, 2007), e eclogitos subordinados (Silveira, 2006). Estudos detalhados de química mineral têm sido conduzidos por aqueles autores para caracterização precisa das assembleias minerais constituintes e no estudo da termobarometria, o piroxênio foi usado. Rivalenti et al. (2000) e Fodor et al. (2002) reconheceram dois tipos texturalmente distintos de xenólitos: (i) porfioclástico, representando uma região mais inferior do manto local que poderia ser interpretada como a parte superior de um “diápiro” da astenosfera, representada pela transição entre os níveis adiabático e convectivo, e (ii) protogranular, de uma região mais rasa (superior) do manto local representada pelo manto litosférico que sofreu baixas taxas de percolação metassomática. Essas estimativas baseiam-se nas temperaturas de equilíbrio calculadas a partir das composições de piroxênios, as quais correspondem a 950-1280°C/1,9-2,7 GPa nos xenólitos porfioclásticos e 710-990°C/1,3-1,8 GPa nos xenólitos protogranulares (Rivalenti et al., 2000, 2007). Os valores foram obtidos em xenólitos coletados nas lavas do Pico do Cabugi, a maior expressão topográfica do vulcanismo Macau na Província Borborema, e em outros quatro *plugs*.

Ainda em Rivalenti et al. (2000, 2007), dados geoquímicos e isotópicos em rocha total e em piroxênios separados da matriz, apontam para a presença de um agente metassomático de

natureza astenosférica e composição essencialmente alcali-basáltica, com características isotópicas tipo-EMI. Esse componente é mais bem reconhecido nos xenólitos profiroclásticos que, segundo os autores, teriam experimentado maior interação metassomática em comparação com os xenólitos protogranulares. A origem deste metassomatismo é associada com alto gradiente geotérmico (~12-15°C/km) interpretado por Fodor et al. (2002) como resultado da passagem da pluma de Fernando de Noronha sob o continente, durante o Cenozóico.

1.3 OBJETIVOS E JUSTIFICATIVA

Os objetivos desta tese de doutorado estão listados a seguir. Antes, no entanto, faz-se necessário informar que a presente tese é a continuidade do trabalho iniciado por Hollanda (2002) cujo objetivo foi acaracterização das fontes mantélicas dos diques toleíticos Ceará-Mirim e basaltos alcalinos Macau. A comparação dessas fontes permitiria discutir a evolução química do manto litosférico subcontinental na Província Borborema, desde o Cretáceo até o Cenozóico. Apesar do volume de dados reunidos por Hollanda (2002), algumas questões ainda permaneceram abertas. Quanto ao Enxame de Diques Ceará-Mirim, temos que:

- i) O enxame principal foi caracterizado do ponto de vista isotópico, especialmente para Sr e Nd, e menos para Pb, enquanto que a caracterização geoquímica e aspectos relacionados à petrogênese (contaminação versus cristalização fracionada, percentual de fusão da fonte, termometria) foram pouco ou nada explorados. Como resultando, Hollanda (2002, também Hollanda et al., 2006) publicaram uma classificação baseada na distribuição de idades modelo T_{DM} , não levando em conta critérios geoquímicos classicamente usados para definir a tipologia de magmas toleíticos continentais como, por exemplo, conteúdo de Ti-Zr-P.
- ii) O enriquecimento em elementos incompatíveis e a marcante anomalia negativa de Nb levou à interpretação de que os magmas toleíticos teriam sido originados a partir de um manto metassomatizado por um componente de subducção, antigo, provavelmente de idade paleoproterozóica. No entanto, nenhuma informação conclusiva foi levantada sobre o enxame menor, alojado a sul do enxame principal. A importância desse sub-enxame deve-se à presença de olivina modal, não identificada nos toleitos do enxame principal. Apenas uma amostra desse sub-enxame foi analizada por Hollanda (2002) e mostrou razão $^{206}\text{Pb}/^{204}\text{Pb}$ moderadamente radiogênica, tendo sido interpretada como influência de uma fonte tipo HIMU. Essa

característica não foi encontrada nos toleitos do enxame principal, menos radiogênicos em Pb, de forma que tornou-se relevante verificar a presença da fonte tipo HIMU e sua abrangência com respeito ao enxame de diques como um todo.

Quanto ao vulcanismo Macau, temos que:

- i) Os dados Sr-Nd obtidos por Hollanda (2002) mostraram superposição entre as composições determinadas para as amostras mais evoluídas do vulcanismo Macau (basaltos e basanitos) e as composições dos diques toleíticos Ceará-Mirim. Logo, passou a ser de extrema relevância discutir a hipótese de que os dois eventos magmáticos teriam compartilhado a mesma fonte litosférica enriquecida. Ainda, a presença de uma fonte tipo HIMU indicada para os diques com olivina no artigo de Hollanda et al. (2006) pedia a investigação de sua presença também nos basaltos Macau.
- ii) Um foco em comum nas discussões de Fodor et al. (1998), Rivalenti et al. (2000) e Knesel et al. (2011) é a relação genética do vulcanismo Macau com a pluma de Fernando de Noronha. O conjunto de dados agora disponível para ambos eventos continental e oceânico permitirá estabelecer similaridades e avançar na discussão.

Por fim, os xenólitos peridotíticos não foram alvo de Hollanda (2002). Os dados Re-Os aqui apresentados representam informação inédita na literatura e serão discutidos com base nas informações já existentes de química mineral, geoquímica e isótopos de Sr, Nd e Pb apresentados principalmente por Fodor et al. (2002) e Rivalenti et al. (2000, 2007). Portanto, esperamos usar os dados isotópicos Re-Os para caracterizar a natureza química (grau de enriquecimento versus empobrecimento) e idade do manto litosférico subcontinental amostrado pelos xenólitos.

CAPÍTULO 2

REVISÃO CONCEITUAL

Em Petrologia, os reservatórios magmáticos reconhecidos no manto são assumidos como tendo características geoquímicas distintas. Diferenciam-se os conceitos “manto empobrecido (ou depletado)” (DM), “manto enriquecido” (EM) e “manto primitivo” (PM). Ao contrário, os termos **litosfera** e **astenosfera** constituem conceitos mecânicos (ou reológicos). O primeiro implica resistência, e está associado às partes da crosta e manto que respondem elasticamente e reversivelmente a uma carga aplicada, contrariamente ao comportamento newtoniano da astenosfera. A integração das duas vertentes conceituais permite então distinguir os reservatórios globais descritos como manto litosférico ou astenosférico, seja empobrecido ou enriquecido (p.ex., Minster e Anderson, 1981; McNutt, 1984; Weiss et al., 1987; White, 1988; McKenzie e Bickle, 1988; Hart e Staudigel, 1989; Menzies, 1990).

2.1 MANTO SUPERIOR ASTENOSFÉRICO E LITOSFÉRICO

A astenosfera consiste em um reservatório convectivo, com espessura média entre 100 e 200 km e viscosidade de $10^{21} - 10^{22}$ Pa.s. É muitas vezes referenciada como 'manto superior', 'manto convectivo' ou simplesmente 'manto empobrecido', de onde normalmente se originam os magmas tipo-MORB. Todos os processos globais relacionados à dinâmica interna, relacionada à tectônica de placas ou plumas, afetam diretamente a assinatura química desse reservatório. A princípio, o manto astenosférico é fértil (altos teores em Fe, Al, Ca, Na, e Ti), mas empobrecido em elementos incompatíveis, e pode ser fonte para magmas primitivos em vários ambientes tectônicos (arcos de ilha, dorsais oceânicas, rifts continentais). O acrônimo para essa característica particular é DM (acrônimo em inglês de *Depleted Mantle*). A litosfera é representada pela crosta e parte do manto superior, consistindo em um reservatório frio e rígido com espessura variável entre 40 e 100 km e viscosidade na ordem de $10^{23} - 10^{25}$ Pa.s. Quando comparado à astenosfera, o manto litosférico é, a princípio, estéril (baixos teores em Fe, Al, Ca, Na, e Ti) e enriquecido em elementos incompatíveis. Sua fertilidade é intrinsecamente

dependente do grau de enriquecimento e de fontes de calor externas que possam promover a fusão parcial, seja por descompressão ou por rebaixamento da temperatura do *solidus* peridotítico na presença de fluidos metassomáticos (p.ex., Dawson 1984; Roden e Murthy, 1985; Nielson e Noller, 1987; Wilshire 1987).

No passado, o manto superior era considerado um reservatório de características DM em toda sua extensão, dado seu potencial para fundir e gerar crosta ao longo do tempo geológico. A partir do trabalho de Anderson (1982) que sugeriu serem os magmas basálticos produtos de misturas de líquidos fracionados de fontes enriquecidas e empobrecidas, teve início a nova concepção de um manto superior geoquimicamente homogêneo. Zindler e Hart (1986) foi um dos trabalhos pioneiros em propor e modelar a existência de distintos reservatórios isotópicos (Sr, Nd e Pb) no manto para explicar a gênese dos basaltos de ilhas oceânicas modernas. A partir daí, os acrônimos EM (I e II) foram definidos para o manto dito 'enriquecido' em elementos incompatíveis, DM manteve-se como 'manto empobrecido' e HIMU foi definido como uma parte do manto superior com valores altamente radiogênicos em Pb, assim diferenciando-se dos demais. Aqueles autores interpretaram as variações para reservatórios tipo-EM e -HIMU como reflexo de contribuições provenientes de sedimentos (continentais + pelágicos) e crosta oceânica alterada em um contexto de subducção (ver também Anderson, 1985), em proporções variáveis. O amplo espectro de variações compostionais hoje reconhecidas no manto superior condiciona a também variabilidade química de magmas OIB, a contrapartida composicional dos magmas tipo-MORB. No entanto, segundo Weiss et al. (1987) a fonte OIB seria melhor correlacionada ao manto inferior se considerada a extensão dos processos de reciclagem para além dos limites da astenosfera, até a descontinuidade de 660 km. Assim, a heterogeneidade química do manto passa a ser característica comum tanto do manto superior quanto em parte do manto inferior.

2.2 RESERVATÓRIOS MAGMÁTICOS: OS *ENDMEMBERS* ISOTÓPICOS

As composições de magmas oceânicos tipo-OIB, os quais têm maior representatividade que os tipo-MORB no manto suboceânico, são os alvos principais para avaliar a heterogeneidade química do manto (p.ex., Tatsumoto, 1987; Zindler e Hart, 1986; Sun e McDonough, 1989; Hofmann, 2003). A heterogeneidade resulta de processos de diferenciação durante a história da Terra que, de maneira contínua, gera crosta rica em elementos incompatíveis e empobrece o manto empobrecido, e ainda enriquece o manto novamente devido a reciclagem de material

crustal em diferentes profundidades. A origem dos vários reservatórios químicos do manto: DM, HIMU, EM1, EM2, FOZO, PREMA e BSE (p.ex., McKenzie e O'Nions, 1983; White, 1985; Zindler e Hart, 1986; Hawkesworth et al., 1986; Hart, 1988; Ben Othman et al., 1989; Plank e Langmuir, 1998; Hart et al., 1992; Sun e McDonough, 1989; White e Hoffman, 1982; Chauvel et al., 1992; Hauri et al., 1993, 1994; Hanan e Graham, 1996, Hanan et al., 2000; Stracke et al., 2005; Workman et al., 2004), são atribuídas a essa ciclicidade dos processo de dinâmica interna.

2.2.1 O RESERVATÓRIO DM

O reservatório DM é definido no manto superior (mais superficial) e é a fonte dos magmas tipo-MORB (Meibom e Anderson, 2003), em geral empobrecidos em elementos incompatíveis em relação ao manto primitivo (CHUR). A subdivisão em magmas E-MORB, N-MORB e T-MORB referem-se a proporções variáveis de alguns elementos traços, sendo reconhecidos por parâmetros tais como razões Rb/Nd e K₂O/TiO₂ (Mahoney et al., 1994; Hall et al., 2006). Segundo Zindler e Hart (1986) pode ser desmembrado em DMA e DMb. As razões em ²⁰⁶Pb/²⁰⁴Pb, ²⁰⁷Pb/²⁰⁴Pb e ⁸⁷Sr/⁸⁶Sr são muito radiogênicas (valores elevados) enquanto ¹⁴³Nd/¹⁴⁴Nd é não-radiogênica (valores elevados) com relação aos outros reservatórios EMs e HIMU (Hoffman, 2003).

- DMA: ¹⁴³Nd/¹⁴⁴Nd ~ 0,51350, ⁸⁷Sr/⁸⁶Sr ~ 0,7021, ²⁰⁶Pb/²⁰⁴Pb ~ 17,40 / ²⁰⁷Pb/²⁰⁴Pb ~ 15,39;
- DMb: ¹⁴³Nd/¹⁴⁴Nd é o mesmo que DMA, ⁸⁷Sr/⁸⁶Sr ~ 0,7019 e as razões Pb/Pb são significativamente menos radiogênicas do que aqueelas de DMA (²⁰⁶Pb/²⁰⁴Pb ~ 15,8 / ²⁰⁷Pb/²⁰⁴Pb ~ 15,15).

2.2.2 O RESERVATÓRIO OIB

Magmas tipo OIB podem ser oceânicos ou continentais, mas são quimicamente e isotopicamente distintos daqueles do tipo MORB por serem enriquecidos em elementos incompatíveis. Hofmann (1997) sugere que o enriquecimento deve ter sido antigo (1 a 2 bilhões de anos) para que a assinatura radiogênica de Sr, Nd e Pb possa ser produzida. Sua origem é motivo ainda de debate, muito embora o envolvimento de plumas já seja um conceito mais amplamente aceito para explicar o enriquecimento por reciclagem profunda de material crustal (ver revisão de Fitton, 2007; também Sleep, 1984; Fitton e James, 1986; Meibom and Anderson,

2003; Ito and Mahoney, 2005). Anderson (1995) pressupõe uma zona semi-viscosa abaixo da litosfera, a qual chama de perisfera, como a fonte provável de magmas tipo OIB. No continente, magmas OIB são, em geral, gerados em contexto extensional ao longo de riftes ativos e passivos.

São reconhecidos três membros principais a partir de magmas OIB os quais são complementares ao manto DM (empobrecido após eventos de fusão parcial): HIMU, EMI e EMII (Zindler e Hart, 1986). Apesar de muitos trabalhos discutirem particularidades da origem desses reservatórios, é consensual que crosta oceânica subductada, crosta continental inferior e crosta continental superior (sedimentos continentais e marinhos), misturados em proporções variáveis ao manto DM, sejam os principais elementos que contribuem para a características isotópicas dominantes em cada um. Um quarto reservatório chamado FOZO é adicionado a esse conjunto, em parte semelhante a HIMU, mas diferenciando-se pelas razões isotópicas de Pb (Hart et al., 1992; Stracke et al., 2005).

- ✓ HIMU (alto $\mu = ^{238}\text{U}/^{204}\text{Pb}$)

HIMU é interpretado como crosta oceânica reciclada previamente empobrecida em elementos incompatíveis (dentre os quais Pb) devido à desidratação durante subducção (p.ex., Hoffman e White, 1982; Chauvel et al., 1992; Hauri et al., 1993; Kelley et al., 2005). Esse reservatório tem razões $^{238}\text{U}/^{204}\text{Pb}$ elevadas o que induz à características muito radiogênicas em Pb, observadas pelos valores muito elevados da razão $^{206}\text{Pb}/^{204}\text{Pb}$, acompanhados por valores baixos para a razão $^{87}\text{Sr}/^{86}\text{Sr}$ (relativo a BSE) e intermediários para $^{143}\text{Nd}/^{144}\text{Nd}$ (relativo ao CHUR). Os magmas OIB-HIMU raramente ocorrem misturados a outros tipos OIB (Stracke et al., 2005), tendo valores médios para $^{143}\text{Nd}/^{144}\text{Nd} \sim 0,5129$, $^{87}\text{Sr}/^{86}\text{Sr} \sim 0,7030$, $^{206}\text{Pb}/^{204}\text{Pb} \sim 21,50$ e $^{207}\text{Pb}/^{204}\text{Pb} \sim 15,85$ (Zindler e Hart, 1986).

- ✓ EMI e EMII

Dois reservatórios com características muito enriquecidas em Sr e Nd são definidos por Zindler e Hart (1986): EMI e EMII (EM – *Enriched Mantle*). O reservatório EMI é caracterizado por valores intermediários para $^{207}\text{Pb}/^{204}\text{Pb}$ (média de $\sim 15,45$) e baixos para $^{206}\text{Pb}/^{204}\text{Pb}$ (média de $\sim 16,80$), valores relativamente altos para $^{87}\text{Sr}/^{86}\text{Sr}$ (média de $\sim 0,7049$), enquanto baixos para $^{143}\text{Nd}/^{144}\text{Nd}$ (média de $\sim 0,5121$). Várias hipóteses têm sido aventadas para a origem do reservatório EMI: (i) litosfera subcontinental delaminada reciclada (p.ex., Hawkesworth et al., 1986; Mahoney et al., 1991; McKenzie e O'Nions, 1983); (ii) reciclagem de sedimentos

pelágicos antigos em zonas de subducção (p.ex., Ben Othman et al., 1989; Plank e Langmuir, 1993); (iii) reciclagem de crosta continental (granulítica) inferior por delaminação (p.ex., Rollinson, 1993); e (iv) mistura de magmas OIB-HIMU e sedimentos continentais (p.ex., Weaver, 1991). Dados para a razão $^{187}\text{Os}/^{188}\text{Os}$ já são mencionadas na literatura para os basaltos das ilhas e *seamounts* Pitcairn, com valores $>0,135$; esses valores sugerem o envolvimento de um componente enriquecido em Rênio e, portanto, altas razões Re/Os (p.ex., Woodhead and Devey, 1993).

O reservatório EMII tem valores relativamente mais altos (relativos a EMI) para as razões $^{207}\text{Pb}/^{204}\text{Pb}$ ($\sim 15,68$), $^{206}\text{Pb}/^{204}\text{Pb}$ ($\sim 18,90$) e $^{87}\text{Sr}/^{86}\text{Sr}$ ($\sim 0,7080$), e baixos para $^{143}\text{Nd}/^{144}\text{Nd}$ ($\sim 0,5121$) (Zindler e Hart, 1986; Chen et al., 2007). EMII tem sua origem atribuída à reciclagem de: (i) crosta continental e sedimentos, (ii) crosta oceânica alterada; e (iii) litosfera subcontinental (p.ex., Hoffman e White, 1982; Rollinson, 1993). Trabalhos sobre basaltos das Ilhas Samoa sugerem que EMII seja um componente derivado de litosfera oceânica metassomatizada, isolada no manto profundo por cerca de $\sim 2,5$ bilhões de anos, a qual teria ascendido na forma de pluma (Workman et al., 2004). As concentrações em elementos traços são pouco conclusivas para diferenciar EMI de EMII (p.ex., Willbold e Stracke, 2006). Em geral, magmas OIB-EM têm teores altos de Ba, Nb, Pb, Sr, Eu e Nd e razões variáveis Ba/Nb e Sr/Nd e baixas Ce/Pb e Nb/U.

✓ FOZO

Os magmas OIB - EMI, EMII, HIMU, e o DM divergem a partir de um foco central que Hart et al. (1992) denominaram FOZO (*Focal Zone*). Esse componente tem composições isotópicas Sr, Nd e Pb intermediárias com respeito aos outros membros. Embora esses autores afirmem que FOZO seja o produto de plumas profundas, Carlson et al. (2006) afirmam que as fontes FOZO estão presentes no manto superior, enquanto que Stracke et al. (2005) sugerem que FOZO está globalmente presente no manto. O debate sobre a origem de FOZO vem das variações compostionais a ele atribuídas. Por exemplo, segundo Hart et al. (1992) as razões isotópicas deste componente seriam $^{143}\text{Nd}/^{144}\text{Nd} > 0,5131$, $^{87}\text{Sr}/^{86}\text{Sr} < 0,7025$, $^{206}\text{Pb}/^{204}\text{Pb}$ entre 19,1–19,7. Hauri et al. (1994) sugerem que composições $^{87}\text{Sr}/^{86}\text{Sr}$ seriam mais radiogênicas, entre $\sim 0,703$ – $0,704$, enquanto as razões $^{143}\text{Nd}/^{144}\text{Nd}$ seriam discretamente menos radiogênicas ($\sim 0,5128$ – $0,5130$), combinadas a razões $^{206}\text{Pb}/^{204}\text{Pb}$ entre 18,5–19,5. Combinações entre essas assinaturas são defendidas por Workman et al. (2003), enquanto que Stracke et al. (2005) faz uma revisão sobre a caracterização de FOZO usando principalmente dados isotópicos de Pb obtidos para as ilhas Cook-Austral (Polinésia Francesa), e comparando-os com dados de basaltos

tipicamente HIMU (St. Helena e o conjunto mais radiogênico de Cook-Austral) e um conjunto de dados globais de basaltos OIB e MORB. A caracterização isotópica dos basaltos continentais apresentada nesta tese foi principalmente baseada na modelagem de Stracke et al. (2005).

REFERÊNCIAS

- ALMEIDA, F.F.M. Distribuição Regional e Relações Tectônicas do Magmatismo Pós – Paleozóico no Brasil. *Revista Brasileira de Geociências*, vol. 16(4): 325-349. 1986.
- ALMEIDA, F.F.M. and CARNEIRO, C.D.R. Magmatic occurrences of post-permian age of the South American Platform. *Boletim do IG-USP-Série Científica*, 20, 71-85, 1989.
- ALMEIDA, F.F.M.; CARNEIRO, C.D.R.; MIZUSAKI, A.M.P. Correlação do magmatismo das bacias da margem continental brasileira com o das áreas emersas adjacentes. *Revista Brasileira de Geociências*, 26 (3): 125-138. 1996.
- ANDERSON, D. L. Isotopic evolution of the mantle: the role of magma mixing. *Earth and Planetary Science Letters*. 57, 1-12. 1982.
- ANDERSON, D.L. 1985. Hotspot magmas can form by fractionation and contamination of MORB. *Nature*, v. 318, p. 145-149.
- ANDERSON, D. L. Lithosphere, asthenosphere and perisphere. *Reviews of Geophysics*, 33, 125-149. 1995.
- ARAUJO, A.L.N.; CARLSON, R.W.; GASPAR, J.C.; BIZZI, L.A. Petrology of kamafugites and kimberlites from the Alto Paranaiba Alkaline Province, Minas Gerais, Brazil. *Contributions to Mineralogy and Petrology* 142, 163-177. 2001.
- ARCHANJO, C.J., TRINDADE, R.I., MACEDO, J.W.P. AND ARAUJO, M.G. Magmatic fabrico f a basaltic dyke swarm associated with Mesozoic rifting in NE Brazil. *Journal of South American Earth Science*, 13 (3), 179-189. 2000.
- BAKSI A.K. & ARCHIBALD D.A. Mesozoic igneous activity in the Maranhão province, northern Brazil: $^{40}\text{Ar}/^{39}\text{Ar}$ evidence for separate episodes of basaltic magmatism. *Earth and Planetary Sciences Letters*, 151:139-153. 1997.
- BELLINI, G., MACEDO, M.H.F., PETRINI, R., PICCIRILLO, E.M., CAVAZZINI, G., COMIN-CHIARAMONT, P., ERNESTO, M., MACEDO, J.W.P., MARTINS, G., MELFI, A.J., PACCA, I.G. and DE MIN, A. Evidence of magmatic activity related to Middle Jurassic and Lower Cretaceous rifting from northeastern Brazil (Ceará-Mirim: K/Ar age, paleomagnetism, petrology and Sr-Nd isotope characteristics. *Chemical Geology*, 97, 9-32. 1992.
- BELLINI, G., MONTES-LAUAR, C.R., DE MIN, A., PICCIRILLO, E.M., CAVAZZINI, G., MELFI, A.J. & PACCA, I.G. Early and Late Cretaceous magmatism from São Sebastião island (SE-Brazil): geochemistry and petrology. *Geochimica Brasiliensis* 4, 59-83. 1990.
- BEN OTHMAN, D., WHITE, W.M. and PATCHETT, J. The geochemistry of marin sediments, island arc magma genesis and crust-mantle recycling. *Earth and Planetary Science Letters*, 94, 1-21. 1989.
- BUIKIN, A. I., KOGARKO, L.N., KOROCHANTSEVA, E.V., HOPP, J. AND TRIELOFF, M. $^{40}\text{Ar}-^{39}\text{Ar}$ Dating of Volcanic Rocks from the Fernando de Noronha Archipelago. *Geochemistry International*, 2010, Vol. 48, No. 10, pp. 1035-1038. 2009.
- CAINELLI C. & MOHRIAK W.U. Some remarks on the evolution of sedimentary basins along the Eastern Brazilian Continental Margin. *Episodes*, 22:206-216. 1999.

- CARLSON, R.W., CZAMANSKE, G., FEDORENKO, V. and ILUPIN, I.A comparison of Siberian meimechites and kimberlites: Implications for the source of high-Mg alkalic magmas and flood basalts.*Geochemistry, Geophysics, Geosystems*, Vol. 7, Issue 11, 2006.
- CHAUVEL, C., A. W. HOFMANN, AND P. VIDAL. HIMU-EM: The French Polynesian connection.*Earth and Planetary Science Letters*, 110, 99–119, 1992.
- CHEN, Y.; ZHANG, Y.; GRAHAM, D.; SU, S. and DENG, J. Geochemistry of Cenozoic basalts and mantle xenoliths in Northeast China.*Lithos*, 96: 108-126, 2007.
- COMIN-CHIARAMONTI, P., GOMES, C.B., PICCIRILLO, E.M. AND RIVALENTI, G. High-TiO₂ basaltic dykes in the coastline of São Paulo and Rio de Janeiro States (Brazil). *Neues Jahrbuch Mineralogische Abhandlungen* 146, 133-150.1983.
- CORDANI, U. G. “K–Ar Ages from Fernando de Noronha,” in *Proceedings of Symposium on ContinentalDrift in the Southern Hemisphere*, Montevideo (Montevideo), p. 85. 1967.
- CORDANI, U.G., ULRICH, M.N.C., ONOE, A.T., VINASCO, V.C.J. Novas determinações de idade pelos métodos K–Ar e Ar–Ar para o arquipélago de Fernando de Noronha. *Revista da Faculdade de Ciências* (1). 2004.
- DAWSON, J. B. Contrasting types of upper-mantle metasomatism? In *Kimberlites II :The Mantle and Crust-Mantle Relationships*, ed. 1. Kornprobst, pp. 289-94. Amsterdam : Elsevier. 393 pp.1984
- FITTON, J. G. The OIB Paradox. Plates, Plumes and Planetary Processes. *Geological Society of America Special Paper* 430, p. 387-412. 2007.
- FITTON, J.G. and JAMES, D. Basic volcanism associated with intraplate linear features. *Philosophical Transactions of the Royal Society of London*, v. A317, p. 253–266. 1986.
- FODOR R.V., MCKEE E.H., ASMUS H.E. K-Ar ages and the opening of the South Atlantic ocean: basaltic rock from the Brazilian margin. *Marine Geology*, 54:M1-M8. 1983/84.
- FODOR, R.V., MUKASA, S.B. AND SIAL, A.N. Isotopic and trace-element indications of lithospheric and asthenospheric components in Tertiary alkalic basalts, northeastern Brazil.*Lithos*, 43.197-217. 1998.
- FODOR, R.V., SIAL, A.N. and GANDHOK, G. Petrology of spinel peridotite xenoliths from northeastern Brazil: lithosphere with a high geothermal gradient imparted by Fernando de Noronha plume. *Journal of South American EarthScience*, 15, 199-214. 2002.
- FODOR, R.V., SIAL, A.N. MUKASA, S.B., McKEE, E.H. Petrology, isotope characteristics, and K-Ar ages of the Maranhão, northern Brazil, Mesozoic basalt province. *Contribution to Mineralogy and Petrology*, 104, 555-567. 1990.
- FODOR R.V. and VETTER S.K. Rift-zone magmatism: petrology of basaltic rocks transitional from CFB to MORB, Southeastern Brazil margin. *Contributions to Mineralogy and Petrology*, 88:307-321. 1984.
- GARDA, G.M. Os diques básicos e ultrabásicos da região costeira entre as cidades de São Sebastião e Ubatuba, Estado de São Paulo. Tese de doutorado, *Universidade de São Paulo*, 156p, 1995.
- GUEDES, E., HEILBRON, M. and VALENTE, S.C. Litogeocíquima e petrografia dos diques máficos da região entre Pedra Selada e Barra do Piraí, RJ, SE do Brasil. Boletim de Resumos Expandidos do 5º Congresso de Geoquímica de Países de Língua Portuguesa & 7º Congresso Brasileiro de Geoquímica, Porto Seguro, SBG-BA, p. 516. 1999.
- HALL, L.S., MAHONEY, J.J., SINTON, J.M., AND DUNCAN, R.A. Spatial and temporal distribution of a C-like asthenospheric component in the Rano Rahi seamount field, East Pacific Rise, 15°–19°S: *Geochemistry Geophysics Geosystems*, v 7. 2006.
- HANAN, B.B., BLICHER-TÖFT, J., KINGSLEY, R. AND SCHILLING, JG. Depleted Iceland mantle plume geochemical signature: Artifact of multicomponent mixing? *Geochemistry, Geophysics, Geosystems*, Vol. 1, No. 1 1003, doi:10.1029/1999GC000009. 2000.

- HANAN, B. B. and D. W. GRAHAM. Lead and helium isotope evidence from oceanic basalts for a common deep source of mantle plumes. *Science* 272, 991-995. 1996.
- HART, S. R. Heterogeneous mantle domains: signatures, genesis and mixing chronologies. *Earth and Planetary Science Letters*, 90, 273-296. 1988.
- HART, S.R., HAURI, E.H., OSCHMANN,L.A., WHITEHEAD, J.A. Mantle Plumes and Entrainment: Isotopic Evidence. *Science*, 256, pp517-520. 1992.
- HART, S.R. and STAUDIGEL, H. Isotopic characterization and identification of recycled components.In *Crust/Mantle Recycling at Convergence Zones*, Hart, S.R. and Gulen, L., editors, pp.15-28. 1989.
- HAURI, E.H. and HART, S.R. Re-Os isotope systematics of HIMU and EMII oceanic island basalts from the South Pacific Ocean.*Earth and Planetary Science Letters*, 114:353-371. 1993.
- HAURI, E.H.; WHITEHEAD, J.A. & HART, S.R. Fluid dynamic and geochemical aspects of entrainment in mantle plumes.*Journal of Geophysical Research*, 99, (B12) 24275-24300. 1994.
- HAWKESWORTH, C.J.; MANTOVANI, M.S.M.; TAYLOR, P.N. & PALACZ, Z. Evidence from the Parana of South Brazil for a continental contribution to Dupal basalts.*Nature*, 322:356-359. 1986.
- HOFMANN, A.W. Mantle geochemistry: The message from oceanic volcanism. *Nature*, 385: 219-229, 1997.
- HOFMANN, A.W. Sampling Mantle Heterogeneity through Oceanic Basalts: Isotopes and Trace Elements. In: Carlson, R.W. (ed.), Treatise on Geochemistry, vol. 2, *Geochemistry of the Mantle and Core*. Elsevier, pp. 61-101, 2003.
- HOFMANN, A.W. and WHITE, W.M. Mantle plumes from ancient oceanic crust. *Earth and Planetary Science Letters*, vol. 11, 421-436. 1982.
- HOLLANDA, M.H.B.M.*Evolução geodinâmica do manto litosférico continental no Domínio Seridó, Província Borborema, NE do Brasil*. Tese de D.Sc. Universidade de Brasilia. 2002.
- HOLLANDA, M.H.B.M., PIMENTEL, M.M., OLIVEIRA, D.C. AND JARDIM DE SÁ, E. F. Lithosphere-asthenosphere interaction and the origino f Cretaceous tholeiitic magmatism in NE Brazil: Sr-Nd-Pb isotopic evidence. *Lithos*, 86, 34-49. 2006.
- HORN, P., MUELLER-SOHNIES, D. AND SCHULT, A. Potassium-argon ages on a Mesozoic tholeiitic dyke swarm in Rio Grande do Norte Brazil. *Revista Brasileira de Geociencias*, 18, 50-53. 1988.
- ITO, G., AND MAHONEY, J.J. Flow and melting of a heterogeneous mantle. 1: method and importance to the geochemistry of of ocean island and midocean ridge basalts: *Earth and Planetary Science Letters*, v. 230, p. 29–46. 2005.
- KELLEY, K.A., PLANK, T., FARR, L., LUDDEN, J., AND STAUDIGEL. Subduction cycling of U, Th, and Pb. *Earth and Planetary Science Letters*, 234(3-4): 369-383, 2005.
- KING S.D. Hotspots and edge-driven convection, *Geology*, 35, 223-226. 2007.
- KING, S.D. & ANDERSON, D.L.An alternative mechanism to flood basalt formation. *Earth and Planetary Science Letters*, 136, 269-279, 1995
- KING, S. D. AND ANDERSON, D.L. Edge-Driven Convection.*Earth and Planetary Science Letters*, 160, 289-296, 1998.
- KNESEL, K.M., SOUZA, Z.S., VASCONCELOS, P.M., COHEN, B.E. AND SILVEIRA, F.V. Young volcanism in the Borborema Province, NE Brazil, shows no evidence for a trace of the Fernando de Noronha plume on the continent. *Earth and Planetary Science Letters*, 302, 38-50. 2011.

- LOBO, J.T., VALENTE, S.C., THOMAZ FILHO, A. & SZATMARI, P. Diabásios da Serra do Mar e basaltos da Bacia de Campos -comparação dos processos de AFC através de modelamento geoquímico quantitativo. Boletim de Resumos Expandidos do 5º Simpósio de Geologia do Sudeste, São Pedro, SBG, p. 56, 1999.
- MAHONEY, J.J., NICOLLET, C. AND DUPUY, C. Madagascar basalts: tracking oceanic and continental sources. *Earth and Planetary Science Letters*, 104, 350-363. 1991.
- MAHONEY, J.J., SINTONJ.M., KURZ, M.D., MACDOUGALL, J.D., SPENCER K.J., LUGMAIR G.W. Isotope and trace element characteristics of a super-fast spreading ridge: East Pacific rise, 13–23°S. *Earth and Planetary Science Letters*, vol. 121, 173-193. 1994.
- MALUSKI, H., COULON, C., POPOFF, M. AND BAUDIN, P. $^{40}\text{Ar}/^{39}\text{Ar}$ chronology, petrology and geodynamic setting of Mesozoic to Early Cenozoic magmatism from the Benue trough, Nigeria. *Journal of the Geological Society of London*, 152, 311-326. 1995.
- MARZOLI, A., RENNE, P.R., AND PICCIRILLO, E.M. $^{40}\text{Ar}/^{39}\text{Ar}$ geochronology of Mesozoic continental basaltic magmatism, and the opening of the central, equatorial and southern Atlantic Ocean. Penrose 2000, *Volcanic Rifted Margins*, University of London, p. 54. 2000.
- MATOS R.M.D. The Northeast Brazilian rift system. *Tectonics* 11(4):766–791. 1992.
- MATOS R.M.D. Tectonic evolution of the Equatorial South Atlantic. In: Mohriak W, Taiwani M (eds) Atlantic rifts and continental margins. *Geophys Monograph 115, American Geophysical Union*, pp 331–354. 2000.
- McKENZIE, D. and BICKLE, M.J. The volume and composition of melt generated by extension of the lithosphere. *Journal of Petrology*, 29, 625-679. 1988.
- McKENZIE, D. and O'NIONS, R. K. Mantle reservoirs and ocean island basalts. *Nature* 301 229-231. 1983.
- MCNUTT, M. Lithospheric flexure and thermal anomalies. *Journal of Geophysical Research* 89(B13). 1984.
- MEIBOM, A. and ANDERSON, D. L. The statistical upper mantle assemblage. *Earth and Planetary Science Letters*, 217, 123-139. 2003.
- MENZIES, M.A. *Petrology and geochemistry of the continental mantle*. Pp. 1-184, Clarendon, Oxford. 1990.
- MINSTER, J.B. AND ANDERSON, D.L. A model of dislocation-controlled rheology of the mantle. *Philosophical Transactions of the Royal Society of London*, 299, 319-356. 1981.
- MIZUSAKI A, M.P., PETRINI, R., BELLINI, G., COMIN-CHIARAMONTI, P., DIAS J., DEMIN A., PICCIRILLO, E.M. Basalt magmatism along the passive continental margin of SE Brazil (Campos basin). *Contributions to Mineralogy and Petrology*, 111:143-160. 1992.
- MIZUSAKI, A.M.P., THOMAS-FILHO, A., MILANI, E.J. AND DE CÉSERO, P. Mesozoic and Cenozoic igneous activity and its tectonic control in northeastern Brazil. *Journal of South American Earth Science*, 15, 183-198. 2002.
- MOHRIAK, W. U., ROSENDAHL, B.R., TURNER, J. P., VALENTE, S. C. Crustal architecture of South Atlantic volcanic margins. In: M.A. Menzies & C. Ebinger (eds.) Volcanic rifted margins. *Geological Society of America*, 362, Ed. Boulder, p. 159-202. 2002.
- NIELSON, J.E. and NOLLER, J.S. Processes of mantle metasomatism: Constraints from observations of composite peridotite xenoliths. *Geological Society of America, Special Papers*, v. 215, p. 61-76. 1987.
- OLIVEIRA, D.C. *O papel do enxame de diques Rio Ceará-Mirim na evolução tectônica do nordeste oriental (Brasil): implicações na formação do Rife Potiguar*. MSc. (dissert.) Universidade Federal de Ouro Preto. 172p. 1992.
- PICCIRILLO, E.M., BELLINI, G., CAVAZZINI, G., COMIN-CHIARA-MONTI, P., PETRINI, R., MELFI, A.J., PINESI, J.P.P., ZANTADESCHI, P., DEMIN, A. Lower Cretaceous tholeiitic Dyke swarms from the Ponta Grossa (southeast Brazil): Petrology, Sr-Nd isotopes and genetic relationships with the Paraná flood volcanics. *Chemical Geology*, 89:19-48. 1990.

PICCIRILLO, E. M. and MELFI, A. J. (Eds.). The Mesozoic Flood Volcanism of the Parana Basin: petrogenetic and geophysical aspects. São Paulo: USP, p. 1-14. 98. 1988.

PLANK, T., LANGMUIR, C.H. Tracing trace element from sediment input to volcanic output at subduction zones. *Nature* 362, 739–742. 1993.

PLANK, T., LANGMUIR, C.H. The chemical composition of subducting sediment and its consequences for the crust and mantle. *Chemical Geology*, 145, pp325–394. 1998.

REGELOUS, M. *Geochemistry of dolerites from the Paraná flood basalt province, southern Brazil*. Tese de doutorado, Open University, 1993.

RIVALENTI, G., MAZZUCHELLI, M., GIRARDI, V.A.V., VANNUCCI, R., BARBIERI, M.A., ZANETTI, A. & GOLDSTEIN, S.L. Composition and processes of the mantle lithosphere in northeastern Brazil and Fernando de Noronha: evidence from mantle xenoliths. *Contribution to Mineralogy and Petrology*, 138, 308-325. 2000.

RIVALENTI, G., ZANETTI, A., GIRARDI, V.A.V., MAZZUCHELLI, TASSINARI, C.C.G. AND BERTOTTO, G.W. The effect of the Fernando de Noronha plume on the mantle lithosphere in north-eastern Brazil. *Lithos*, 94, 111-131. 2007.

RODEN, M. F. AND MURTHY, V. R. Mantle metasomatism. *Annual Review of Earth and Planetary Sciences*, 13: 269-96. 1985.

ROLLINSON, H. *Using Geochemical Data: Evaluation, Presentation, Interpretation*. Prentice Hall. England, 1993. 352 p. 1993

SIAL A.N., LONG L.E., PESSOA D.A.R., KAWASHITA K. Potassium-argon ages and strontium isotope geochemistry of Mesozoic and Tertiary basaltic rocks, Northeastern Brazil. *Anais da Academia Brasileira de Ciências*, 53: 115-122. 1981.

SILVEIRA, F.V. *Magmatismo Cenozóico da porção central do Rio Grande do Norte, NE do Brasil*. Tese de doutorado, UFRN, 220p. 2006.

SLEEP, N.H. Tapping of magmas from ubiquitous mantle heterogeneities - an alternative to mantle plumes: *Journal of Geophysical Research*, v. 89, p. 29–41. 1984.

SMITH, P.E., EVENSEN, N.M., YORK, D., SZATMARI, P., OLIVEIRA, D.C. Single-crystal ^{40}Ar - ^{39}Ar dating of pyrite: no fool's clock. *Geology* 29, 403–406. 2001.

STRACKE, A., BIZIMIS, M. AND SALTERS, V.J.M. Recycling oceanic crust: quantitative constraints. *Geochemistry, Geophysics, Geosystems*, 4(3), 8003, DOI:10.1029/2001GC000223. 2003.

STRACKE, A.; HOFFMAN, A.W. and HART, S.R. FOZO, HIMI, and the rest of the mantle zoo. *Geochemistry, Geophysics, and Geosystems*, 6(5): Q05007. doi:10.1029/2004GC000824. 2005.

SUN, S.-S and McDONOUGH, W.F. Chemical and isotopic systematics of oceanic basalts: implications for mantle composition and processes. In: Saunders, M.J. Magmatism in the ocean basins. Londres. *Geological Society Special Publication* 42: 313-345, 1989.

TATSUMOTO, M. Isotopic composition of lead in oceanic basalt and its implication to mantle evolution. *Earth and Planetary Science Letters* 38(1): 63-87. 1987.

THOMAZ FILHO, A., MIZUSAKI, A.M.P., MILANI, E.J., CESERO, P. Rifting and magmatism associated with the South America and Africa breakup. *Revista Brasileira de Geociências*, 30:17-19. 2000.

VALENTE, S.C., ELLAM, R.L., MEIGHAN, I.G., FALLICK, A.E. Geoquímica isotópica, modelo geodinâmico e petrogêne-se dos diabásios do cretácio Inferior no Enxame de Diques Máficos da Serra do Mar (EDSM) na área de do Rio de Janeiro, RJ. In: SBG –MG, Congresso Brasileiro de Geologia, 40, *Boletim de Resumos*, p. 471. 1998.

VALENTE, S.C., ELLAM, R.L., MEIGHAN, I.G. and FALLICK, A.E. The evolution of the Early Cretaceous tholeiitic dykes of Rio de Janeiro by AFC under high fO₂ conditions: Major and trace element, Sr-Nd-O data and

quantitative modelling. Boletim de Resumos do 7º Simpósio Sul Brasileiro de Geologia e 2º Encontro de Geologia do MERCOSUL, Foz do Iguaçu. *Boletim de Resumos...*, Foz do Iguaçu, SBG, p. 94. 1999.

WEAVER, B.L. 1991. The origin of ocean island end-member compositions: trace element and isotopic constraints. *Earth and Planetary Science Letters*, 104, 381-397. 1991.

WEISS, D., DEMAFFE, D., CAVET, S. and JAVOY, M. Sr, Nd, O and H isotopic ratios in Ascension Island lavas and plutonic inclusions; cogenetic origin. *Earth and Planetary Science Letters*, 82 (1987) 255-268. 255. 1987.

WHITE, W.M. Sources of oceanic basalts: Radiogenic isotopic evidence. *Geology*, 13:115-118, 1985.

WHITE, W. M., HOFMANN, A. W.Sr and Nd isotope geochemistry of oceanic basalts and mantle evolution, *Nature*, 296, 821-825. 1982.

WHITE, R.S. The Earth's crust and lithosphere. *Journal of Petrology* special issue, 1-10. 1988.

WILLBOLD, M. AND STRACKE, A. Trace element composition of mantle end-members: Implications for recycling of oceanic and upper and lower continental crust. *Geochemistry, Geophysics, Geosystems*, vol.7, 1-30DOI: 10.1029/2005GC001005. 2006.

WILSHIRE, H.G. A model of mantle metasomatism *Geological Society of America Special Papers*, 215, p. 47-60. 1987.

WOODHEAD, J.D. and DEVEY, C.W. Geochemistry of the Pitcairn seamounts, I: Source character and temporal trends. *Earth and Planet. Sci. Lett.* 116: 81-99. 1993.

WORKMAN, R.K.; HART, S.R.; JACKSON, M.; REGELOUS, M.; FARLEY, K.A.; BLUSZTAJN, J.; KURZ, M. and STAUDIGEL, H. Recycled metasomatised lithosphere as the origin of the Enriched Mantle II (EM2) end-member: Evidence from the Samoan Volcanic Chain. *Geochemistry, Geophysics, Geosystems*, 5(4), Q04008, doi:10.1029/2003GC000623. 2004.

ZINDLER A. and HART S. Chemical geodynamics. *Annual Review of Earth and Planetary Sciences*, 14: 493-571. 1986.

CAPÍTULO 3

ARTIGO SUBMETIDO AO PERIÓDICO *LITHOS*

ABSTRACT

The Ceará Mirim dyke swarm (northeastern Brazil) is composed of Cretaceous tholeiites with plagioclase, clinopyroxene (\pm olivine), Fe-Ti oxides and pigeonite in its groundmass. These tholeiites have been subdivided into three groups: (i) high-Ti olivine tholeiites, (ii) evolved high-Ti tholeiites ($TiO_2 \geq 1.5$ wt.%; $Ti/Y > 360$), and (iii) low-Ti tholeiites ($TiO_2 \leq 1.5$ wt.%; $Ti/Y \leq 360$), with all exhibiting distinct degrees of enrichment in incompatible elements relative to the Primitive Mantle. Negative Pb anomalies are found in all three groups, while Nb-Ta abundances similar to those of OIB-type magmas are found in the olivine tholeiites, with moderate to higher depletion being observed, respectively, in the evolved high-Ti and low-Ti tholeiites. The low-Ti tholeiites had clearly been contaminated with crustal (felsic) materials during ascent. The initial isotopic compositions of olivine tholeiites show uniform and unradiogenic Sr (~0.7035–0.7039) combined with (in part) radiogenic Nd and Pb (>19.1) ratios, which together reveal an indisputable contribution of FOZO component in their genesis. The other tholeiite groups show variable Sr-Nd ratios to relatively consistent $^{206}Pb/^{204}Pb$ ratios clustering toward an isotopically enriched (EMI-type) component. When examined jointly with the negative spike in Nb, this enriched signature reflects the involvement of a subduction-modified lithospheric mantle as a source of the evolved high-Ti and low-Ti tholeiites. Thus, we propose that FOZO and EMI (and likely minor E-MORB) have coexisted and contributed to varying extents to the generation of CMDS primary melts, which has been segregated at 75 to 60 km in depth at the garnet-spinel facies transition. Mechanism(s) that promoted melting were most likely non-plume related, and several alternative models must to be examined further. We find, however, that the role of plate-boundary forces linked to the opening of the Atlantic Ocean have promoted passive rifting and that resulting asthenosphere upraise cannot be excluded as a potential control of CMDS origin.

Keywords: Ceará-Mirim dyke swarm; Mesozoic continental tholeiitic basalts; enriched sub-continental lithospheric mantle; FOZO mantle component

PETROLOGY OF CONTINENTAL THOLEIITIC MAGMAS FORMING A 350 KM-LONG MESOZOIC DYKE SWARM IN NE BRAZIL: CONSTRAINTS OF GEOCHEMICAL AND ISOTOPIC DATA

Emmanuel Donald Ngonge^{1*}, Maria Helena Bezerra Maia de Hollanda¹, Carlos José Archanjo¹, Diógenes Custódio de Oliveira²

¹ Department of Mineralogy and Geotectonics, Institute of Geosciences, University of São Paulo, Rua do Lago, 562, 05508-080, São Paulo SP, Brazil

²Petrobras/UO-RNCE/EXP/ABIG, Av. Eusebio Rocha, 1000, 59064-100, Natal RGN, Brazil

*Corresponding author: donald@usp.br; +55.11.98471.3526

3.1 INTRODUCTION

Rifting and tholeiitic magmatism characterized the breakup and drifting of the South American and African continents in the Mesozoic. Cretaceous Paraná-Etendeka flood basalts ($1 \times 10^6 \text{ km}^3$) that cover part of southern South America and Africa rank as some of the largest igneous provinces in the world (Cordani and Vandoros, 1967; Peate, 1997). In contrast, small volumes of tholeiitic magma emplaced as radial to linear set of dykes mark the rifting stage of Equatorial (Bellieni et al., 1992; Hollanda et al., 2006) and of Central Atlantic magmatism (CAMP, e.g., Marzoli et al., 1999). Our study focuses on the Ceará Mirim dyke swarm (hereinafter CMDS) which includes roughly tens of dykes covering an area of approximately 350 km in length in northeastern Brazil (Fig. 3.1).

One of the most challenging aspects of the study of continental tholeiites relates to the identification of their mantle sources. As precursor magmas migrate upwards through the lithosphere, assimilation and fractional crystallization (AFC) processes can modify magma compositions and thus conceal the original characteristics of primary melts. As a result, geochemical and isotopic features generated by continental tholeiitic basalts cannot be fully distinctive in constraining their mantle sources. In spite of this, their genesis is mostly credited to high melting degrees (>5%) (Jacques and Green, 1980) of enriched spinel lherzolites representing the lithospheric mantle component and/or to asthenosphere (deeper levels) becoming increasingly alkaline with increasing depths of partial melting. For instance, Thompson et al. (2001) proposed that the Southern Etendeka flood basalts were generated from a wholesale hydrous melting of overlying sub-continental lithospheric mantle as a result of heat

transfer from the rising Tristan da Cunha plume. Furthermore, Ewart et al. (2004) argued for time-integrated interactions of the Tristan da Cunha plume with DM-type asthenosphere and subducted sediment components. In contrast, the Northern Paraná tholeiitic basalts were recently re-interpreted following the partial melting of an old metasomatized sub-continental lithospheric mantle with no apparent involvement of the Tristan da Cunha plume (Rocha-Júnior et al., 2012, 2013). In studying further north in the CAMP-Maranhão tholeiitic province, Merle et al. (2011) proposed that magmatism includes variable contributions of the enriched lithospheric mantle mixed with asthenosphere components and contaminated by ultra-alkaline melts.

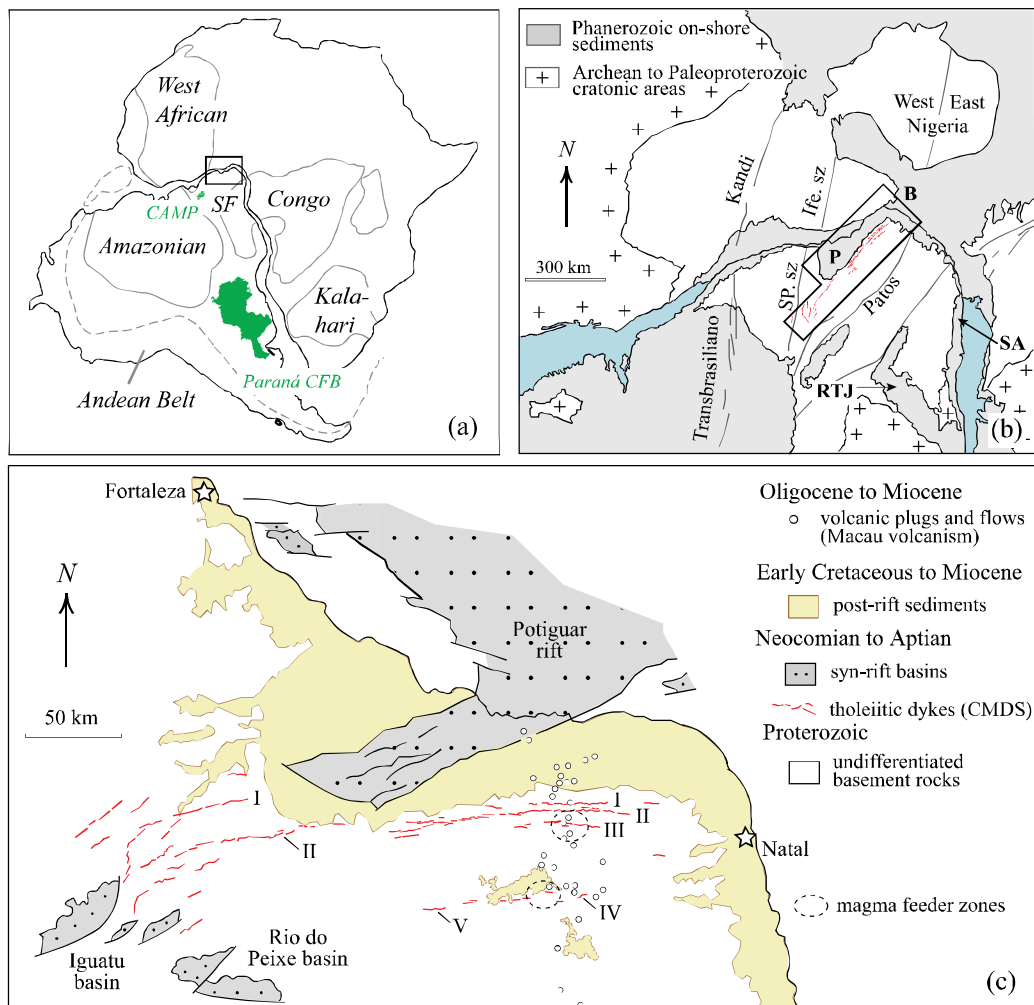


Figure 3.1. (a) Schematic illustration of the West Gondwana with focus on the main Neoproterozoic cratonic areas – Amazonian, São Francisco-Congo, West African and Kalahari. The study area is shown in the box; CAMP-Maranhão (Parnaíba) and Paraná-Etendeka igneous provinces are shown regardless of craton positions. (b) Pre-drift reconstruction of the main geological features of the northeastern Borborema Province and of the West African counterparts (shields of Nigeria and Cameroon) with an emphasis on the major Brasiliano/Pan-African ductile shear zones and major Mesozoic rift systems (B: Benue, RTJ: Recôncavo-Tucano-Jatobá, SA: Sergipe-Alagoas, P: Potiguar). (c) Zoomed-in image of (b) with the geographic location of the CMDS highlighted in red. Sub-swarms defined based on Bellieni's et al. (1992) paleomagnetic study are shown as I–V. Open circles denote the distribution of plugs and lava

flows related to Tertiary Macau volcanism. See the text for general comments.

The present paper assembles a significant dataset on the petrography, mineral chemistry, major and minor elements and Sr-Nd-Pb isotope geochemistry of the CMDS. The swarm consists of a linear set of dykes that have intruded into Precambrian rocks of northeastern Brazil. Though they do not exactly serve as a major igneous province like CAMP or Paraná-Etendeka, their geochemical and isotopic features can provide reliable information on (1) which continental mantle reservoirs were available as fertile sources in the Cretaceous and on (2) how they interacted to generate tholeiitic magmatism. Our objective is to assess the petrological evolution of the CMDS through an updated geochemical characterization of magmas and possible mantle sources involved following the earlier works of Bellieni et al. (1992) and Hollanda et al. (2006). Effects of fractional crystallization and crustal contamination, which are frequently found in continental magmatism are also examined. Comparisons are made with other Mesozoic igneous provinces in South America and Africa to discuss possible chemical similarities.

3.2 GEOLOGICAL BACKGROUND

Atlantic pre-drift reconstructions of the Borborema Province (northeastern Brazil) share numerous geological features with Western Central Africa (Nigeria, Cameroon). Well-known features include the continuity of continental-scale shear zones that can be traced from NE Brazil to SE Nigeria along NE to E-W directions (Fig. 3.1a, b). In the Borborema Province, these shear zones normally present high-temperature (usually low-pressure) ductile conditions (Vauchez et al., 1995; Viegas et al., 2014). Some of these structures accommodated late brittle deformation processes (e.g., normal, strike-slip or locally reverse faults) related to Cambrian-Ordovician to Cenozoic extensional events that led to the development of within-plate rifted basins (e.g., Sénant and Popoff, 1991; Françolin et al., 1994). Rifting processes were influential in breaking up this major continental area, especially from the Early Jurassic to the Late Cretaceous, resulting in the opening of the Equatorial and Central segments of the Atlantic Ocean. A striking outcome of this global event has been the generation of continental volcanism and hydrocarbon traps related to both onshore and offshore basins (e.g., Chang et al., 1992).

In contrast to the large volumes of magma extrusion associated with the syn-rift stage of the southern Atlantic margin (the Paraná-Etendeka Province; see review of Peate, 1997), the Equatorial rift basins are characterized by modest quantities of magmatic rock (e.g., Benkhelil, 1989). The most significant magmatic activity found in the Borborema Province corresponds

with the CMDS, which marks early rift stages of the Potiguar basin. The dykes are essentially tholeiitic and vertically cross cut the Precambrian basement exposed along the southern border of the Portiguar basin (Fig. 3.1c). The swarm is composed by at least 100 dykes of one- to 150-meters in width and of up to one kilometer in length; a few dykes exceeding 100 kilometers have been reported in aeromagnetic survey (Oliveira, 1992). The dykes show E-W and NE-SW trends in the southern and western areas of the Potiguar basin, respectively. The arcuate orientation of the CMDS is suggestive of NW-SE shift in the minimum stress axis at the western part of the swarm (Oliveira, 1992).

Geochronological studies on the CMDS have only been supported by K-Ar determinations. They show that the dykes were emplaced over a wide age interval between 145 and 125 Ma (see compilation of Misusaki et al., 2002). Such an interval is consistent with paleomagnetic studies (Bellieni et al. 1992), which have shown that most of the dykes record magnetization directions acquired during the Cretaceous. A small collection of the E-W dykes show poles compatible with the Middle Jurassic, which were apparently validated by Bellieni et al. (1992) based on K-Ar ages (179–161 Ma). Even when considering misinterpretations related to K-Ar method, which is unable to recognize Ar loss or excess components, the ages available for the CMDS show a strong correlation with those from tholeiitic basalts of the Northern Benue Trough in West Africa, which provided $^{40}\text{Ar}/^{39}\text{Ar}$ ages in the range of 147 and 123 Ma (Maluski et al., 1995). Mesozoic magmatic products in the Benue Trough and Cenozoic to Recent volcanism found along the Cameroon Line (e.g., Marzoli et al., 2000) have been interpreted as a continuing result of a complex and long-lived interaction between a deep mantle plume (St. Helena HIMU-type) and enriched sub-continental lithospheric and depleted (N-MORB) asthenospheric mantle sources during the opening of the Equatorial Atlantic (e.g., Coulon et al., 1996).

3.3 ANALYTICAL PROCEDURES

Detailed geochronological study to discuss about the emplacement age of the CMDS fall beyond the scope of this paper. However, to effectively constrain a precise age for dyke emplacement to recalculate the initial isotopic compositions discussed here we present an (up to now) unpublished $^{40}\text{Ar}/^{39}\text{Ar}$ dating of one representative tholeiite (sample CM-12) performed in 2001 at the Geochronological Research Center of the University of São Paulo (Brazil). Clear and fresh plagioclase grains (35–60 mesh) were separated from the rock and were irradiated under

the IPEN/CNEN IEA-R1 nuclear reactor. The grains were then loaded into multigrain aliquots and analyzed using laser incremental-heating techniques. Instrumentation, operational condition and correction information can be found in Vasconcelos et al. (2000). Data are listed in Table 3.1.

Table 3.1. $^{40}\text{Ar}/^{39}\text{Ar}$ data obtained for the tholeiite CM-12

Run ID#	Laser (W)	$^{40}\text{Ar}/^{39}\text{Ar}$	$^{38}\text{Ar}/^{39}\text{Ar}$	$^{37}\text{Ar}/^{39}\text{Ar}$	$^{36}\text{Ar}/^{39}\text{Ar}$	$^{40}\text{Ar}*/^{39}\text{Ar}$	^{40}Ar (nA)	^{40}Ar (moles)	% $^{40}\text{Ar}_{\text{rad}}$	Age (Ma)	\pm
0480-01A	0.3	279.19	0.1678	3.7608	0.7973	44.14	1.75	3.40E-14	15.7	266.84	25.29
0480-01B	0.5	34.59	0.0160	2.9178	0.0470	21.02	0.18	3.49E-15	60.5	131.97	3.77
0480-01C	0.8	38.19	0.0269	2.7314	0.0594	20.93	0.16	3.08E-15	54.6	131.47	4.84
0480-01D	1.1	52.41	0.0300	3.0378	0.1170	18.16	0.17	3.18E-15	34.5	114.59	7.95
0480-01E	1.4	52.13	0.0286	3.1906	0.1119	19.39	0.21	3.98E-15	37.0	122.10	5.12
0480-01F	1.7	58.57	0.0362	3.5967	0.1219	22.93	0.13	2.47E-15	38.9	143.54	9.34
0480-01G	2.0	52.66	0.0368	3.2721	0.1351	13.06	0.12	2.26E-15	24.7	83.11	9.88
0480-01H	2.4	50.30	0.0200	4.0275	0.0989	21.51	0.11	2.02E-15	42.5	134.94	9.91
0480-01I	2.8	59.06	0.0311	4.7115	0.1312	20.79	0.17	3.33E-15	35.0	130.62	8.98
0480-01J	5.0	68.07	0.0359	5.8051	0.1818	14.93	0.13	2.45E-15	21.7	94.71	15.72
0480-02A	0.4	561.98	0.3796	1.0309	1.9356	-9.93	0.66	1.23E-14	-1.8	-65.88	171.33
0480-02B	0.8	300.90	0.1810	5.2976	0.9442	22.47	1.24	2.35E-14	7.4	140.74	26.35
0480-02C	1.4	76.97	0.0426	4.2144	0.1876	22.00	0.45	8.70E-15	28.4	137.91	6.77
0480-02D	2.0	35.40	0.0255	1.7347	0.0693	15.09	0.18	3.32E-15	42.5	95.70	5.55
0480-02E	2.6	36.93	0.0038	2.1611	0.0520	21.81	0.08	1.51E-15	58.9	136.75	6.88
0480-02F	3.5	36.72	0.0155	1.8318	0.0672	17.05	0.10	1.98E-15	46.3	107.81	6.32
0480-02G	4.2	48.64	0.0166	2.2944	0.0912	21.95	0.11	2.15E-15	45	137.60	9.51
0480-02H	5.0	61.88	0.0283	4.6040	0.1406	20.84	1.11	2.13E-14	33.4	130.88	2.78
0480-03A	0.4	119.45	0.0907	0.3641	0.3732	9.20	0.33	6.31E-15	7.7	58.96	23.01
0480-03B	0.8	69.09	0.0494	0.4704	0.2009	9.77	0.66	1.27E-14	14.1	62.55	6.34
0480-03C	1.4	39.67	0.0225	0.8300	0.0655	20.40	0.53	9.88E-15	51.4	128.25	3.47
0480-03D	2.0	27.01	0.0150	0.6636	0.0221	20.54	0.28	5.21E-15	76.0	129.11	1.77
0480-03E	2.6	25.90	0.0126	0.5244	0.0162	21.18	0.19	3.60E-15	81.7	132.93	2.56
0480-03F	3.5	25.60	0.0127	0.4438	0.0185	20.18	0.21	3.99E-15	78.8	126.88	1.24
0480-03G	4.2	28.04	0.0166	0.5094	0.0282	19.77	0.18	3.30E-15	70.4	124.39	1.75
0480-03H	5.0	36.48	0.0202	1.2579	0.0565	19.93	1.82	3.46E-14	54.5	125.36	1.84

Irradiation ID: SPA0101-25, Date: October 7th, 2001.

J = 0.00361000 ± 0.00000166

Over 90 samples representative of the CMDS were available for this study, and some of them have been examined for their structural, geochemical and isotopic characteristics in Archanjo et al. (2000, 2002) and Hollanda et al. (2006). Thin sections were used to investigate petrography features using a conventional optical microscope, and 20 were examined for chemistry data on major mineral contents using electron microprobe techniques at the Institute of Geosciences (University of Brasilia, Brazil) and at the Federal University of Rio de Janeiro (Brazil). In the former experiment, mineral chemistry analyses were performed on a JEOL JXA 8600 Superprobe while applying an accelerating voltage of 15 KeV and a beam current of 10 nA, whereas in the Rio de Janeiro lab analyses were carried out on a JXA 8230 Superprobe applying

a voltage of 15 KeV for the analysis of olivine, pyroxene and plagioclase and of 20 KeV for oxides, and a beam current of 20 nA. Corrections of matrix effects and data reduction tasks were routinely conducted using PROZA systematic (Bastin and Heijligers, 1990). Descriptions of the mineral chemical analyses are presented in Appendix A.1.

Fifty-six representative samples were used to support our interpretations on elemental geochemistry features, of which 13 were earlier reported on in Holland et al. (2006). The complete geochemical results found in the present study are listed in Table 3.2. Major and trace (including rare earth) element data obtained through this study were collected from ACME Analytical Laboratories Ltd, Canada. Analytical procedures involved LiBO₂ fusion followed by X-ray fluorescence (for major oxides and LOI, plus Ba) and dilute acid digestion followed by ICP-MS analysis for minor and rare earth elements, corresponding with a combination of 4X4B commercial package codes. Metals and total Pb levels were also determined by ICP-MS following aqua regia digestion as required for the package code 1DX. Otherwise, most Sr, Nd and Pb isotope compositions presented in this paper were also previously presented in Holland et al. (2006) (Table 3.3), while six of the analyses are original and were performed at the Geochronological Research Center of the University of São Paulo (Brazil).

For the Sr, Nd and Pb isotopic analyses, approximately 100 mg of whole-rock powder was dissolved into Savillex® beakers via sub-boiling purified HF:HNO₃ acid digestion and was then refluxed in 6 M HCl for fluoride removal. Sr and rare earth elements were collected from the matrix solution using Eichrom Sr-Spec® resin eluted with 0.05 M HNO₃ and a combination of two sets of ion-exchange columns packed with RE-Spec® (for rare earth elements) and LN-Spec® resins (for Sm and Nd). Nd and Sm elements were collected using 0.26 M and 0.55 M HCl, respectively. Natural isotopic compositions were measured by thermal ionization mass spectrometry (TIMS) in a multicollector Thermo Scientific Triton machine set in dynamic mode. The Sr and Nd isotope ratios were mass fractionated and normalized to ⁸⁶Sr/⁸⁸Sr = 0.1194 and ¹⁴⁶Nd/¹⁴⁴Nd = 0.7219, respectively. Measurements of the NBS-987 and JNd-1 standards made during the period of analysis yielded natural ⁸⁷Sr/⁸⁶Sr = 0.710248±0.000039 and ¹⁴³Nd/¹⁴⁴Nd = 0.512101±0.000006 values at 2σ level, while total procedure blanks were recorded at 640 (Sr) and 120 (Nd) pg. ⁸⁷Rb/⁸⁶Sr and ¹⁴⁷Sm/¹⁴⁴Nd ratios were determined from Rb, Sr, Sm and Nd concentrations obtained via ICP-MS.

Finally, an aliquot of the matrix solution was loaded into a Biorad AG 1-X8® (200-400#) anion exchange column for Pb extraction. The matrix was eluted using 0.7 M HBr and Pb collected in 6 M HCl over successive stages. Total blanks were in the range of 50-100 pg. Pb-isotope ratios were acquired in static mode on a seven-collector Finnigan MAT-262 TIMS

spectrometer. Mass fractionation was corrected for 0.095% a.m.u. NBS-981 standard measurements yielded average values of $^{206}\text{Pb}/^{204}\text{Pb} = 16.898 \pm 0.007$, $^{207}\text{Pb}/^{204}\text{Pb} = 15.439 \pm 0.009$ and $^{208}\text{Pb}/^{204}\text{Pb} = 36.535 \pm 0.029$ (2σ ; $n = 60$).

3.4 RESULTS

3.4.1 $^{40}\text{Ar}/^{39}\text{Ar}$ GEOCHRONOLOGY

Three plagioclase multigrain aliquots extracted from the tholeiite CM-12 were dated, but one (#0480-02) failed to provide a reliable age, and thus its heating spectra are not shown in Figure 3.2. The other two aliquots yielded concordant ages, with one resulting from a plateau of 127.1 ± 1.3 Ma defined with ~90% of the total $^{39}\text{Ar}_K$ released (#0480-03). The other (#0480-01) provided a heating spectrum that remained mildly disturbed by $^{39}\text{Ar}_K$ recoil loss at lower temperatures. However, although more imprecise, a plateau age of 129 ± 4 Ma calculated from ~80% of the total $^{39}\text{Ar}_K$ released is comparable to the former. Combined plateau steps of the two multigrain aliquots yielded a mean weighted age of 126.9 ± 4 Ma, which we consider to be the best estimate of tholeiite CM-12 age.

3.4.2 PETROGRAPHY AND MINERAL CHEMISTRY

Rocks constituting the CMDS are doleritic basalts that assemble modal Ca-plagioclase+pyroxene+opaque minerals±olivine. Depending on dyke widths, textures vary from fine-grained at the chilled margins to mid-grained in the central zones, with intergranular and, occasionally, intersertal arrangements present. Some display plagioclase-pyroxene-(±olivine)-

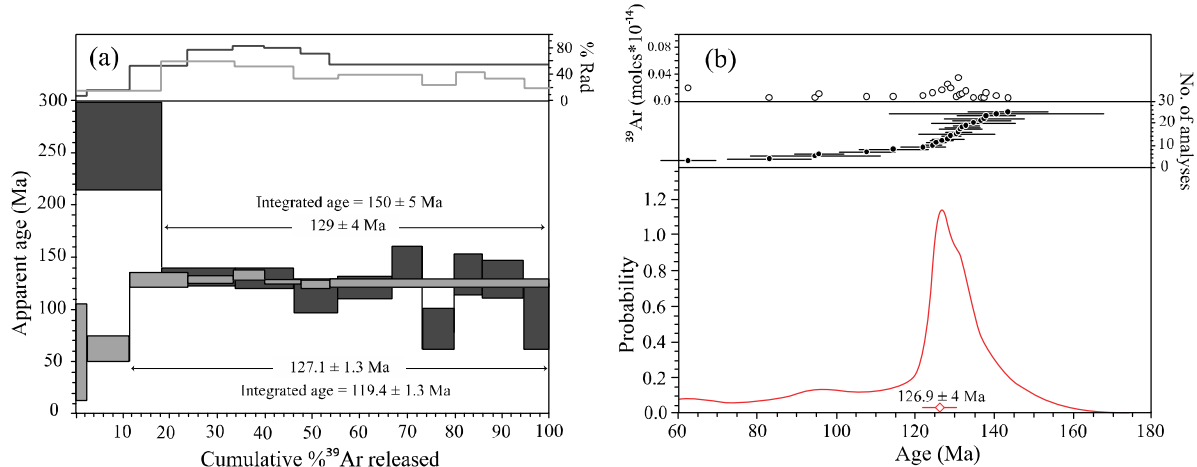


Figure 3.2. (a) $^{40}\text{Ar}/^{39}\text{Ar}$ step-heating diagram for two multigrain replicates (#0480-01 and -03) of the tholeiite CM-12. The error boxes of each step are given at the 1σ level, while errors for the plateau and integrated ages are shown at the 2σ level. (b) Age-probability curve presenting a mean age of 126.9 ± 4 Ma

after the combination of the plateau steps defined in (a).

phyric textures. Phenocryst abundances range from 20 to 30% vol. When dyke widths exceed 10 meters, mineral assemblages exhibit a coarse-grained gabbroic texture. Olivine constitutes a phenocryst phase (up to 5 mm) in ~15% of the dykes (those cropping out from the southern section of the main swarm), occasionally enclosing smaller laths of plagioclase and providing the rock with sub-ophitic and poikilitic textures. Seriate-textured dykes are rare. Fe-Ti oxides (3–4% vol.) include magnetite and ilmenite of symplectic intergrowth exsolution textures (titano-magnetite); some rare ilmenite co-exists in the groundmass in needle-like and skeletal forms, especially in the gabbroic dykes.

The CMDS has long been considered to be tholeiitic in composition (Bellieni et al., 1992; Hollanda et al., 2006). Here, we first grouped the dykes into olivine tholeiites for those containing modal olivine (with the exception of pyroxene and plagioclase) and into tholeiites for those devoid of modal olivine. A more accurate classification based on geochemical features is presented below.

A representative mineral assemblage of the olivine tholeiites includes 45:20:30:5% vol. of plagioclase: pyroxene:olivine:opaque (Fe-Ti) oxides. Clinopyroxene and plagioclase are found either as phenocryst and/or groundmass phases, while olivine is only found as phenocryst, and Fe-Ti minerals form the fine-grained matrix. Anorthite (An) compositions in plagioclase are composed of labradorite to andesine (An_{62-46}) in normally zoned phenocrysts and of dominantly andesine (An_{54-40}) in microlitic laths of the matrix. Microprobe analyses show that olivine phenocryst compositions are unimodal with forsterite content from the center (Fo_{69-55}) to the late-stage rims ($Fo_{66-55.5}$), although one of the phenocryst grains is more Mg-rich with $Fo_{81.5-76}$. Pyroxene microphenocrysts are diopsidic ($Wo_{45.9}En_{40.4}Fs_{13.7}$; Fig. 3.3a) to sub-calcic augite in the groundmass ($Wo_{37.7}En_{46}Fs_{16.2}$; Fig. 3.3b) together with rare pigeonite (according to one analysis shown in Appendix A.1).

For most of the tholeiitic dykes, the common modal assemblage is 55:35:10 (% vol.) of plagioclase:pyroxene:Fe-Ti minerals. Anorthite compositions in plagioclase are 62–29% An, though albite ($An_{3.8-11.1}$) was detected along the rims of some laths in sample CM-02. In the Ca-Mg-Fe diagram of Figure 3.3c a set of analysis plots at the 45 mol.% Ca threshold with compositions of diopside ($Wo_{46.1-45.2}En_{39.1-36.8}Fs_{13.4-16.1}$) and sub-calcic augite ($Wo_{46.1-45.2}En_{39.1-36.8}Fs_{13.4-16.1}$) as those presented in the olivine tholeiites. The microphenocrysts are mainly augite, occasionally exhibiting Fe enrichment along the rims. Pigeonite serves as a dominant phase in the coarse groundmass (Fig. 3.3d).

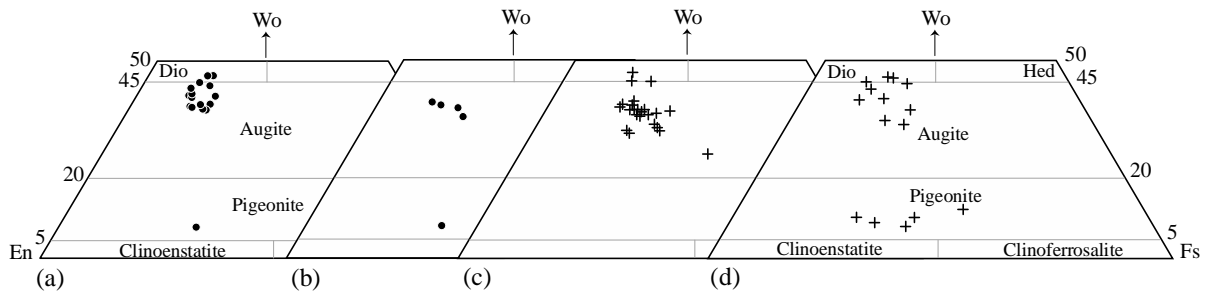


Figure 3.3. Ca-Mg-Fe ternary plot used for the classification of pyroxenes analyzed for the CMDS tholeiites. Pyroxenes occur as: (a) microphenocrysts and (b) coarse-grained matrixes in the olivine tholeiites and as (c) – (d) microphenocrysts and coarse-grained matrixes in the tholeiites.

3.4.3 MAJOR AND TRACE ELEMENT COMPOSITIONS

Major and minor element compositions are listed in Table 3.2. In the TAS diagram (Fig. 3.4a) all CMDS samples are basaltic (basalts-trachybasalts-andesites), though two samples show silica contents that are more highly evolved towards andesitic compositions. All are tholeiitic according to Miyashiro's (1979) diagram (Fig. 3.4b). From the normative compositions, three groups were identified. The group with modal olivine (olivine tholeiites) shows normative quartz values of 0–2, whereas another shows higher values of 8–15, and the other shows relatively moderate values of 7–9. The most basic sample in our dataset is DCO-125 with MgO of 10.2 wt.% and silica content of 47.5 wt.%. This is the only sample that is hypersthene+olivine normative. All of the other samples are hypersthene+quartz normative.

The chemical classification proposed here uses the Ti-P-Zr triad to define continental tholeiites, for which a bound of 2 wt.% TiO₂ is used as the main geochemical criterion for subdivision into low-Ti and high-Ti magmas (Bellieni et al., 1984; Fodor et al., 1985, 1990; Mantovani et al., 1985; Peate et al., 1992; Peate and Hawkesworth, 1996; Ewart et al., 1998; Marques et al., 1999; De Min et al., 2003; Jourdan et al. 2007). As such a value is arbitrary according to Peate et al. (1992), we use a value of 1.5 wt.% as a more appropriate measure for our dataset, and this value is used together with a Ti/Y ratio of ~360. Such a ratio serves as a more robust qualifier for fractionated magmas than the TiO₂-wt.% as noted in Peate et al. (1992). The also arbitrary value of 360 is used here to distinguish between high and low-Ti tholeiites of the CMDS in corresponding with the value of 310 defined by these authors in relation to the Paraná flood basalts. Relative abundances of SiO₂ and MgO and ratios of incompatible elements are assessed as diagnostic criteria for further discussion on the petrogenesis processes.

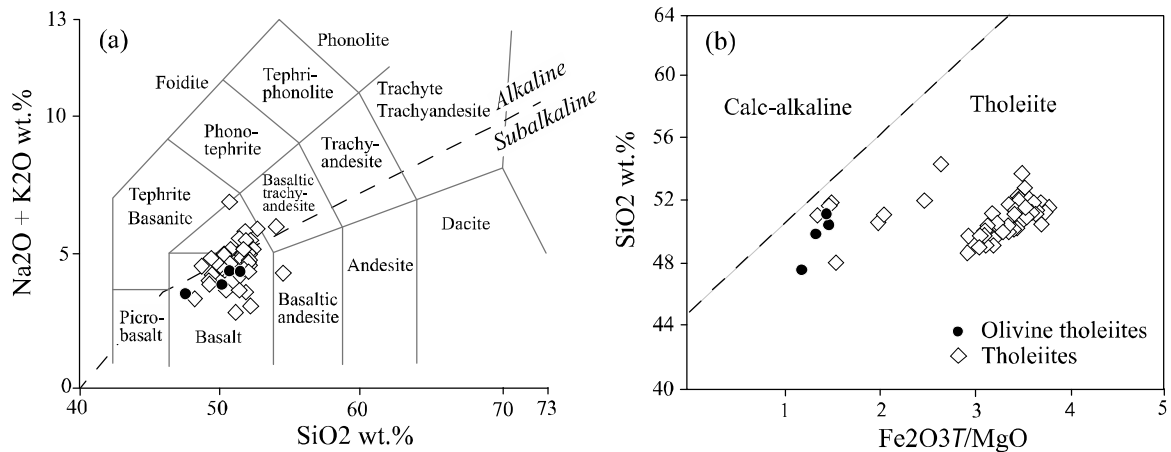


Figure 3.4. Major element classification for the CMDS tholeiites based on (a) TAS and (b) SiO₂ versus Fe₂O_{3T}/MgO diagrams.

From our dataset, two olivine tholeiites present loss of ignition (LOI) values of >2.5 wt.%, and these are not considered in our comments. A plot of MgO versus TiO₂ wt.% (Fig. 3.5a) shows that the olivine tholeiites and most of the tholeiites are high in TiO₂ thus closely matching Pitanga and Paranapanema compositions of the Paraná province, with olivine tholeiites exhibiting higher MgO content levels. Six samples show low-Ti composition plotting in the same field as low-Ti magmas of the CAMP-Maranhão and Paraná provinces. Such patterns are also observed in the Ti/Y–Ti/Zr diagram (Fig. 3.5b), thus allowing us to subdivide the CMDS tholeiites into three well-defined groups. When examining the distribution of the high-Ti tholeiite samples, we found a sharp gap of 7.3–5.0 wt.% in MgO content leading us to subdivide them into high-Ti olivine tholeiite (MgO >7.3 wt.%) and evolved high-Ti tholeiite (3.5< MgO<5.0 wt.%) groups as proposed for the CAMP-Maranhão tholeiites (Merle et al., 2011). However, such a decrease in MgO content does not correlate with increasing silica content, suggesting that the two groups were likely not derived through the fractionation of the same parental magma. In applying other geochemical criteria proposed by Peate et al. (1992) to differentiate between high-Ti magma types of the Paraná flood basalts, we observe that Fe₂O₃, P₂O₅, Sr and Zr (and other large ion lithophile (LIL) and high field strength (HFS) elements) can also be used to distinguish between the two high-Ti groups of the CMDS, with evolved high-Ti tholeiites exhibiting higher Fe and P oxide levels and being more enriched with Zr, Sr, Ba and Rb. Thus, the evolved high-Ti tholeiites may be defined as high-Ti-P-Zr (HTPZ) magmas, while the olivine tholeiites may be defined as high-Ti-P magmas with low-Zr.

		Localization	SiO ₂	Al ₂ O ₃	Fe ₂ O _{3T}	MnO	MgO	CaO	Na ₂ O	K ₂ O	TiO ₂	P ₂ O ₅	LOI	SUM
Geochemical group	Sample name	(UTM coordinate)	Major elements wt.%											
<i>Evolved high-Ti tholeiites</i>														
	DCO-60	395.95/9262.43	53.9	16.12	10.37	0.16	2.86	7.07	3.87	2.08	2.33	0.66	1.61	101.1
	DCO-71	822.54/9364.58	50.6	16.39	9.59	0.12	4.59	7.34	4.85	1.98	2.66	0.50	1.92	100.6
	DCO-72	806.66/9368.53	51.7	13.47	13.76	0.19	3.97	6.28	3.65	2.14	2.89	0.53	1.74	100.4
	DCO-83		51.3	12.43	15.58	0.20	4.40	7.60	2.59	1.72	3.48	0.45	###	####
	DCO-132	799.65/9316.98	51.3	12.48	15.17	0.20	4.06	7.03	2.80	2.11	3.31	0.49	1.62	100.4
	DCO-133	783.37/9319.25	51.5	12.80	14.76	0.21	3.81	7.17	2.93	2.02	3.17	0.53	1.43	100.4
	DCO-134	786.41/9319.36	51.1	12.85	15.31	0.21	4.12	7.49	2.85	1.77	3.41	0.50	0.85	100.6
	DCO-138	768.85/9320.35	51.6	12.69	15.15	0.22	3.88	7.23	2.90	1.97	3.32	0.53	0.69	100.3
	DKFL-02		51.2	12.68	15.19	0.20	4.08	7.20	2.74	1.73	3.25	0.54	1.50	100.4
	DKJU		51.4	12.66	15.31	0.20	4.05	7.02	2.85	1.95	3.38	0.51	1.03	100.4
	DKSV-1		51.4	12.68	15.29	0.19	3.95	7.09	2.83	1.74	3.34	0.52	1.14	100.3
	HD-27	250.74/9414.83	49.4	12.02	15.65	0.20	4.77	7.71	2.73	1.58	3.95	0.40	1.28	99.7
	HD-28		52.2	12.69	13.78	0.21	3.86	7.13	3.04	2.12	3.10	0.78	1.10	100.1
	HD-32A	216.44/9369.33	52.1	12.75	13.05	0.20	3.64	6.48	3.31	2.21	2.85	0.80	1.81	99.2
	HD-32B	216.44/9369.33	52.0	12.74	13.84	0.20	3.76	7.13	3.01	2.00	3.07	0.78	1.24	99.9
	Average (n = 46)		50.9	12.85	14.45	0.20	4.20	7.30	2.98	1.83	3.31	0.53	1.37	
	Standard deviation (SD)		1.2	0.82	1.33	0.02	0.45	0.47	0.43	0.26	0.39	0.11	0.48	
	SD %		2.4	6.4	9.2	8.6	10.6	6.4	14.3	14.4	11.8	20.9	35.3	
<i>Low-Ti tholeiites</i>														
	DCO-03	580.85/9379.85	52.1	14.40	11.21	0.18	7.03	10.58	2.33	0.75	1.18	0.16	0.55	100.5
	DCO-04	587.47/9359.94	52.0	13.79	13.28	0.20	4.93	8.35	2.90	1.40	1.53	0.21	1.46	100.1
	DCO-06	808.01/9381.38	51.8	14.38	11.11	0.18	7.15	10.13	2.59	0.97	1.17	0.15	0.70	100.4
	DCO-08	572.01/9398.65	51.3	15.38	11.56	0.19	5.41	9.50	2.64	0.98	1.22	0.16	1.15	99.5
	DCO-14	502.22/9387.64	51.1	13.93	10.71	0.17	7.47	10.63	2.24	0.63	1.10	0.12	0.96	99.1
	DCO-27	698.24/9368.54	48.2	16.12	12.93	0.18	7.95	10.33	2.90	0.42	0.89	0.09	0.66	100.7
	Average (n = 6)		51.1	14.67	11.80	0.18	6.66	9.92	2.60	0.86	1.18	0.15	0.91	
	Standard deviation (SD)		1.3	0.83	0.96	0.01	1.10	0.80	0.25	0.31	0.19	0.04	0.32	
	SD %		2.6	5.6	8.1	5.2	16.5	8.0	9.7	36.0	16.0	24.8	34.7	

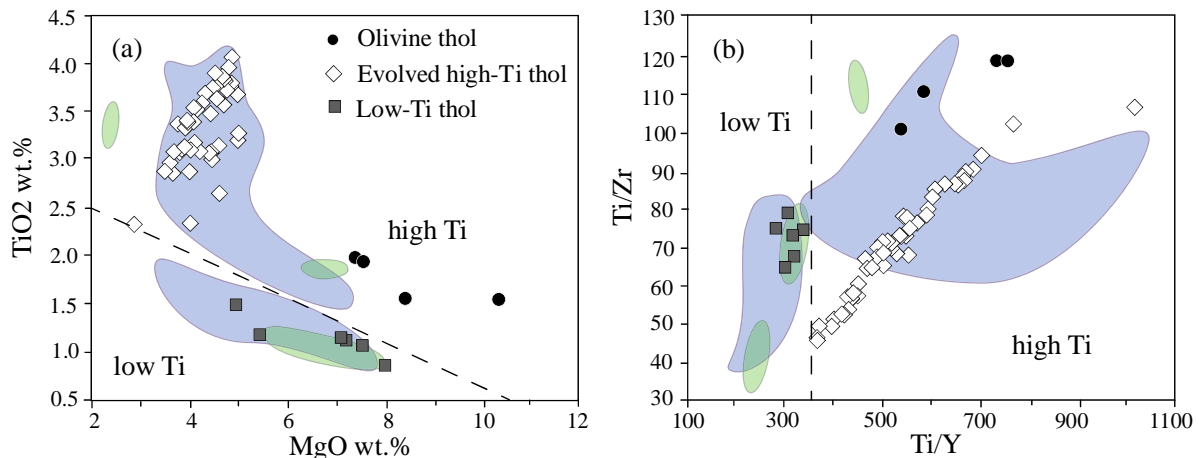


Figure 3.5. (a) Mg versus Ti oxides and (b) Ti/Y versus Ti/Zr plots for discrimination between high- and low-Ti magmas. Fields for both high-Ti and low-Ti suites of the Paraná (blue) and CAMP-Maranhão (green) provinces are shown for purposes of comparison; for Paraná, we do not discriminate between the distinct high-Ti and low-Ti magma types. Sources used include the following: Peate (1997), Merle et al. (2011) and Rocha-Júnior et al. (2013).

From major oxides shown in the MgO plots, each of the three groups shows patterns compatible with slight or moderate degrees of fractional crystallization (Fig. 3.6). SiO_2 , Na_2O and P_2O_5 (and K_2O , to a minor extent) increase with decreasing MgO levels in all groups, while CaO (and in part Fe_2O_3) and $\text{Al}_2\text{O}_3/\text{CaO}$ ratios decrease, indicating that pyroxene and plagioclase served as major fractionating phases. Oxide minerals may have served as either fractionating or accumulating phases depending on whether Fe and Ti decreased against MgO or not.

Chondrite-normalized REE patterns are shown as average patterns in Figure 3.7a. All of the analyzed samples are several times richer in light rare earth elements than the chondritic average composition. The low-Ti tholeiites present a very slight Eu negative anomaly denoting minor plagioclase precipitation, while the olivine tholeiites show discrete plagioclase accumulation patterns. All of the groups show nearly flat patterns in heavy rare earth elements ($\text{Dy}/\text{Yb}_N = 1.3 - 1.7$), highlighting sparse residual garnet in their sources. All primitive mantle-normalized incompatibility profiles of the three groups look similar with the exception of distinct degrees of enrichment observed for the evolved high-Ti tholeiites and of a positive spike in Nb observed in the olivine tholeiites rather than depletion patterns seen in the other groups (Fig. 3.7b). While the evolved high-Ti tholeiite pattern resembles the average OIB as indicated by the fitting in high field strength element abundances and Pb negative anomalies, no correspondence is found regarding Nb behaviors. For these tholeiites, Nb-Ta depletion is moderate and becomes more pronounced in the low-Ti tholeiites. By contrast, the olivine tholeiites show Nb-Ta abundances that are similar to those of OIB magmas, with their average incompatible element compositions matching those of E-MORB magmas.

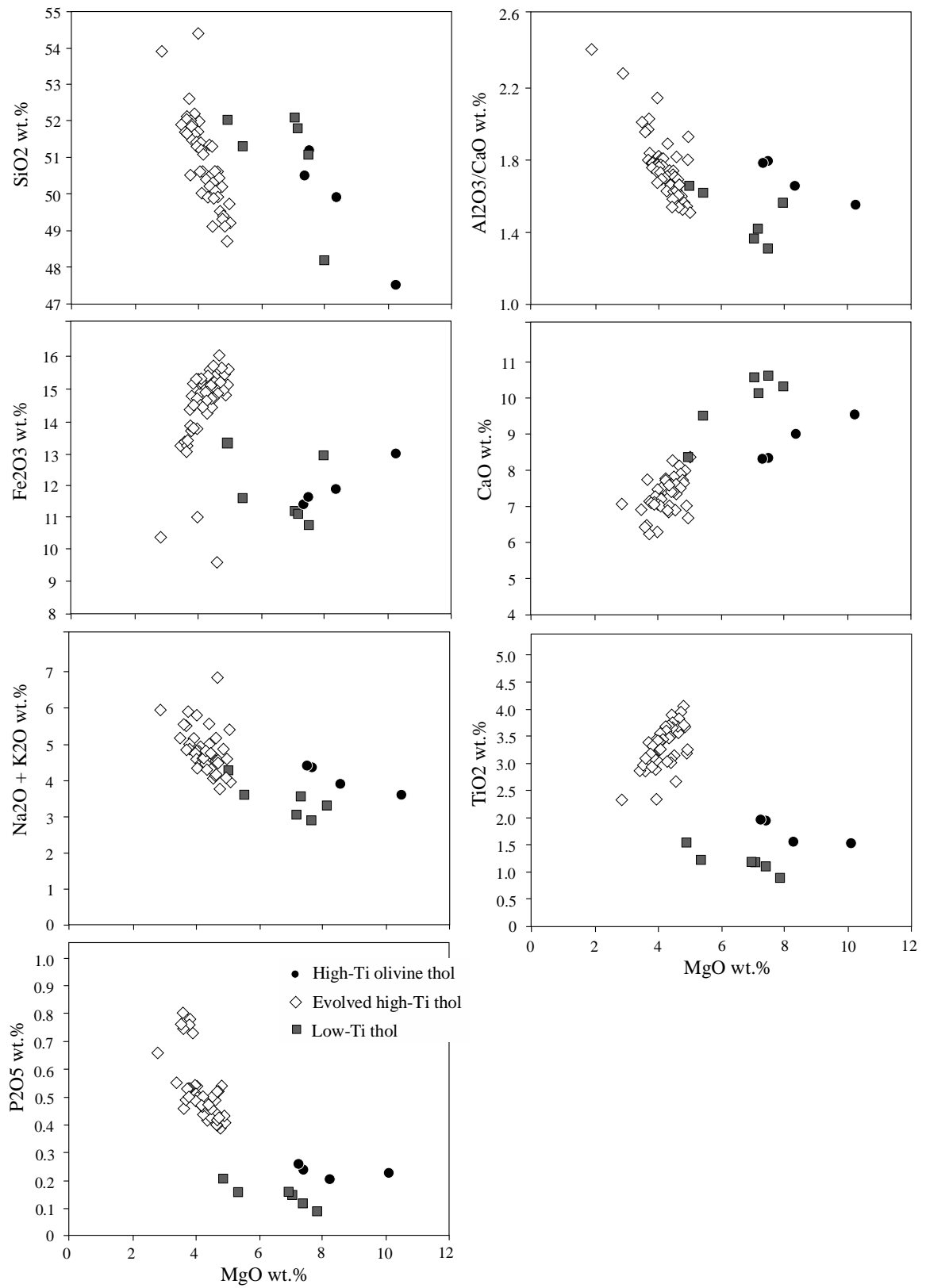


Figure 3.6. Variation diagrams of major elements against MgO.

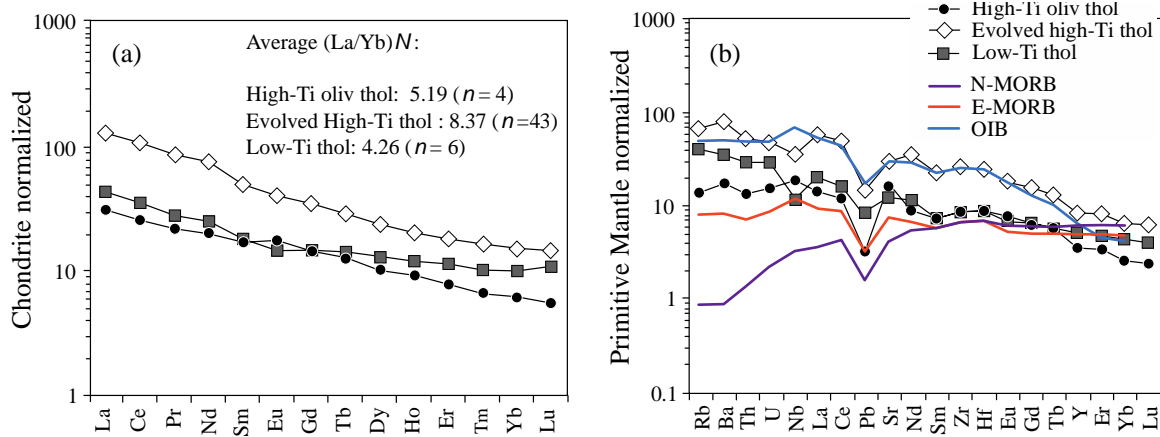


Figure 3.7. Profiles for average abundances of (a) chondrite-normalized REE and (b) PM-normalized incompatible element patterns. Comparison are made between OIB, N- and E-MORB average compositions presented by Sun and McDonough (1989). Normalization parameters are drawn from (a) Boynton (1984) and (b) Sun and McDonough (1989). N denotes the number of samples analyzed and considered in average patterns of each tholeiite group.

3.4.4 SR-Nd-Pb ISOTOPIC COMPOSITIONS

Most of the Sr-Nd-Pb isotopic compositions discussed here were previously reported on in Holland et al. (2006). They are reproduced in Table 3.3 in italics together with new results obtained for the olivine and low-Ti tholeiites (three samples for each group). We also include new Pb isotopic compositions obtained for the evolved high-Ti (DCO-17, -25, -71, -83) and low-Ti (DCO-08, -14) tholeiites, some of which also previously studied for Sr-Nd systematics by the same authors. Samples that were omitted owing to their higher LOI values were also not considered for isotopic modeling. For the same reason, we did not examine some of the isotopic compositions presented by Holland et al. (2006). To allow for uniform comparisons between the samples, all isotopic parent/daughter ratios were (re)calculated using concentrations obtained in this study by LA-ICPMS (listed in Table 3.2), while all initial radiogenic ratios were calculated to the $^{40}\text{Ar}/^{39}\text{Ar}$ age of 127 Ma. We note that even when using a time span of roughly 15 m.y. for the emplacement of the CMDS as suggested by the published K-Ar ages, the shift in the initial isotope ratios is negligible for Sr and Nd and for $^{207}\text{Pb}/^{204}\text{Pb}$ and $^{208}\text{Pb}/^{204}\text{Pb}$ ratios. For $^{206}\text{Pb}/^{204}\text{Pb}$, the deviation should be <1%, which would not change our interpretation of the CMDS petrogenesis.

When the Sr-Nd radiogenic ratios are plotted on a binary diagram, the CMDS tholeiites spread towards variable Sr combined with chondritic to unradiogenic Nd isotopic compositions

Table 3. Sr, Nd and Pb isotopic compositions of the CMDS tholeiites.

Sample name	$^{87}\text{Sr}/^{86}\text{Sr}$	$^{143}\text{Nd}/^{144}\text{Nd}$	$^{206}\text{Pb}/^{204}\text{Pb}$	$^{207}\text{Pb}/^{204}\text{Pb}$	$^{208}\text{Pb}/^{204}\text{Pb}$	$^{87}\text{Rb}/^{86}\text{Sr}$	$^{147}\text{Sm}/^{144}\text{Nd}$	$^{87}\text{Sr}/^{86}\text{Sr}$	$^{143}\text{Nd}/^{144}\text{Nd}$	$\varepsilon(\text{Nd})$	$^{206}\text{Pb}/^{204}\text{Pb}$	$^{207}\text{Pb}/^{204}\text{Pb}$	$^{208}\text{Pb}/^{204}\text{Pb}$	
	measured (<i>t</i> = 0) isotopic ratios					calculated isotopic ratios			calculated (<i>t</i> = 127 Ma) isotopic ratios					
<i>Olivine tholeiites</i>														
DCO-125	0.70348	0.512646	18.406	15.548	38.160	0.0521	0.1545	0.70339	0.512518	0.84	17.987	15.528	37.680	
DCO-136	0.70365	0.512837	19.100	15.645	38.873	0.0672	0.1655	0.70353	0.512699	4.36	18.244	15.603	37.473	
DCO-137	0.70377	0.512769	19.954	15.821	39.904	0.0865	0.1597	0.70361	0.512636	3.16	19.130	15.781	39.148	
DKTt-01	0.70388	0.512105	20.128	15.846	39.934	0.0834	0.1851	0.70373	0.511951	-10.40	19.246	15.803	38.924	
<i>Evolved high-Ti tholeiites</i>														
DCO-02	0.70425	0.512266	18.315	15.593	38.592	0.1443	0.1372	0.70399	0.512152	-6.29	17.753	15.566	37.788	
DCO-17	0.70624	0.512421	18.292	15.572	38.538	0.1961	0.1438	0.70589	0.512301	-3.38	17.535	15.535	37.326	
DCO-25	0.70511	0.512234	18.276	15.572	38.546	0.2540	0.1340	0.70465	0.512123	-6.87	17.944	15.556	38.090	
DCO-26	0.70426	0.512277	18.317	15.588	38.573	0.1757	0.1307	0.70394	0.512168	-5.97	17.719	15.559	37.767	
DCO-29	0.70533	0.512241	18.332	15.594	38.780	0.2164	0.1183	0.70494	0.512143	-6.48	18.040	15.580	38.355	
DCO-60	0.70677	0.512368	18.775	15.634	39.043	0.1535	0.1271	0.70644	0.512262	-4.14	17.860	15.590	37.516	
DCO-71	0.70512	0.512172	17.560	15.389	37.976	0.0782	0.1509	0.70498	0.512047	-8.35	17.084	15.366	37.446	
DCO-72	0.70682	0.512423	18.352	15.603	38.781	0.2487	0.1314	0.70637	0.512314	-3.14	18.088	15.590	38.357	
DCO-83	0.70570	0.512261	18.243	15.561	38.458	0.2383	0.1315	0.70527	0.512152	-6.30	17.577	15.529	37.560	
HD-27	0.70399	0.512493	18.338	15.609	38.646	0.1886	0.1410	0.70365	0.512376	-1.93	17.743	15.580	37.817	
HD-28	0.70607	0.512463	18.263	15.565	38.583	0.2206	0.1287	0.70567	0.512356	-2.31	17.395	15.523	37.292	
HD-32B	0.70456	0.512445	18.283	15.586	38.582	0.1467	0.1277	0.70430	0.512339	-2.65	17.797	15.562	37.834	
<i>Low-Ti tholeiites</i>														
DCO-03	0.70652	0.512494	18.616	15.642	38.713	0.2475	0.1372	0.70607	0.512380	-1.84	18.167	15.620	38.174	
DCO-04	0.71194	0.512349	18.941	15.697	39.133	0.4687	0.1466	0.71109	0.512227	-4.83	17.999	15.651	37.983	
DCO-06	0.70453	0.512555	18.629	15.653	38.720	0.3279	0.1363	0.70394	0.512442	-0.64	18.408	15.642	38.322	
DCO-08	0.70767	0.512302	18.721	15.688	38.918	0.3275	0.1346	0.70708	0.512190	-5.50	18.234	15.664	38.221	
DCO-14	0.70625	0.512494	18.505	15.615	38.493	0.2499	0.1690	0.70580	0.512354	-2.36	17.999	15.590	37.789	
DCO-27	0.70469	0.512133	18.518	15.582	38.937	0.0853	0.1416	0.70454	0.512015	-8.96	17.563	15.536	37.583	

(Fig. 3.8a). Pb isotopic ratios represent, in turn, high and low values (Fig. 3.8b, c). The olivine tholeiites show nearly consistent initial $^{87}\text{Sr}/^{86}\text{Sr}$ ratios (0.70339–0.70373), but $^{143}\text{Nd}/^{144}\text{Nd}$ ratios that are partly low (sample DKTt-01) and partly chondritic to high (samples DCO-125, -136, -137) values. There is no ideal coupling between their Nd and Pb isotopic compositions, except for that of sample DCO-137, which has initial $^{206}\text{Pb}/^{204}\text{Pb}$ and $^{207}\text{Pb}/^{204}\text{Pb}$ ratios of 19.130 and 15.781, respectively ($\Delta 7/4 = +21.6$; $\Delta 7/4$ is the vertical deviation of $^{207}\text{Pb}/^{204}\text{Pb}$ from the Northern Hemisphere Reference Line, NHRL, as defined by Hart et al., 1984), for $\varepsilon_{\text{Nd}T} = +3.16$. The other depleted Nd value ($\varepsilon_{\text{Nd}T} = +4.39$) comes from the DCO-136 sample, which has a moderate initial $^{206}\text{Pb}/^{204}\text{Pb}$ value (18.244), while sample DKTt-01 has a combination of lowest Nd (0.511951; $\varepsilon_{\text{Nd}T} = -10.4$) and highest $^{206}\text{Pb}/^{204}\text{Pb}$ (19.246) and $^{207}\text{Pb}/^{204}\text{Pb}$ (15.803; $\Delta 7/4 = +22.5$) ratios. Together, these samples fit along a Pb/Pb “errochron” of c. 2.6 Ga (MSWD = 5.7) (Fig. 8b). For DKTt-01, decoupling occurs when its negative $\varepsilon_{\text{Nd}T}$ is associated with a nearly chondritic $^{147}\text{Sm}/^{144}\text{Nd}$ ratio of 0.1851. This cannot be attributed to simple crustal contamination, as its $^{87}\text{Sr}/^{86}\text{Sr}$ ratio of 0.70373 is lower than that of Bulk Silicate Earth (BSE).

The evolved high-Ti tholeiites also show a wide range of isotopic compositions corresponding to unradiogenic Nd isotopic ratios integrated with either lower or higher Sr values (Fig. 8a). Initial $^{87}\text{Sr}/^{86}\text{Sr}$ ratios vary from 0.70365 to 0.70644 and the $^{143}\text{Nd}/^{144}\text{Nd}$ ratios range

between 0.512376 and 0.512047 ($\varepsilon_{\text{NdT}} = -8.35$ to -1.93). Pb isotopic compositions for these tholeiites are low: $^{206}\text{Pb}/^{204}\text{Pb}$ (17.395 to 18.088), $^{207}\text{Pb}/^{204}\text{Pb}$ (15.523 to 15.590) and $^{208}\text{Pb}/^{204}\text{Pb}$

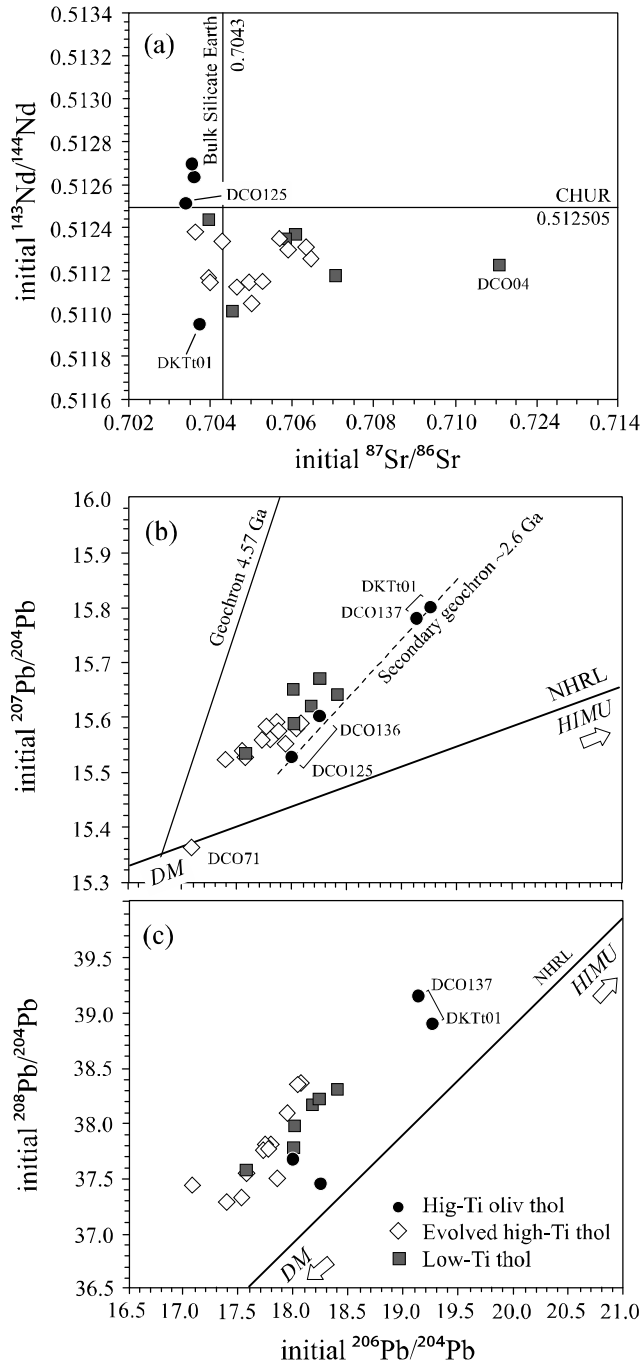


Figure 3.8. Initial (a) $^{87}\text{Sr}/^{86}\text{Sr}$ versus $^{143}\text{Nd}/^{144}\text{Nd}$, (b) $^{206}\text{Pb}/^{204}\text{Pb}$ versus $^{207}\text{Pb}/^{204}\text{Pb}$ and (c) $^{206}\text{Pb}/^{204}\text{Pb}$ versus $^{208}\text{Pb}/^{204}\text{Pb}$ plots showing the distribution of the CMDS isotopic compositions. All ratios are plotted back to 127 Ma.

(37.292 to 38.357). All of these data values fall well above the NHRL with $\Delta 7/4$ values of between +10.8 and +16.5 distributed along a linear trend sub-parallel to it (Fig. 3.8b, c). One evolved high-Ti tholeiite (DCO-71 sample), however, plots near the low Pb endmember of the NHRL. Finally, the low-Ti tholeiites show initial Sr-Nd isotopic compositions that are very

similar to those of evolved high-Ti tholeiites ($^{87}\text{Sr}/^{86}\text{Sr} = 0.70394\text{--}0.70607$; $\varepsilon_{\text{Nd}_T} = -0.64$ to -8.96), but with slightly higher levels of radiogenic Pb ($^{206}\text{Pb}/^{204}\text{Pb} = 17.563$ to 18.408 ; $^{207}\text{Pb}/^{204}\text{Pb} = 15.536$ to 15.651). One exception is the DCO-04 sample, which has the highest $^{87}\text{Sr}/^{86}\text{Sr}$ ratio of 0.71109.

3.5 DISCUSSION ON THE PETROGENETIC PROCESSES

3.5.1 MAGMA GENERATION

Assumptions regarding chemical interaction between lithospheric and asthenospheric mantle sources/melts have been recurrent in discussions on the genesis of continental tholeiitic magmas (e.g., Peate and Hawkesworth, 1996; Jourdan et al., 2007; Price et al., 2014). The rigid lithospheric mantle is presumed to be molten as a result of heat transferred through upwelling thermal anomalies or through physico-chemical interactions with hotter asthenospheric melts. In both cases, the asthenosphere and lithosphere are able to record chemical signatures as consequence of the mixing of melts that form the magmas generated.

The Lindsley (1983) pyroxene geothermometer shows temperatures of between 950° and 1,200°C for magmas crystallizing with augite+pigeonite(\pm clinoenstatite) assemblage, as found for the CMDS tholeiites. Ratios and contents of the major elements (Al, Ti, Mg) estimated for clinopyroxene highlight pressure conditions of the crystallizing magma. Ti/Al > 0.5 in most of the augite crystals of the olivine tholeiites and tholeiites of the CMDS denote that crystallization occurred preferentially at shallow crustal levels. In fact, measured Ca (0.15% < CaO < 0.34%) and Cr (Cr₂O₃ < 0.1 wt%) content levels in the olivines might be taken as chemical qualifiers of the conclusion that crystallization likely occurred primarily under lower pressure conditions and at temperatures of ~1,250°C ($10^{-6} f\text{O}_2$) (based on estimates made according to methods presented by Roeder and Emslie, 1970). However, < 0.25 values of CaO measured in crystals from the same samples corroborate the fact that crystallization began at deeper levels before cooling occurred at lower pressures, and this is supported by the broad variations in Al^{vi}/Al^{iv} ratios observed. According to Sack and Carmichael (1984), both low pressure and temperature levels favor Ti accommodation in pyroxene.

The evolved high-Ti tholeiite group is more enriched in rare earth elements ($\sum \text{REE} = 116\text{--}279$; $(\text{La/Yb})_N \sim 8.4$) depicting a relatively higher melt fraction in garnet lherzolite contributions than in spinel when compared to the olivine ($\sum \text{REE} = 58\text{--}91$; $(\text{La/Yb})_N \sim 5.2$) and low-Ti ($\sum \text{REE} = 64\text{--}115$; $(\text{La/Yb})_N \sim 4.3$) tholeiites. The diagram shown in Figure 9 compares

$(\text{Dy/Yb})_N$ to $(\text{La/Yb})_N$ ratios in modeling magma generation levels while also providing an estimate of melting degrees and fractions (Thirlwall et al., 1994). This relationship allows us to infer that spinel lherzolite melting will result in minimal variations in the Dy/Yb ratio, as garnet, if present, will retain Dy (a heavy-REE) preferentially. Garnet lherzolite melting will generate higher values of Dy/Yb and more significant depletions of heavy-REE. We plotted the studied samples as groups to identify mixing lines between spinel and garnet lherzolite melts. Two mixing lines (one linking the olivine tholeiites and the low-Ti tholeiites and the second defined by the evolved high-Ti tholeiites) converge at $(\text{Dy/Yb})_N = 0.7$ and $(\text{La/Yb})_N = 2.5$, which represents hypothetical values for a spinel lherzolite (lithospheric) source enriched with incompatible elements. The two most basic samples (our use of them is only indicative) of the olivine (DCO-125) and the low-Ti (DCO-27) tholeiites are highlighted as different symbols in Fig. 9. These two groups apparently form an array similar to that of a single suite fitted by a mixing line between melts derived from partial melting of at least 10% of spinel lherzolite and melts derived from ~4% of garnet lherzolite. Both exhibit a melt fraction of 2:3 for spinel and garnet lherzolite, respectively. A fair difference is found between the two groups in terms of their magma segregation depths: ~75 km for the olivine tholeiites and ~60 km for the low-Ti tholeiites, calculated from major element data using Scarrow and Cox's (1995) method for apparent pressures ($P[\text{Kbar}] = 213.6 - 4.05 \text{ SiO}_2$) and Albarède's (1992; $T^\circ\text{C} = 2000 * \text{MgO}/(\text{SiO}_2 + \text{MgO}) + 969$, with $\pm 40^\circ\text{C}$ error margin) method for temperatures. The difference between the two may be attributed to the fact that the low-Ti tholeiites are more evolved. However, according to Chayes (1966), TiO_2 -rich basalts result from high pressure and deep-seated peridotite partial melting while low- TiO_2 basalts are generated from magmas formed at higher levels and at higher partial melting degrees. Prytulak and Elliot (2007) argue that small amounts (generally less than 10%) of recycled oceanic crust in the peridotitic mantle serve as a probable geochemically consistent explanation for the enrichment of TiO_2 in OIB magmas. The presence, therefore, of both low-Ti and high-Ti type basalts in the CMDS may be attributed to mantle heterogeneity. The evolved high-Ti tholeiites in turn exhibit higher La/Yb_N ratios (7–10) that corroborate their higher levels of enrichment in LIL elements. Corresponding parental magma were generated via ~10% partial melting of enriched lithospheric mantle spinel lherzolite with the contribution of <2% of garnet lherzolite in proportion of ~1:2, respectively. This denotes a higher garnet lherzolite contribution that may partly be responsible for the higher Ti contents found.

The degrees of partial melting estimated here agree with the findings of Jacques and Green (1980) and Takahashi and Kushiro (1983) for the generation of tholeiitic magmas. The

CMDS plot between the main garnet and spinel lherzolite melting curves (as in Fig. 3.9) suggests that the various magmas were generated at the garnet-spinel lherzolite transition zone (Thirwall et al., 1994). Therefore, we conclude that CMDS magma generation were likely constrained through a mixing of deep mantle (60–70% garnet-facies melts) and shallow mantle (30–40% spinel-facies melts) sources. The origin and roles of the deep (or asthenospheric) and shallow (or enriched lithospheric) mantle sources in the petrogenesis of the CMDS are discussed in the following sections.

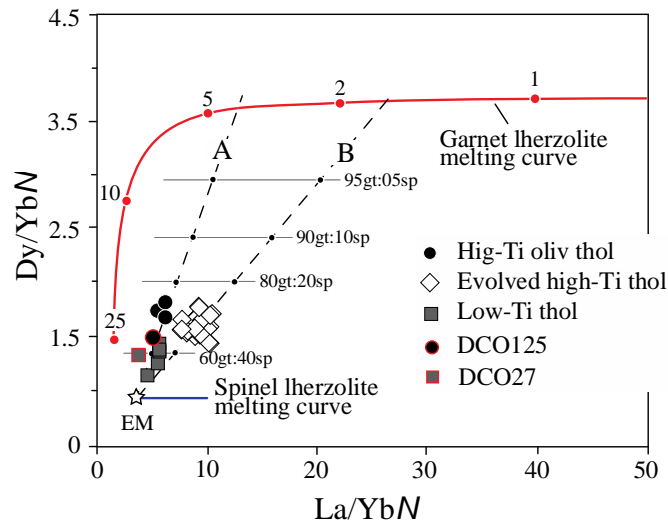


Figure 3.9. Model of mixing curves between spinel (in blue) and garnet (in red) lherzolite melts using normalized-Dy/Yb and La/Yb ratios to estimate rates of partial melting and magma sources for the CMDS tholeiitic magmas. The normalized ratios of EM (enriched mantle) are: $(Dy/Yb)_N = 0.7$ and $(La/Yb)_N = 2.5$, plotted from the convergence of the two modeled mixing lines along the spinel lherzolite melting curve.

3.5.2 EVALUATION OF LOW-PRESSURE CRUSTAL CONTAMINATION

The effects of crustal contamination on the CMDS require further attention given their variable and enriched Sr-Nd isotope compositions, especially for the evolved high-Ti and low-Ti tholeiite groups. As already mentioned, the CMDS intrudes Proterozoic crustal rocks that are primarily represented by c. 2 Ga acid to intermediate migmatitic gneisses, which were in turn covered by Neoproterozoic platformal to deep-water pelitic sediments, the whole intruded by Ediacaran acid to basic granitoids aged in c. 600–570 Ma. As a group, this complex set of rocks represents high silica crustal material with quite radiogenic Sr and unradiogenic Nd isotopic signatures (Van Schmus et al., 2003; Souza et al., 2007; Archanjo et al., 2013; Hollanda et al., 2003, 2011, 2015) and, therefore, potential contaminants for the CMDS magmas. For the olivine tholeiitic dykes, for which $^{87}\text{Sr}/^{86}\text{Sr}$ are low (0.7034–0.7037) and where $\varepsilon_{\text{Nd}_T}$ values of three of the four samples are positive ($\varepsilon_{\text{Nd}_T} = +0.8$ to $+4.4$), only the sample DKTt-01 sample has a strongly negative $\varepsilon_{\text{Nd}_T}$ value (-10.4) similar to those values reported for the basement rocks. In spite of divergence from radiogenic Nd isotopic values depicted by the other olivine tholeiites,

the initial $^{87}\text{Sr}/^{86}\text{Sr}$ ratio of 0.70373 and trace element contents of the DKTt-01 dyke correspond well with the mean values for the group. Such a discrepancy characterizes mafic magmas rising as dykes as a result of rapid heat transfer and turbulent flows, thus favoring the incomplete homogenization of the assimilated material (Huppert and Sparks, 1985) and producing compositional heterogeneities that are significant enough to be attributed to conventional AFC processes. Otherwise, it may also reflect isotopic imbalances related to the mantle source rather than effects of crustal assimilation during ascent.

To evaluate whether crustal contamination was responsible for the development of variations in the isotopic and trace element compositions of the evolved high-Ti tholeiites and the low-Ti tholeiites, we plot the average compositions of each Precambrian orthogneisses and GLOSS (Global Subducting Sediment) in Figure 3.10 as contaminants, with the latter representing a proxy for upper continental crust as proposed by Plank and Langmuir (1998). In this figure, K_2O is compared to the initial $^{87}\text{Sr}/^{86}\text{Sr}$ ratios for all of the samples, as well the $^{87}\text{Sr}/^{86}\text{Sr}$ ratio to Sr concentrations. Although most of the samples show a typical trend of fractional crystallization, the presence of a slight deviation in the $^{87}\text{Sr}/^{86}\text{Sr}$ ratio with increasing K_2O contents denotes that crustal assimilation must have marginally influenced the geochemistry of the evolved high-Ti tholeiites. In contrast, the low-Ti tholeiites show a stronger tendency towards AFC. More substantial levels of assimilation are found for sample DCO-04, which shows a higher initial $^{87}\text{Sr}/^{86}\text{Sr}$ ratio (0.71109) and which also represents the more evolved one of the group (MgO 4.93 wt.%; SiO_2 52.0 wt.%). One major contribution of crustal contamination to the low-Ti magmas is also related to lower $\text{P}_2\text{O}_5/\text{K}_2\text{O}$ ratio values (~0.18) relative to those of the evolved high-Ti tholeiites (~0.3), even so these values are even significantly higher than values found for the regional basement gneissic rocks (average 0.04; Souza et al., 2007).

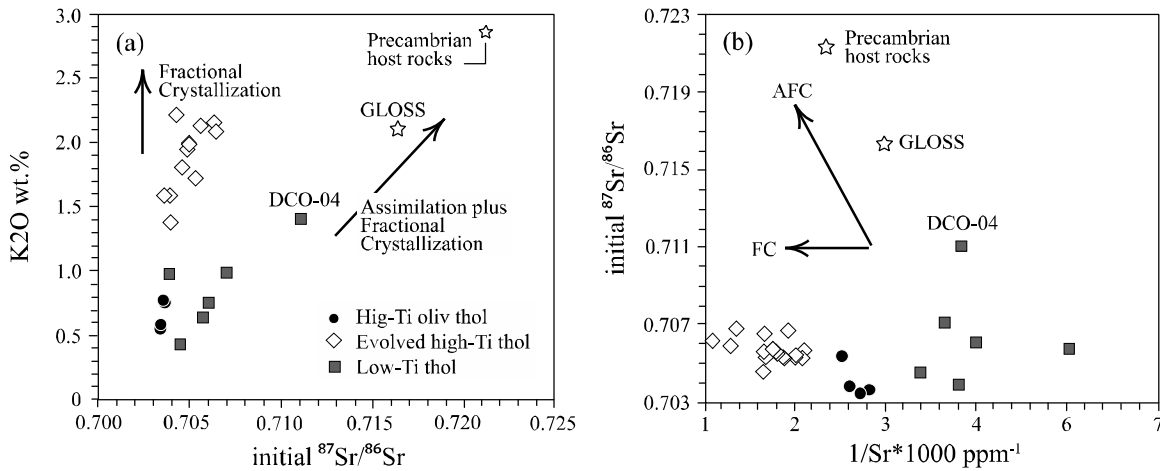


Figure 3.10. (a) Initial $^{87}\text{Sr}/^{86}\text{Sr}$ versus K_2O and (b) $^{87}\text{Sr}/^{86}\text{Sr}$ versus $1/\text{Sr} \times 1,000$ plots used to evaluate low-pressure crustal contamination levels in the CMDS tholeiitic magmas. The potential contaminants are assumed to form the regional, Precambrian gneissic basement and hypothetical GLOSS (Global Subduction Sediments; after Plank and Langmuir (1998)). Average data for Precambrian orthogneisses are drawn from Hollanda et al. (2003) and Souza et al. (2007).

3.5.3 CONSTRAINTS ON MANTLE SOURCES FOR THE CMDS THOLEIITES

Incompatible trace element and isotopic data can be effectively used to discuss the characterization of mantle sources for mafic rocks. In Figure 3.11, we re-plot incompatibility profiles as previously shown in Figure 7b to compare patterns of the CMDS samples with other Mesozoic (Jurassic and Cretaceous) continental tholeiites from South America and Africa. The Northern Benue tholeiites and St. Helena OIB (currently found in the southern Atlantic Ocean) were used to evaluate the influence of a HIMU-type component in the genesis of olivine tholeiites once part of the samples of this group show moderately radiogenic Pb isotopic compositions. Average compositions of both high-Ti and low-Ti tholeiites of the Jurassic CAMP-Maranhão (NE Brazil) and Cretaceous Paraná provinces were used to equate to CMDS-evolved high-Ti and low-Ti tholeiites, respectively. Given the discovery of similarities in major element abundances, we preferentially conducted comparisons with those of evolved high-Ti tholeiites of the CAMP-Maranhão province rather than with those of the silica undersaturated high-Ti group (Merle et al., 2011), while as a reference to the high-Ti Paraná tholeiites, we used Paranapanema and Pitanga types instead of Urubici and Ribeira types. The Esmeralda-Paraná ($\text{Ti/Zr} > 60$) was used to conduct comparisons with the CMDS low-Ti tholeiites (we recommend that the reader consult Peate (1997) for further details on the discrimination of the Paraná tholeiitic magmas).

We find clear similarities between incompatible trace element patterns in the olivine tholeiites, St. Helena magmas and Northern Benue tholeiitic basalts, though gentler fractionation and lower (2-3 times) abundance levels are found for most of the elements in the CMDS olivine tholeiites (Fig. 3.11a). These patterns may be attributable to by either (but not fully exclusive of) larger degrees in the partial melting of a source containing residual garnet or to some contribution of a mantle component approximating to E-MORB. In fact, Kawabata et al. (2011) argue that St. Helena primary magmas are produced through the 1-2% melting (perhaps <1% according Stracke et al., 2003) of a hybrid peridotitic source that leaves garnet in the residue. This differs from our estimate of 10% melting of a spinel:garnet peridotite as a source of olivine tholeiites. Notwithstanding reasonable parallelism to an E-MORB-type profile (see back Fig. 3.7b), the negative spike patterns in Pb, Nb enrichment trends ($\text{Nb}/\text{U} = 30\text{--}60$) and trace element ratios (as La/Nb , Nb/Th , Ce/Pb , Nb/Pb) of the olivine tholeiites most closely approximate to those of HIMU rather than with those of E-MORB. This suggest that the radiogenic Pb component is required to reproduce the geochemistry of olivine tholeiites and that it likely dominated over a more depleted mantle source that may be similar to E-MORB. Pb depletion in HIMU-type basalts has been proven to derive from a major contributions of recycled oceanic crust in the mantle source (e.g., Kawabata et al., 2011), which may also be responsible for Rb, Ba, La, Ce and Sr impoverishment relative to other OIBs, while Nb enrichment patterns would result from its preferential retention into refractory minerals after the dehydration of subducting lithospheric slabs (e.g., Brenan et al., 1994; Hanyu and Nakamura, 2000). With the exception of Ba, two samples of this tholeiite group are more plentiful in water-soluble elements (Rb to U), but as LOI values are low for all of the studied samples (0.25–0.85 wt.%), these differences may to be primary and potentially source-related.

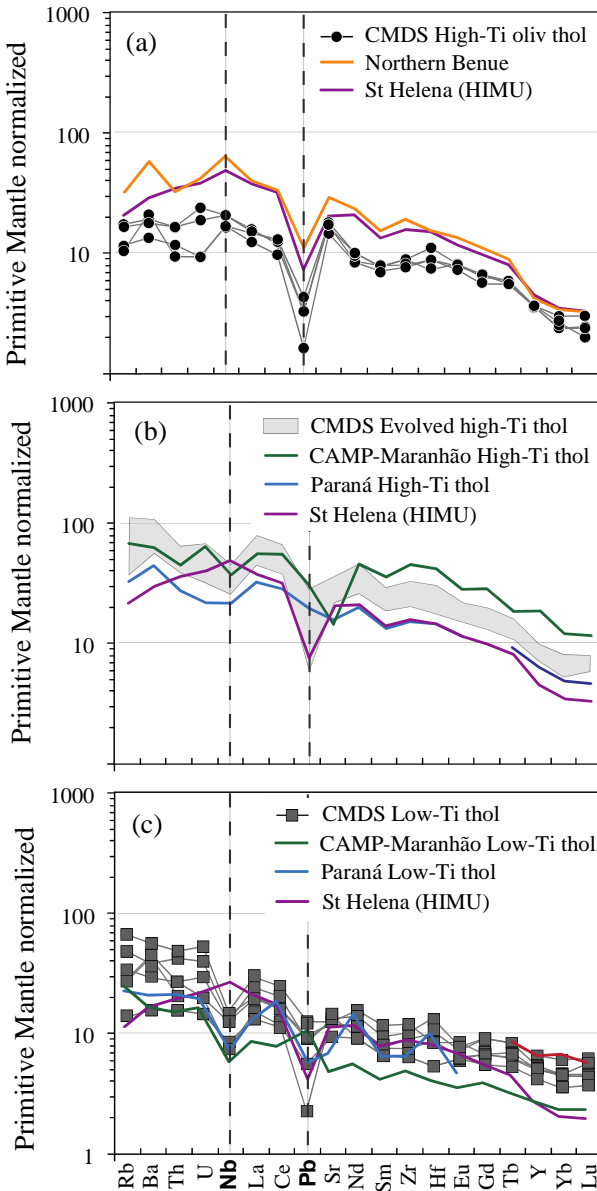


Figure 3.11. Incompatible element profiles for (a) olivine tholeiites, (b) high-Ti evolved tholeiites and (c) low-Ti tholeiites. Samples in (a) and (b) are plotted individually; given the number of geochemical analyses obtained for the evolved high-Ti tholeiites ($n=46$), we represent them as a field (grey area). Average compositions for HIMU-type OIB (St Helena), and high- and low-Ti tholeiites of the Paraná and CAMP-Maranhão igneous provinces are shown for purposes of comparison. Sources data were drawn from: CAMP-Maranhão – De Min et al. (2003) and Merle et al. (2011), Paraná – Peate (1997) and Rocha-Junior et al. (2013), Northern Benue G1 basalts – Coulon et al. (1996) and HIMU – Kawabata et al. (2011).

The evolved high-Ti tholeiites are richer in LIL and HFS elements than the other two groups. Their patterns bear some similarities with those of St. Helena OIBs with relative abundances of moderately to weakly incompatible (La to Lu) elements, although they are independently more significant in the CMDS. The most striking differences pertain to Rb-to-Th enrichment and to a well-marked negative Nb anomaly (Fig. 3.11b) found in the evolved high-Ti tholeiites, which is also present and more prominent in the low-Ti tholeiites (Fig. 3.11c). As Nb is strongly fractionated into refractory minerals assembled into dehydrated oceanic slab, its depletion is commonly shared by magmas derived from sub-arc lithospheric mantle materials modified by a subduction component (e.g., Tatsumi and Kogiso, 1997). However, average Nb/U ratios of ~25 and ~15 are observed for the evolved high-Ti and low-Ti tholeiites, respectively,

and their Nb/Th and Th/U ratios are all higher than those values found for IAB magmas (Ryerson and Watson, 1987), denoting that a subduction-related lithospheric mantle should not be the sole source of the primitive melts of these CMDS tholeiites.

Metasomatized (enriched) sub-arc lithospheric mantle involvement has also been found for other Mesozoic tholeiitic magmas in South America. In spite of variations in their whole trace element contents, the fit between the trace element patterns of evolved high-Ti tholeiites of the CMDS and high-Ti equivalents of the Paraná igneous province is outstanding, with the exception of an apparent lack of negative Pb spike found in the latter. Otherwise, the CAMP representatives tend to be slightly more abundant in moderately to weakly incompatible elements (from Nd to Lu) than the evolved high-Ti tholeiites, resulting in gentler profiles typically expected when garnet occupies a minor phase in the source, or when melting has occurred at large degrees. In addition, the CMDS tholeiites do not exhibit the negative anomaly in Sr as the CAMP and Paraná magmas, which may also indicate some differences in magma fractionation. Regarding the low-Ti magmas, the average trace element abundances of the CMDS tholeiites also do not fully match those of the Esmeralda or CAMP. Notwithstanding, the LIL enrichment and negative Nb anomaly are conspicuous for all three low-Ti groups, and this contrasting Pb behavior suggests depletion in the mantle sources of the CMDS and Paraná tholeiites and enrichment in CAMP. In the CMDS, the Pb anomaly decreases with differentiation, likely reflecting distinct and variable effects of AFC processes on these magmas ‘diluting’ such supposedly original source-related feature.

Sr-Nd-Pb isotope data on the CMDS were first plotted in binary diagrams shown in the Figure 8, which are known as Zindler and Hart’s (1986) and Holmes-Houtermans’s (Holmes, 1946; Houtermans, 1946) models. The data reveal the considerable compositional scattering. Despite the variability in terms of Nd, it is clear that only two olivine tholeiites (samples DCO-137 and DKtt-01) show strong tendencies towards radiogenic Pb, whereas the whole group displays uniform and unradiogenic Sr (0.7034–0.7037) compositions. The other evolved high-Ti and low-Ti tholeiites were found to be quite dispersed towards weakly to strongly radiogenic Sr and unradiogenic Nd and Pb. In the diagrams in Figure 3.12, we compare the isotopic compositions of CMDS tholeiites to those of the modern MORB-OIBs. As we believe that Pb isotopes are central to better determining mantle sources contributing to CMDS tholeiite genesis, we use a set of four companion plots proposed by Stracke et al. (2005) to differentiate between FOZO (the FOcal ZOne component) presented by Hart et al. (1992) and the typical HIMU-type OIBs found in St. Helena and on some of the Cook-Austral islands. In the diagrams, our results are plotted as present-day isotopic compositions to maintain coherence with those values for

modern ocean basalts. In all companion plots, FOZO represents a fairly radiogenic Pb and unradiogenic Sr component dismembered from HIMU. As shown in the Holmes-Houtermans's diagram on $^{208}\text{Pb}/^{204}\text{Pb}$ – $^{206}\text{Pb}/^{204}\text{Pb}$ (Fig. 3.12a), and in the $^{207}\text{Pb}/^{206}\text{Pb}$ versus $^{208}\text{Pb}/^{206}\text{Pb}$ chart (Fig. 3.12b), two olivine tholeiites fully match to the field defined by FOZO, with $^{206}\text{Pb}/^{204}\text{Pb} = 19.95$ and 20.13 and $^{208}\text{Pb}/^{204}\text{Pb} = 39.9$ and 39.93 for, respectively, the DCO-137 and DKTt-01 samples, and with $^{207}\text{Pb}/^{206}\text{Pb} \sim 0.79$. However, they slightly deviate from FOZO when considering their $^{208}\text{Pb}^*/^{206}\text{Pb}^*$ and Nd isotopic values (Fig. 3.12c, d), where $^{208}\text{Pb}^*/^{206}\text{Pb}^*$ ($= \frac{^{208}\text{Pb}/^{204}\text{Pb}_{\text{measured}} - ^{208}\text{Pb}/^{204}\text{Pb}_{\text{CDtroilite}}}{(^{206}\text{Pb}/^{204}\text{Pb}_{\text{measured}} - ^{206}\text{Pb}/^{204}\text{Pb}_{\text{CDtroilite}})}$; Galer and O'Nions, 1985) expresses the time-integrated Th/U ratio. The Pb isotopic compositions of the two other olivine tholeiites (samples DCO-125 and DCO-136) are more unradiogenic and are positioned within the overlapping field between Atlantic MORB and other OIBs (non-HIMU types). However, as shown in Stracke et al. (2005), MORBs and non-HIMU OIBs should represent magmas generated from mixing between FOZO and a depleted (DM) Pb component, diverging at variable degrees towards isotopically enriched compositions (e.g., EMI or EMII).

The Pb isotopic compositions of all of the other samples of both evolved high-Ti and low-Ti tholeiites must be described given the significant effects of an enriched end-member. Regardless we find some evidence for crustal contamination in these two tholeiite groups that must to be more extensive in the low-Ti magmas, their Pb isotopic compositions are quite uniform for strongly variable $^{87}\text{Sr}/^{86}\text{Sr}$ ratios. This suggests that Pb systematics in these tholeiites mostly approximate with original values and thus may be used to constrain their mantle source(s). For example, the most radiogenic in Sr (DCO-04 sample) was modelled to exhibit a higher degree of contaminant assimilation, but exhibit the more radiogenic $^{206}\text{Pb}/^{204}\text{Pb}$ ratio higher than the olivine tholeiite DCO-125, which display no patterns of crustal contamination. As a whole, both evolved high-Ti and low-Ti tholeiites plot within an overlapping region between Atlantic MORB and non-HIMU OIBs in Figure 3.12 together with the two unradiogenic Pb olivine tholeiites. Assuming that Pb systematics also provide the most significant isotopic differences between the two enriched EMI and EMII end-members (an estimation would be $^{206}\text{Pb}/^{204}\text{Pb} \sim 18.8$ according the dataset used by Stracke et al., 2003) and that the tholeiites have measured $^{206}\text{Pb}/^{204}\text{Pb}$ ratio < 18.8 , we propose that an EMI-type reservoir must serve as the enriched source component of the CMDS tholeiites. In fact, Zr/Nb, Ba/Nb, Th/Nb and Ba/La ratios of these tholeiites are in good agreement to those averaged by Weaver (1991) for EMI OIBs, even though there is an actual consensus that trace element systematics does not allow unambiguous discrimination between EMI- and EMII-types (Willbold and Stracke, 2006).

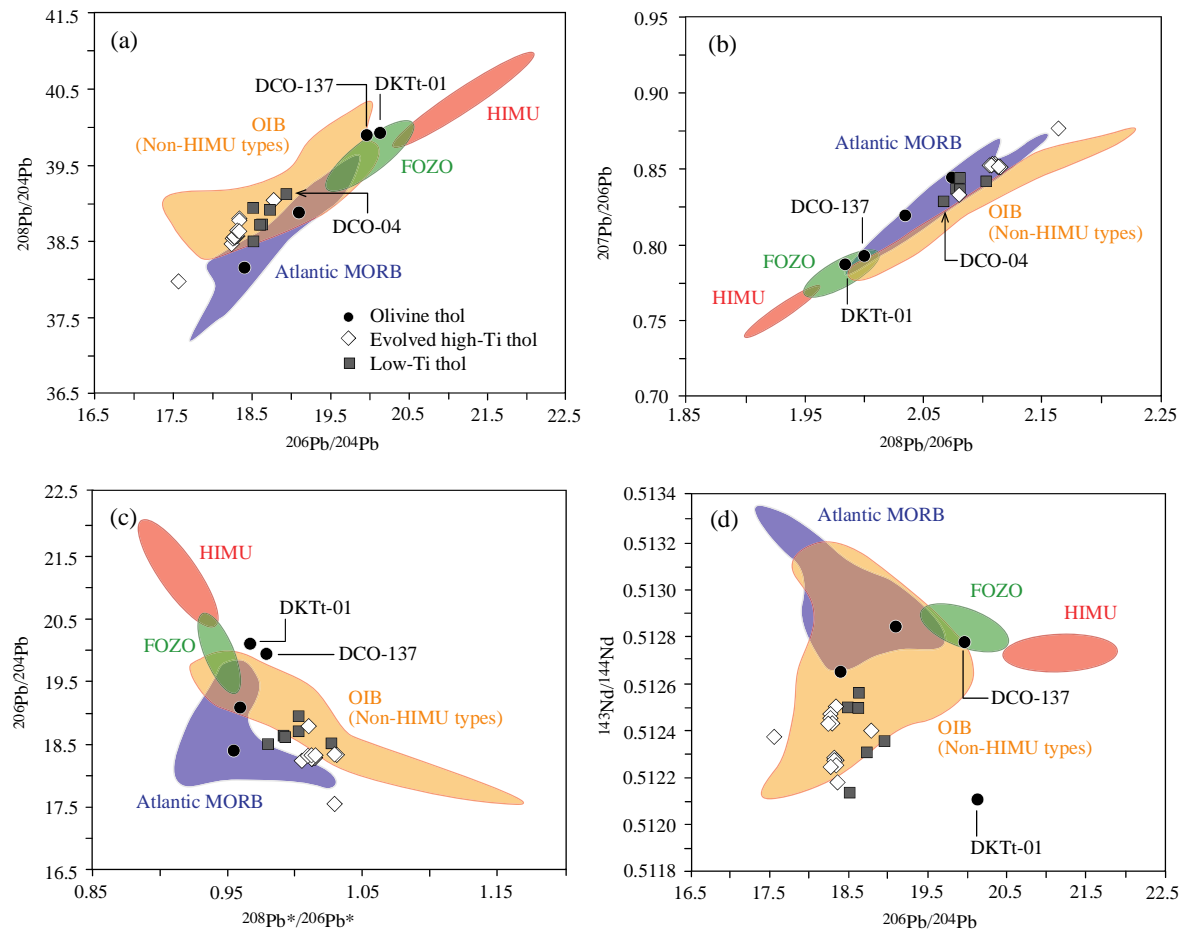


Figure 12. Isotopic companion plots used to differentiate FOZO and HIMU components and to compare their Pb and Nd signatures with those of the CMDS tholeiitic groups. Fields for Atlantic MORB and non-HIMU OIBs as defined by Stracke et al. (2005) are also included for comparison (fields for both Pacific and Indian MORB are not shown).

We conclude that the trace element (enrichment in Nb and depletion in Pb relative to U and Th) and FOZO signatures, now well constrained from some of the CMDS olivine tholeiites, should be ascribed to an asthenospheric (deeper) component. As widely discussed in literature the FOZO origin is related to long-term recycling oceanic crust with moderately time-integrated $^{238}\text{U}/^{204}\text{Pb} (= \mu)$ ratios compared to those of the classical HIMU-type reservoir (e.g., Hart et al., 1992; Stracke et al., 2003, 2005). The ubiquitously enriched signature found in the other tholeiite groups was in turn likely dominant at narrower mantle depths. Such enriched mantle source are credited to the sub-continental lithospheric mantle, which was chemically modified (metasomatized) by subduction-related processes as predicted by striking negative Nb anomaly reported for all of the studied samples. The Nd-model ages >1 Ga calculated for the CMDS tholeiites (Hollanda et al., 2006) underscore a need for the long-term preservation of such

ancient (Proterozoic) enriched signatures of at least concurrent lithospheric melting and extensional thinning as a consequence of the Atlantic Ocean opening at the Cretaceous.

3.6 GEODYNAMIC CONSIDERATIONS

Two geochemical subdivisions for the CMDS are proposed in the works of Bellieni et al. (1992) and Hollanda et al. (2006). According these authors, the CMDS was predominantly composed of high-Ti tholeiites grouped into four sub-swarms (I to IV), with three of them recording magnetic poles of the Upper Jurassic/Lower Cretaceous and with one (sub-swarm II) possibly becoming crystallized in the Lower Jurassic. A small set of dykes (sub-swarm V) defined as “alkaline” in composition was once shown to include modal olivine and was shown to have poles consistent with the Lower Cretaceous ages. Sub-swarms I to III are found to form the main E-W swarm, while sub-swarms IV and V are smaller in length and are found to the south of the main branch. In turn, Hollanda et al. (2006) divided the swarm into eastern, central and western tholeiites to explain the prevalence of lower Nd isotope compositions in the dykes of the central part compared to dykes of the eastern and western regions. These authors also highlight the dominance of (evolved) high-Ti tholeiites in the swarm and, in minor occurrences typically confined to the western region, the low-Ti tholeiites. In view of the dataset assembled in this paper, we propose a new subdivision of CMDS tholeiites into three major geochemical groups. The first consists of evolved high-Ti tholeiites representing the main swarm (~80%), encompassing sub-swarms I to III presented by Bellieni and colleagues. The second group consists of low-Ti tholeiites forming ~10% of the main swarm and preferentially exposed in its western part. The third group found exclusively to the south of the main swarm (sub-swarm IV) consists of olivine tholeiites (~10%). These magmas moved up through the lithosphere likely along (at least) two main feeder zones found at the intersection of both main and southern swarms with Tertiary plugs of the Macau volcanism (see back Fig. 3.1). Such zones were mapped from vertical flow fabrics (via steep-dipping magnetic lineation) measured over a set of 60 dykes including the evolved high-Ti and olivine tholeiites following Archanjo's et al. (2000, 2002) anisotropy of magnetic susceptibility study. This whole region is positioned across a large negative geoid anomaly documented in the NE Borborema Province and modeled as a low density (thermal) zone situated at between 17 and 78 km in depth (Chaves, 2010). This interval embraces our estimates of melting depths of between 60 and 75 km for the CMDS.

No single measure can evaluate which mechanism may have promoted the melting of both sub-continental lithospheric and asthenospheric sources beneath NE Brazil at the Cretaceous. Three thought-provoking models have been proposed for the origins of intraplate magmatism, and although they have been largely used to explain the formation of large (volume) igneous provinces, they may be employed in examining the CMDS. For example, the plume model invokes an upwelling of hot materials from the deep mantle driven by thermal buoyancy, arriving at the base of the lithosphere as a large head (>1,000 km in diameter) followed by a narrower tail (e.g., Richards et al., 1989; Campbell and Griffiths, 1990). Such a mechanism may help explain the formation of CMDS in view of a likely geographic overlap of NE Brazil and the St. Helena hotspot during Cretaceous (~130 Ma; Sengor, 1995), it does not endorsed by Ernesto et al. (2002), and in regards to our conclusions on the existence of radiogenic Pb OIB-type magmas (the olivine tholeiites) forming the swarm. However, assuming that FOZO serves as a more realistic component and in accepting that it is “*...a ubiquitously dispersed, small-scale component [expected to reside] in possibly the entire mantle...*” according Stracke et al. (2005), there is no need to relate the origin of the CMDS to the St. Helena plume. In addition, plume-related igneous provinces require the emplacement of large (extrusive and/or intrusive) magma volumes over a short time period in a focused area, leading to the presence of high-Mg rocks (picrite) and to connection with an age-progressive trail and a present-day hotspot (see Ernst, 2014). All of these predictions are not met in the case of the CMDS, although there a few systematic geochronological studies have been conducted on this issue.

An alternative model proposed on the origins of continental basaltic magmas envisages that thermal insulation induced by thick lithospheric (“cratonic”) roots can raise the temperature of the asthenosphere, generating flows moving laterally towards thinner lithospheric areas (King and Anderson, 1995, 1998). As the asthenosphere ascends into small-scale convective flows, it may trigger lithospheric melting or decompression and melting itself. The main issue for this model concerns the factual spatial link between magmatism and cratonic edges. In fact, the CMDS is located roughly 600–700 km away from the present-day northern edge of the São Francisco-Congo (SFC) craton formed during the Neoproterozoic, a distance that may prove sustainable for the effects of such convective cells (King, 2007). Finally, one non-thermal model involves the delamination and detachment of a thickened lithospheric keel followed by sinking into the convective asthenosphere (Anderson, 2005; Lustrino, 2005). The asthenosphere in turn wells up, passively replacing the lithosphere. It is true that orogenic lithospheric thickening is presumed to have occurred at end of the Neoproterozoic (~600 Ma) as a result of collisional events that assembled West Gondwana (e.g., Ganade Araújo et al., 2014). However, major

drawbacks to assuming both edge-driven and delamination models relate to the time delay between the onset of convective thermal instability at the edge of a major lithospheric (the SFC) discontinuity and delamination (a few hundred million years) and mantle melting in the Cretaceous. Nevertheless, these two models cannot be excluded as a whole, and a combination of them with local effects of plate-boundary stresses that were time-related to the Atlantic Ocean opening (which may certainly explain the association between rifting and lithospheric thinning and that between asthenospheric upwelling and intraplate (mafic) magmatism) may be explored in future works.

3.7 CONCLUSIONS

From the results presented in this study the following conclusions can be drawn:

- (1) CMDS tholeiites can be subdivided into three geochemical groups based on their major and trace element compositions: (high-Ti) olivine tholeiites, evolved high-Ti tholeiites and low-Ti tholeiites;
- (2) Chemical variability observed for each group are governed by fractional crystallization combined with moderate (for the low-Ti tholeiites) to negligible crustal assimilation processes. Fractionation is primarily favored by olivine, pyroxene, plagioclase and Fe-Ti minerals from evolving primary magmas;
- (3) Primitive mantle-normalized incompatibility profiles show that all of the groups are prevalent in LIL and HFS elements. Nb(-Ta) enrichment was only found in the olivine tholeiites, while noteworthy levels of depletion were found in the evolved high-Ti and low-Ti tholeiites. These contrasting Nb signatures strongly imply the involvement of a deeper OIB-type (asthenospheric) source and of the sub-continental (arc-type) lithospheric mantle in the genesis of the CMDS, melted at depths of between 75 and 60 km corresponding with the garnet-spinel facies transition;
- (4) The OIB-type source shown isotopic similarities with the FOZO component (plus some interaction with E-MORB), which is especially evident from the radiogenic Pb ratios of the olivine tholeiites. Primary magmas that generated the evolved high-Ti and low-Ti tholeiites likely evolved from a dominant EMI (subduction-type) reservoir with some interactions with FOZO melts, as shown by patterns of considerable Nb and Pb depletion, respectively;

(5) While the primary control for the origin of the CMDS was not deeply assessed in this paper, we would be biased to believe that its formation primarily results from passive (plate-boundary stress) rifting rather than from mantle plume activity.

ACKNOWLEDGMENTS

This article was written as part of the E.D. Ngonge's Ph.D. thesis. Ngonge was supported by CAPES. M.H.B.M. Hollanda and C.J. Archanjo received grants from the Brazilian National Research Council (CNPq), which were used to finance part of this research project. The analytical tests and field trips were carried out under the auspices of CNPq through Project 473.638/2011-8. We thank D.W. Peate and P. Hawkesworth for providing useful comments on early versions of the manuscript and A. Marzoli and P. Hollings for providing constructive criticism and suggestions that certainly improved the final version.

REFERENCES

- Albarède, F. 1992. How deep do common basaltic magmas form and differentiate? *Journal of Geophysical Research*, 97: 10997–11009.
- Anderson, D.L. 2005. Large igneous provinces, delamination, and fertile mantle. *Elements*, 1: 271-275.
- Archango, C.J., Trindade, R.I.F., Macedo, J.W.P., Araújo, M.G.S. 2000. Magnetic fabric of a basaltic dyke swarm associated with Mesozoic rifting in northeastern Brazil. *Journal of South American Earth Sciences*, 13: 179-189.
- Archango, C.J., Araújo, M.G.S., Launeau, P. 2002. Fabric of the Rio Ceará-Mirim mafic dyke swarm (Northeastern Brazil) determined by anisotropy of magnetic susceptibility and image analysis. *Journal of Geophysical Research*, 107(B3), 2046: 1-13.
- Archango, C.J., Viegas, L.G.F., Hollanda, M.H.B.M., Souza, L.C., Liu, D. 2013. Timing of the HT/LP transpression in the Neoproterozoic Seridó Belt (Borborema Province, Brazil): constraints from U-Pb (SHRIMP) geochronology and implications for the connections between NE Brazil and West Africa. *Gondwana Research*, 23: 701-714.
- Bastin, G.F., Heijligers, H.J.M. 1990. Progress in electron-probe microanalysis. *Material-wissenschaft und Werkstofftechnik*, 21: 216-221.
- Bellieni, G., Comin Chiaramonti, P., Marques, L.S., Melfi, A.J., Piccirillo, E.M., Nardy, A.J.R., Roisemberg, A. 1984. High- and low-TiO₂ flood basalts from the Parana plateau (Brazil): petrology and geochemical aspects beraing on their mantle origin. *Neues Jahrbuch Miner. Abh.* 150(3): 273-306.
- Bellieni, G., Macedo, M.H.F., Petrini, R., Picirillo, E.M., Cavazzini, G., Comin-Chiaramonti, P., Ernesto, M., Macedo, J.W.P., Martins, G., Melfi, A.J., Pacca, I.G., De Min, J. 1992. Evidence of magmatic activity related to Middle Jurassic to Early Cretaceous rifting from northeastern Brazil (Ceará-Mirim): K/Ar age, palaeomagnetism, petrology and Sr-Nd isotope characteristics. *Chemical Geology*, 97: 9-32.
- Benkhelil, J. 1989. The origin and evolution of the Cretaceous Benue Trough (Nigeria). *Journal of African Earth Sciences*, 8 (2/3/4): 251-282.
- Boynton, W.V. 1984. Geochemistry of the rare earth elements: meteorite studies. In P. Henderson (Ed.), *Rare-Earth Element Geochemistry*, Elsevier: 63-114.
- Brenan, J.M., Shaw, H.F., Phinney, D.L., Ryerson, F.J. 1994. Rutile-aqueous fluid partitioning of Nb, Ta, Hf, Zr, U and Th: implications for high field strength element depletions in island-arc basalts. *Earth and Planetary Science Letters*, 128: 327-339.
- Campbell, I.H. 2005. Large igneous provinces and the mantle plume hypothesis. *Elements*, 1: 265-269.
- Campbell, I.H., Griffiths, R.W. 1990. Implications of mantle plume structure for the evolution of flood basalts. *Earth and Planetary Science Letters*, 99: 79-93.
- Chang, H.K., Kowsmann, R.O., Figueiredo, A.M.F., Bender, A.A. 1992. Tectonics and stratigraphy of the East Brazil Rift system: an overview. *Tectonophysics*, 213: 97-138.
- Chaves, C.A.M. 2010. Inversão linear de anomalias do geóide da Província Borborema: variação composicional ou perturbação térmica no manto? Master thesis, Instituto de Astronomia, Geofísica e Ciências Atmosféricas, Universidade de São Paulo, 163 pp.
- Chayes, F. 1966. Alkaline and subalkaline basalts. *American Journal of Science*, 264: 128-145.
- Cordani, U. G., and P. Vandoros. 1967. Basaltic rocks of the Parani basin, in *Problems in Brazilian Gondwana Geology*, edited by J. J. Bigarella, R. D. Becker, and J. D. Pinto, pp. 207-231.
- Coulon, C., Vidal, P., Dupuy, C., Baudin, P., Popoff, M., Maluski, H., Hermitte, D. 1996. The Mesozoic to Early Cenozoic Magmatism of the Benue Trough (Nigeria); Geochemical Evidence for the Involvement of the St Helena Plume. *Journal of Petrology*, 37: 341-358.

- De Min, A., Piccirillo, E.M., Marzoli, A., Bellieni, G., Renne, P.R., Ernesto, M., Marques, L.S. 2003. The Central Atlantic Province (CAMP) in Brazil: petrology, geochemistry, $^{40}\text{Ar}/^{39}\text{Ar}$ ages, paleomagnetism and geodynamic implications. In: Hames, W.E., McHone, J.G., Renne, P.R., Ruppel, C. (Eds.), The Central Atlantic Magmatic Province: insights from fragments of Pangea. AGU Geophysical Monographs, 136: 209-226.
- Ernesto, M., Marques, L.S., Piccirillo, E.M., Molina, E.C., Ussami, N., Comin-Chiaromanti, P., Bellieni, G. 2002. Paraná magmatic province-Tristan da Cunha plume system: fixed versus mobile plume, petrogenetic considerations and alternative heat sources. *Journal of Volcanology and Geothermal Research*, 118: 15-36.
- Ernst, R.E. 2014. Large Igneous Provinces. Cambridge University Press, 653 pp.
- Ewart, A., Milner, S.C., Armstrong, R.A., Duncan, A.R. 1998. Etendeka volcanism of the Goboboseb Mountains and Messum Igneous complex, Namibia. Part I: Geochemical evidence of Early Cretaceous Tristan plume melts and the role of crustal contamination in the Parana-Etendeka CFB. *Journal of Petrology*, 39: 191-225.
- Ewart, A., Marsh, J.S., Milner, S.C., Duncan, A.R., Kamber, B.S., Armstrong, R.A. 2004. Petrology and geochemistry of Early Cretaceous bimodal Continental Flood Volcanism of the NW Etendeka, Namibia. Part 1: Introduction, mafic lavas and re-evaluation of mantle source components. *Journal of Petrology*, 45, 59-105.
- Fodor, R.V., Corwin, C., Roisenberg, A. 1985. Petrology of Serra Geral (Paraná) continental flood basalts, southern Brazil: crustal contamination, source material and South Atlantic magmatism. *Contributions to Mineralogy and Petrology*, 91: 54-65.
- Fodor, R.V., Sial, A.N., Mukasa, S.B., McKee, E.H. 1990. Petrology, isotope characteristics and K-Ar ages of the Maranhão, northern Brazil Mesozoic basalt province. *Contributions to Mineralogy and Petrology*, 104: 555-567.
- Françolin, J.B.L., Cobbold, P.R., Szatmari, P. 1994. Faulting in the Early Cretaceous Rio do Peixe basin (NE Brazil) and its significance for the opening of the Atlantic. *Journal of Structural Geology*, 16(5): 647-661.
- Galer, S.J.G., O'Nions, R.K. 1985. Residence time of thorium, uranium and lead in the mantle with implications for mantle convection. *Nature*, 316: 778-782.
- Ganade-Araújo, C.E., Rubatto, D., Hermann, J., Cordani, U.G., Caby, R., Basei, M.A.S. 2014. Ediacaran 2,500-km-long synchronous deep continental subduction in the West Gondwana Orogen. *Nature Communications*, doi: 10.1038/ncomms6198.
- Hanyu, T., Nakamura, E. 2000. Constraints on HIMU and EM by Sr and Nd isotopes re-examined. *Earth, Planets and Space*, 52: 61-70.
- Hart, S.R. 1984. A large-scale isotope anomaly in the southern hemisphere mantle. *Nature*, 309: 753-757.
- Hart, S.R. 1988. Heterogeneous mantle domains: signatures, genesis and mixing chronologies. *Earth and Planetary Science Letters*, 90: 273-296.
- Hart, S.R., Hauri, E.H., Oschmann, L.A., Whitehead, J.A. 1992. Mantle plumes and entrainment – isotopic evidence. *Science*, 256: 517-520.
- Hollanda, M.H.B.M., Pimentel, M.M., Jardim de Sá, E.F. 2003. Paleoproterozoic subduction-related metasomatic signatures in the lithospheric mantle beneath NE Brazil: inferences from trace element and Sr–Nd–Pb isotopic compositions of Neoproterozoic high-K igneous rocks. *Journal of South American Earth Science*, 15(8): 885- 900.
- Hollanda, M.H.B.M., Pimentel, M.M., Oliveira, D.C., Jardim de Sá, E.F. 2006. Lithosphere–asthenosphere interaction and the origin of Cretaceous tholeiitic magmatism in Northeastern Brazil: Sr–Nd–Pb isotopic evidence. *Lithos*, 86: 34-49.
- Hollanda, M.H.B.M., Archanjo, C.J., Souza, L.C., Liu, D., Armstrong, R. 2011. Long-lived Paleoproterozoic granitic magmatism in the seridó-Jaguaribe domain, Borborema Province – NE Brazil. *Journal of South American Earth Sciences*, 32: 287-300.

- Hollanda, M.H.B.M., Archanjo, C.J., Bautista, J.R., Souza, L.C. 2015. Detrital zircon ages and Nd isotope compositions of the seridó and Lavras da Mangabeira basins (Borborema Province, NE Brazil): evidence for exhumation and recycling associated with a major shift in sedimentary provenance. *Precambrian research*, 258: 186-207.
- Holmes, A. 1946. An estimate of the age of the Earth. *Nature*, 157: 680-684.
- Houtermans, F.G. 1946. Die isotopenhäufigkeiten im natürlichen blei und das alter des urans. *Naturwissenschaften*, 33: 185-186.
- Huppert, H.E., Sparks, R.S.J. 1985. Cooling and contamination of mafic and ultramafic magmas during ascent through continental crust. *Earth and Planetary Science Letters*, 74: 371-386.
- Jaques, A.I. and Green, G.H. 1980. Anhydrous melting of peridotite at 0-15kb and the genesis of tholeiitic basalts. *Contributions to mineralogy and petrology*, 73, 287-310.
- Jourdan, F., Bertrand, H., Schärer, U., Blichert-Toft, J., Féraud, G., Kampunzu, A.B. 2007. Major and trace element and Sr, Nd, Hf and Pb isotope compositions of the Karoo large igneous province, Botswana-Zimbabwe: lithosphere vs mantle plume composition. *Journal of Petrology*, 48(6): 1043-1077.
- Kawabata, H., Hanyu, T., Chang, Q., Kinura, J-I., Nichols, A.R.L., Tatsumi, Y. 2011. The petrology and geochemistry of St. Helena alkali basalts: evaluation of the oceanic crust-recycling model for HIMU-OIB. *Journal of Petrology*, 52(4): 791-838.
- King, S.D. 2007. Hotspots and edge-driven convection. *Geology*, 35: 223-226.
- King, S.D., Anderson, D.L. 1995. An alternative mechanism of flood basalt formation. *Earth and Planetary Letters*, 136: 269-279.
- King, S. D., Anderson, D.L. 1998. Edge-driven convection. *Earth and Planetary Science Letters*, 160: 289-296.
- Lindsley, D.H. 1983. Pyroxene thermometry. *American Mineralogist*, 68:477-493.
- Lustrino, M. 2005. How the delamination and detachment of lower crust can influence basaltic magmatism. *Earth-Science Reviews*, 72: 21-38.
- Maluski, H., Coulon, C., Popoff, M., Baudin, P. 1995. $^{40}\text{Ar}/^{39}\text{Ar}$ chronology, petrology and geodynamic setting of Mesozoic to early Cenozoic magmatism from the Benue Trough, Nigeria. *Journal of the Geological Society, London*, 152: 311-326.
- Mantovani, M.S.M., Marques, L.S., Sousa, M.A., Civetta, L., Atalia, L., Innocenti, F. 1985. Trace element and strontium isotope constraints on the origin and evolution of Paraná continental flood basalts of Santa Catarina state (southern Brazil). *Journal of Petrology*, 26: 187-209.
- Marques, L.S., Dupré, B., Piccirillo, E.M. 1999. Mantle source compositions of the Paraná Magmatic Province (southern Brazil): evidence from trace element and Sr-Nd-Pb isotope geochemistry. *Journal of Geodynamics*, 28: 439-458.
- Marzoli, A., Renne, P.R., Piccirillo, E.M., Ernesto, M., Bellieni, G., De Min, A. 1999. Extensive-200-million-year-old continental flood basalts of the Central Atlantic Magmatic Province. *Science*, 284: 616-618.
- Marzoli, A., Piccirillo, E.M., Renne, P.R., Bellieni, G., Iacumin, M., Nyobe, J.B., Tongwa, A.T. 2000. The Cameroon Volcanic Line revised: petrogenesis of continental basaltic magmas from lithospheric and asthenospheric mantle sources. *Journal of Petrology*, 42: 1,197-1,218.
- Merle, R., Marzoli, A., Bertrand, H., Reisberg, L., Verati, C., Zimmermann, C., Chiaradia, M., Bellieni, G., Ernesto, M. 2011. $^{40}\text{Ar}/^{39}\text{Ar}$ ages and Sr-Nd-Pb-Os geochemistry of CAMP tholeiites from Western Maranhão basin (NE Brasil). *Lithos*, 122: 137-151.
- Misusaki, A.M.P., Thomaz-Filho, A., Milani, E.J., Césaro, P. 2002. Mesozoic and Cenozoic igneous activity and its tectonic control in northeastern Brazil. *Journal of South American Earth Sciences*, 15: 183-198.
- Miyashiro, A. 1974. Volcanic rock series in island arcs and active continental margins: *American Journal of Science*, 274: 321-355.

- Oliveira, D.C. 1992. O papel do enxame de diques Rio Ceará-Mirim na evolução tectônica do nordeste oriental (Brasil): implicações na formação do rifte Potiguar. Master thesis, University of Ouro Preto, Brasil, 172 pp.
- Pearce, J.A. 2008. Geochemical fingerprint of oceanic basalts with applications to ophiolite classification and the search for Archean oceanic crust. *Lithos*, 100: 14-48.
- Peate, D.W. 1997. The Paraná-Etendeka province. In: Large Igneous Provinces: Continental, Oceanic and Planetary Flood Volcanism. AGU Geophysical Monographs, 100: 217-245.
- Peate, D. W., Hawkesworth, C. J. 1996. Lithospheric to asthenospheric transition in Low-Ti flood basalts from southern Paranti, Brazil. *Chemical Geology*, 127: 1-24.
- Peate, D.W., Hawkesworth, C.J., Mantovani, M.S.M. 1992. Chemical stratigraphy of the Paraná lavas (South America): classification of magma types and their spatial distribution. *Bulletin of Volcanology*, 55: 119-139.
- Plank, T., Langmuir, C.H. 1998. The chemical composition of subducting sediment and its consequences for the crust and mantle. *Chemical Geology*, 145: 325-394.
- Price, R.C., Nicholls, I.A., Day, A. 2014. Lithospheric influences on magma compositions of late Mesozoic and Cenozoic intraplate basalts (the Older Volcanics) of Victoria, south-eastern Australia. *Lithos*, 206-207: 179-200.
- Prytulak, J. and Elliott, T. 2007. TiO₂ enrichment in ocean island basalts. *Earth and Planetary Science Letters* 26, 388-403.
- Richards, M.A., Duncan, R.A., Courtillot, V.E. 1989. Flood basalts and hotspot tracks – plume heads and tails. *Science*, 246: 103-107.
- Rocha-Júnior, E.R.V., Puchtel, I.S., Marques, L.S., Walker, R.J., Machado, F.B., Nardy, A.J.R., Babinsky, M., Figuerirido, A.M.G. 2012. Re-Os isotope and highly siderophile element systematic of the Paraná continental flood basalts (Brazil). *Earth and Planetary Science Letters*, 337: 164-173.
- Rocha-Júnior, E.R.V., Marques, L.S., Babinski, M., Nardy, A.J.R., Figueiredo, A.M.G., Machado, F.B. 2013. Sr-Nd-Pb isotopic constraints on the nature of the mantle sources involved in the genesis of the high-Ti tholeiites from northern Paraná continental flood basalts (Brazil). *Journal of South American Earth Sciences*, 46: 9-25.
- Roeder and Emslie, 1970. Olivine-liquid equilibrium. Contribution to mineralogy and petrology, 29: 275-289.
- Ryerson, F.J., Watson, E.B. 1987. Rutile saturation in magmas: implication for Ti-Nb-Ta depletion in island-arc basalts. *Earth and Planetary Science Letters*, 86: 225-239.
- Sack, R.O., Carmichael, I.S.E. 1984. Fe₂↔Mg₂ and TiAl₂↔MgSi₂ exchange reactions between clinopyroxenes and silicate melts. *Contributions to Mineralogy and Petrology*, 85: 103-115.
- Scarborough, J.H., Cox, K.G. 1995. Basalts generated by decompressive adiabatic melting of mantle plume-a case study from the Isle of Skye, NW Scotland. *Journal of Petrology*, 36: 3-22.
- Sénant, J., Popoff, M. 1991. Early Cretaceous extension in northeast Brazil related to the South Atlantic opening. *Tectonophysics*, 198: 35-46.
- Sengor, A.M.C. 1995. Sedimentation and tectonics of fossil rifts. In: Busby, C.J., Ingersoll, R.-V. (Eds.), *Tectonics of Sedimentary Basins*, Oxford: Blackwell, pp.53-117.
- Souza, Z.S., Martin, H., Peucat, J.-J., Jardim de Sá, E.F., Macedo, M.H.F. 2007. Calc-alkaline magmatism at the Archean-Proterozoic transition: the Caicó complex basement (NE Brazil). *Journal of Petrology*, 48: 2149-2185.
- Stracke, A., Bizimis, M., Salters, V.J.M. 2003. Recycling oceanic crust : quantitative constraints. *Geochemistry, Geophysics, Geosystems*, 4(3), 8003, doi: 10.1029/2001GC000223.
- Stracke, A., Hofmann, A.W., Hart, S.R. 2005. FOZO, HIMU, and the rest of the mantle zoo. *Geochemistry, Geophysics, Geosystems*, 6(5), Q05007, doi: 10.1029/2004GC000824.
- Sun, S.S., McDonough, W.F. 1989. Chemical and isotopic systematic of oceanic basalts: implications for mantle composition and processes. In: Saunders, A.D., Norry, M.J. (Eds.), *Magmatism in the Ocean Basins*, Geological Society Special Publications, 42: 313–345.

- Takahahshi, E., Kushiro, I. 1983. Melting of a dry peridotite at high pressures and basalt magma genesis. *American Mineralogist*, 68: 859-879.
- Tatsumi, Y., Kogiso, T. 1997. Trace element transport during dehydration processes in the subducted oceanic crust: 2, Origin of chemical and physical characteristics in arc magmatism. *Earth and Planetary Science Letters*, 148: 207-221.
- Thirwall, M.F., Upton, B.G.J., Jenkins, C. 1994. Interaction between continental lithosphere and the Iceland plume-Sr-Nd-Pb isotopic geochemistry of Tertiary basalts, NE Greenland. *Journal of Petrology*, 35: 839-879.
- Thompson, R.N., Gibson, S.A., Dickin, A.P. 2001. Early Cretaceous basalt and picrite dykes of the Southern Etendeka region, NW Namibia: windows into the role of the Tristan mantle plume in
- Van Schmus, W.R., Brito Neves, B.B., Williams, I.S., Hackspacher, P.C., Fetter, A.H., Dantas, E.L., Babinski, M. 2003. Seridó Group of NE Brazil, a Late Neoproterozoic pre- to syn-collisional flysch basin in West Gondwanaland?: insights from SHRIMP U-Pb detrital zircon ages. *Precambrian Research*, 127: 287-327.
- Vasconcelos, P.M., Onoe, A.T., Kawashita, K., Soares, A.J., Teixeira, W. 2002. $^{40}\text{Ar}/^{39}\text{Ar}$ geochronology at the Instituto de Geociências, USP: instrumentation, analytical procedures and calibration. *Anais Academia Brasileira de Ciências*, 74: 297-342.
- Vauchez, A., Neves, S., Caby, R., Corsini, M., Egydio-Silva, M.E., Arthaud, M., Amaro, V. 1995. *Journal of South American Earth Sciences*, 8(3/4): 247-266.
- Viegas, L.G.F., Archanjo, C.J., Hollanda, M.H.B.M., Vauchez, A. 2014. Microfabrics and zircon U-Pb (SHRIMP) chronology of mylonites from the Patos shear zone (Borborema Province, NE Brazil). *Precambrian Research*, 243: 1-17.
- Weaver, B.L. 1991. Trace element evidence for the origin of ocean-island basalts. *Geology*, 19, 123-126.
- Willbold, M., Stracke, A. 2006. Trace element composition of mantle end-members: implications for recycling of oceanic and upper and lower continental crust. *Geochemistry, Geophysics, Geosystems*, 7(4), doi:10.1029/2005GC001005.
- Wilson, M., Patterson, R. 2001. Intraplate magmatism related to hot fingers in the upper mantle: Evidence from the Tertiary-Quaternary volcanic province of western and central Europe. In: R. Ernst & K. Buchan (Eds.). *Mantle Plumes: Their identification through time*. Geological Society of America Special Paper, 352: 37-58.
- Zindler, A., Hart, S.R. 1986. Chemical geodynamics. *Annual Review of Earth and Planetary Sciences*, 14: 493-571.

CAPÍTULO 4

ARTIGO SUBMETIDO AO PERIÓDICO

JOURNAL OF VOLCANOLOGY AND GEOTHERMAL RESEARCH

ABSTRACT

The Macau Volcanic Field (MVF) is an example of Cenozoic intraplate alkaline volcanism exposed over Precambrian rocks in northeastern Borborema Province, NE Brazil. Here, we present the elemental geochemistry and Sr-Nd-Pb isotope results for nephelinites, basanites and (olivine) alkali and tholeiitic basalts with the purpose to assess their magmatic history from source to crystallization. These silica-undersaturated lavas have compositions close to primitive magmas ($10 < \text{MgO} < 15$ wt.% and $200 < \text{Ni} < 500$ ppm) and important enrichment in large ion lithophile and Nb-Ta elements. As a group, they have experienced fractional crystallization of olivine, clinopyroxene and (to a minor extent) plagioclase with negligible crustal assimilation. We have modeled the mantle sources of the MVF basanites and alkali basalts from a garnet-bearing domain existing at the lithosphere-asthenosphere boundary (80–90 km deep), whereas the nephelinites were derived from the convective asthenosphere at ~120 km (melting temperature of ~1,470°C). K/Nb–K/La and Rb/Sr– $^{87}\text{Sr}/^{86}\text{Sr}$ ratio constraints support that the generation of the MVF magmas occurred in the presence of amphibole (plus clinopyroxene) with minor influence of phlogopite. Correlations between the Sr, Nd and Pb isotope compositions indicate mixing between FOZO and EM-type components, likely with minor involvement of DM. The combination of the FOZO-EM signature was also suggested for Early Cretaceous tholeiite dykes that intruded in the same geographic area as MVF, suggesting persistence of FOZO as a lithospheric component for a period near 80 m.y. up to the Cenozoic. The EM component, in turn, represents a deep component derived from metasomatizing fluid-melts that have interacted with an underlaid lithospheric mantle showing FOZO-like characteristics. Because there is no evidence for mantle plume activity or even passive asthenosphere upwelling related to extensive lithospheric thinning processes at the Cenozoic in the Borborema Province, we suggest that melting to generate the MVF magmas would be related with permeability and enrichment degree prevailing in the potentially adiabatic LAB-asthenosphere system existing in that region.

Keywords: Continental alkaline basalts, FOZO endmember, Enriched lithospheric mantle, Borborema Province.

**PETROGENESIS OF ALKALINE ROCKS OF THE MACAU VOLCANIC FIELD,
NORTHEASTERN BRAZIL**

Emmanuel Donald Ngonge^{1*}, Maria Helena Bezerra Maia de Hollanda¹, Márcio Martins Pimentel², Diógenes Custódio de Oliveira³

¹ Department of Mineralogy and Geotectonics, Institute of Geosciences, University of São Paulo, Rua do Lago 562, 05508-080, São Paulo SP, Brazil

² Institute of Geosciences, University of Brasília, 70910-900, Brasília DF, Brazil

³Petrobras/UO-RNCE/EXP/ABIG, Av. Eusebio Rocha 1000, 59064-100, Natal RGN, Brazil

*Corresponding author: donald@usp.br; +55.11.98471.3526

4.1 INTRODUCTION

The Macau volcanism (hereafter named Macau Volcanic Field – MVF) is the most recent magmatic activity documented in the Precambrian shield of the South American platform since the widespread eruption of tholeiitic and alkaline magmatic events related to the opening of the Atlantic Ocean in the Mesozoic (e.g., Paraná Igneous Province, CAMP-Maranhão, Ceará Mirim Dyke Swarm). The rocks of the MVF are exposed in northeast Brazil (northeastern Borborema Province) forming tens of individual eruptive centers spatially distributed in a volcanic field over an area of thousands of square kilometers. The eruptive centers represent an inactive intraplate volcanic system encompassing vents and lava flows that erupted dominantly basaltic magmas. In that sense, they may correspond to ‘monogenetic or polygenetic’ volcanic fields depending on whether the eruptions had occurred as single or multiple episodes (e.g., Connor and Conway, 2000). Monogenetic volcanic fields have been described in different tectonic settings encompassing various areas, number (volume) of centers and longevities (e.g., O'Reilly and Zhang, 1995; Baker et al., 1997; Shaw et al., 2003; Evarts et al., 2009; Kiyosugi et al., 2012; Agustín-Flores et al., 2011; McGee et al., 2013; Boivin and Thouret, 2014). The magma supply feeding each individual volcano is commonly low and, as a result, forms single and usually short-lived eruptions. In contrast, polygenetic volcanoes erupt repeatedly and are sustained by high supply rates to maintain heat and mass flow (e.g., Connor and Conway, 2000; Németh, 2010).

Magma erupted from monogenetic volcanoes can trend along the mixing line between sodic (silica-saturated to -undersaturated) to potassic compositions, in general, resulting in major plate-boundary stresses linked to both intraplate and arc-related settings (e.g., Baker et al., 1997; McGee et al., 2013). Mechanisms to promote melting to feed these volcanoes have been ascribed to either active or passive upwelling of large- to small-scale thermal anomalies related to the convective asthenosphere. A common genetic feature shared by many of these magmatic events is the concurrent involvement of lithospheric and asthenospheric mantle sources. Because the eruptive activity and crustal residence time for each individual volcano are geologically brief, they usually display minor chemical variability because neither wall-rock assimilation nor fractional crystallization are expected to occur in large scale (Kereszturi and Németh, 2013). Thus, the volcanoes have been studied to understand the chemical evolution of the sub-continental lithospheric mantle by providing information about the melting depth/rate and metasomatic interactions in the course of rifting and ongoing lithospheric thinning processes.

Here we present a number of elemental geochemical and isotopic (Sr-Nd-Pb) data for the basalts belonging to the MVF to integrate the investigation of its magmatic history from the source to crystallization. Because the petrology of the MVF has been outlined in previous works (Sial et al., 1981; Fodor et al., 1995, 1998; Knesel et al., 2011, as well a number of unpublished Ph.D. theses), we focus on defining the nature of the mantle (lithospheric and/or asthenospheric) source(s) of such basalts to further support our discussion of the chemical evolution of the sub-continental mantle beneath the northeastern Borborema Province. Therefore, we compared the chemistry of the MVF basalts to that of Cretaceous tholeiites intruded at the same continental area as well as the Fernando de Noronha lavas presently exposed as a group of small oceanic islands 250 km offshore (at ~3°S–32.5°W). We show that these two magmatic events share common OIB-type source(s), although sampling distinct lithospheric mantle domains.

4.2 GEOLOGICAL OVERVIEW

Northeast Brazil comprises the Borborema Province, a geological entity that was part of the West Gondwana supercontinent assembled in the Brasiliano/Pan-African orogeny (e.g., Van Schmus et al., 2008). The Borborema Province preserves vast areas of (Archean to) Paleoproterozoic gneissic to migmatitic rocks, which were the basement for several Meso- to Neoproterozoic sedimentary and volcano-sedimentary basins, all of which metamorphosed and deformed during the orogeny. Neoproterozoic granites also comprise a significant portion of the

Borborema Province in close spatial (but not always cogenetic) association with intermediate to mafic rocks (e.g., Hollanda et al., 2003). Continental-scale shear zones are pervasive, either controlling the ascent and emplacement of these granitoid magmas or representing major boundaries between distinct geological domains. These Neoproterozoic structures are mostly NE- and E-trending and developed under high-temperature and low-pressure ductile conditions (Vauchez et al., 1995; Viegas et al., 2014), usually with late brittle reactivation to accommodate the development of intraplate and marginal rifted basins (e.g., Sénan and Popoff, 1991; Françolin et al., 1994; Bezerra and Vita-Finzi, 2000; Castro et al., 2012). Some of these basins evolved after plate-boundary stresses related to the Gondwana breakup in the Mesozoic.

The Potiguar Basin is an example of a rift reactivated from older Precambrian structures. The basin consists of NE-trending asymmetric grabens developed during the Atlantic opening in the Cretaceous (Matos, 1992). Two mafic magmatic events, exposed in the same geographic area, were temporally related to the basin evolution: (i) tholeiite magmas assembled as the Ceará Mirim dyke swarm (CMDS) and (ii) alkali basalt centers formed the MVF. The CMDS comprises dominantly high-Ti tholeiites (low MgO <5 wt.%) and subordinate low-Ti tholeiites forming a 350-km long E-W trending dyke swarm intruded into the basement rocks. A minor swarm (<100-km long) occurs to the south of the main swarm and is composed of high-Ti olivine tholeiites. The CMDS has been considered the Brazilian counterpart of the tholeiitic magmatism exposed at the Northern Benue Rift (SE Nigeria), the latter corresponding to continental products of the St Helena hotspot during the Cretaceous (Coulon et al., 1996). Recently, Ngonge et al. (submitted) reported isotopic evidence that excludes the direct involvement of the St. Helena plume in the CMDS genesis by modeling the FOZO component as the best source for those olivine tholeiites. The authors confirmed the prediction of Hollanda et al. (2006), who argued that the evolved high-Ti (and low-Ti) tholeiites would be derived from a sub-continental lithospheric mantle exhibiting chemistry similar to a sub-arc mantle modified by an ancient, subduction-related component.

The MVF consists of tens of unconnected eruptive centers forming necks, plugs and lava flows dispersed by approximately 300 km in the N-S direction (Fig. 4.1). These centers are strongly eroded; therefore, it is impossible to estimate the volume of magma erupting at the surface. The MVF encompasses basanites to andesite basalts displaying modal olivine, which show a very uniform chemical signature characterized by small effects of fractional crystallization and negligible crustal contamination (Sial et al., 1981; Fodor et al., 1998; Knesel et al., 2011). A detailed study of the $^{40}\text{Ar}/^{39}\text{Ar}$ geochronology was recently reported in the unpublished PhD thesis of F.V. Silveira (2006). The ages range between 52 and 7 Ma, i.e., a time

interval of approximately forty-five million years of episodic magmatic activity. The results for the youngest (and also smaller) eruptive centers were published in Knesel et al. (2011) and show partial temporal overlap with the eruption of the basaltic lavas of Fernando de Noronha dated at 12–1.3 Ma (Perlingeiro et al., 2013).

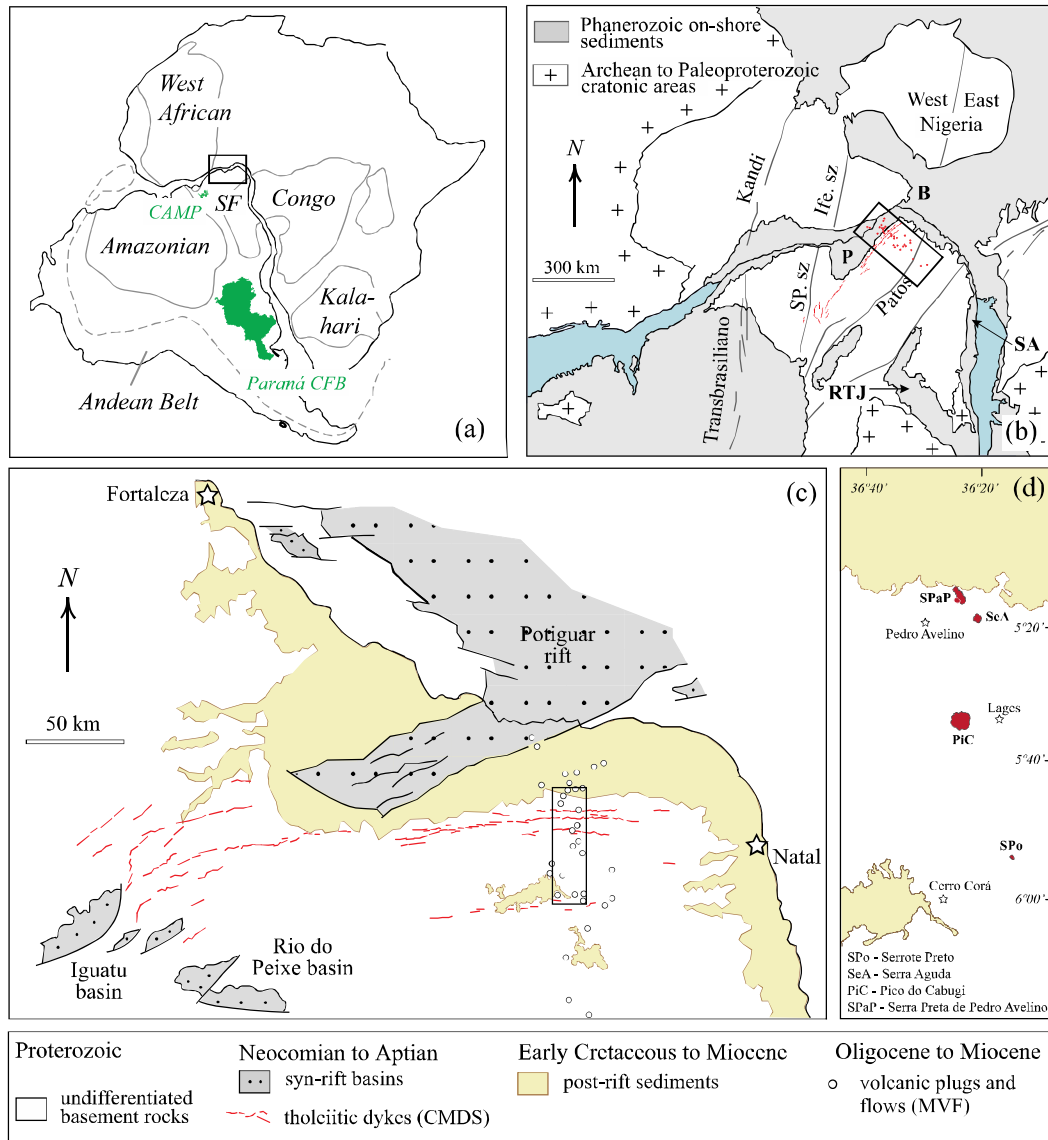


Figure 4.1. (a) Schematic illustration of the West Gondwana with focus on the main Neoproterozoic cratonic areas – Amazonian, São Francisco-Congo, West African and Kalahari. The study area is shown in the box; CAMP-Maranhão (Parnaíba) and Paraná-Etendeka igneous provinces are shown regardless of craton positions. (b) Pre-drift reconstruction of the main geological features of the northeastern Borborema Province and of the West African counterparts (shields of Nigeria and Cameroon) with an emphasis on the major Brasiliano/Pan-African shear zones and major Mesozoic rift systems (B: Benue, RTJ: Recôncavo-Tucano-Jatobá, SA: Sergipe-Alagoas, P: Potiguar). (c) Zoomed-in image of (b) with the geographic location of the MVF eruptive centers (open circles) and CMDS (red lines). (d) Zoomed-in image of (c) to highlight the location of SPo, SeA, PiC and SPaP eruptive centers; minor centers are not shown. See the text for general comments.

The MVF lavas are strongly enriched in incompatible elements relative to the primitive mantle, a feature that typically resembles OIB magmas. The variability of their isotopic compositions was attributed to mixing between asthenospheric (HIMU- plus DM-like) melts interacting with an enriched (EMI-type) lithospheric component (Fodor et al. 1998). In studying a number of peridotite xenoliths hosted in the MVF basalts, Rivalenti et al. (2007) ascribed the EMI signature to an asthenospheric origin similar to the xenoliths from Fernando de Noronha lavas (Rivalenti et al., 2000; Fodor et al., 2002) to support the genetic link between the lithospheric mantle in these two areas (see also Gerlach et al., 1987). These interpretations were challenged by new $^{40}\text{Ar}/^{39}\text{Ar}$ determinations that show no age progression in samples collected both offshore and onshore (Knesel et al., 2011). In contrast with the plume model, the authors propose that the MVF lavas erupted by an edge-driven mechanism (King and Anderson, 1995, 1998).

4.3 SAMPLING STRATEGY

Thirty-four elemental geochemical and isotopic results support the present contribution. A portion of these results was previously reported in the unpublished PhD thesis of the co-author M.H.B.M. Hollanda, including all Sr-Nd isotope data for samples tagged HD and DCO, as well some geochemical results. The old and the new data analyzed for this study are reproduced in Tables 4.1 and 4.2.

From approximately sixty eruptive centers of the MVF, we selected four with good exposures and relatively fresh rocks to determine the major and trace elements. They are Serrote Preto (SPo), Serra Aguda (SeA), Pico do Cabugi (PiC) and Serra Preta de Pedro Avelino (SPaP) – names borrowed from the eruptive centers and known in the literature. According to geochemical similarities, especially with respect to the trace element compositions, samples collected from other eruptive centers have been grouped into any of those four groups. We also analyzed eight other samples for Sr, Nd and Pb isotopes (except samples HD-49 and DCO-98, which were not analyzed for Pb) for which the geochemical data are not available. Because we could not classify them, we opted to consider this subset separately, naming it ‘minor eruptive centers’.

The SPo eruptive center is a small denuded plug approximately 200 meters in diameter and 100 meters high. Samples classified into this subset came from the eruptive center and from other surrounding minor occurrences. Nine samples were analyzed for geochemistry and Sr-Nd

isotopic compositions, but only one was analyzed for Pb isotopes. Four and nine samples, respectively, were investigated from the SeA and PiC eruptive centers. Both represent eroded subrounded volcanic necks of, respectively, ~1 and 5 km in diameter, with PiC having the highest elevation (650 m) of the MVF. Sr-Nd and geochemical data are available for all samples, but Pb isotopes were measured for only three samples of the SeA and six samples of the PiC subsets. Finally, SPaP is a NW-trending fault-controlled lava plateau approximately 5 km long. Six samples were collected at the base of the plateau, and three from a small satellite plug located at the southwestern edge. Geochemistry and Sr-Nd isotopic compositions were measured for all samples, and Pb isotopes were measured for five samples. Finally, ten samples collected from sparse and minor eruptive centers were analyzed for Sr and Nd, and six were analyzed for their Pb isotope compositions. Details on the analytical procedures for mineral chemistry, elemental and isotopic geochemistry can be found as footnotes in Tables 4.1–4.3.

4.4 RESULTS

4.4.1 PETROGRAPHY AND MINERAL CHEMISTRY

The MVF lavas are olivine-phyric displaying textures ranging from tiny-sized microlitic porphyritic in the SPaP samples to microgranular porphyritic in SPo, SeA and PiC. Occasionally, the lavas show intergranular and seriate arrangements. The mineral assemblage includes olivine+clinopyroxene+plagioclase+Fe-Ti oxides, but sub- to millimetric xenocrysts of olivine and pyroxene, as well millimetric peridotite xenoliths are common, mainly in the SPaP lavas. Olivine, pyroxene and plagioclase microphenocrysts comprise approximately 30–40% of the mode, whereas glass may reach up to 30% of the groundmass, especially in the samples showing microlitic texture. Except for the samples of the SPo, for which the mineral chemistry was not investigated, the Fo content in olivine varied from 88 to 77 mol.%, in agreement with both fractional crystallization and equilibrium with peridotitic mantle sources. According to Fodor et al. (1995, 1998), all olivine with $\text{Fo} > 88$ mol.% must be derived from the hosted peridotite xenoliths and is considered as xenocrysts. Pyroxene is essentially diopsidic ($\text{Wo}_{50.8-45.8}\text{En}_{47.2-33.7}\text{Fs}_{14.8-4.1}$) with TiO_2 wt.% varying from 2 to 5 and Mg# (0.86–0.72) compatible with the Fo values measured in olivine. The chemical compositions of plagioclase microphenocrysts from PiC and SeA are dominantly labradorite ($\text{An}_{60.8-71.8}$), although a few crystals with resorbed rims found in SeA display $\text{An}_{29.8-31.5}$, which we assume as xenocrysts. It is common to observe plagioclase (and minor pyroxene) microphenocrysts exhibiting sieved textures, which were

Table 1. Average mineral chemistry of olivine, clinopyroxene and plagioclase of the MVF eruptive centers

Mineral														
<i>Olivine</i>	SiO ₂	Al ₂ O ₃	Cr ₂ O ₃	FeO	MgO	NiO	CaO	Sum	Fo	Fa				
SeA (n = 3)	38.88	0.02	0.03	17.93	42.05	0.22	0.29	99.41	80.6	19.4				
PiC (n = 6)	38.51	0.00	0.02	19.75	40.39	0.19	0.42	99.27	78.4	21.6				
<i>Clinopyroxene</i>	SiO ₂	TiO ₂	Al ₂ O ₃	Cr ₂ O ₃	FeO	MnO	MgO	CaO	Na ₂ O	NiO	Sum	Wo	En	Fs
SeA (n = 6)														
minimum	39.45	0.00	0.03	0.00	14.40	0.21	44.14	0.08	0.02	0.31	98.65	0.1	85.6	14.2
maximum	52.99	0.34	5.33	0.66	2.43	0.05	16.11	21.28	1.01	0.06	100.24	44.9	47.2	4.1
PiC (n = 20)														
minimum	37.332	0.045	0.037	0	25.464	0.371	35.65	0.469	0.006	0.06	99.434	0.7	72.9	26.4
maximum	51.17	1.323	2.98	0.508	5.534	0.045	15.234	22.244	0.383	0.068	99.489	45.9	43.7	9.0
SPaP (n = 10)														
minimum	39.423	0.026	0.028	0.015	16.795	0.285	42.982	0.301	0.034	0.011	99.9	0.4	83.0	16.5
maximum	47.25	2.977	7.789	0.004	5.964	0.106	11.321	22.163	0.516	0	98.09	50.8	36.1	10.9
<i>Plagioclase</i>	SiO ₂	Al ₂ O ₃	FeO	CaO	Na ₂ O	K ₂ O	Sum	An	Ab	Or				
SeA (n = 3)	56.83	27.01	0.45	8.48	5.64	1.35	99.76	42.1	50.1	7.8				
PiC (n = 9)	51.67	30.47	0.99	12.79	3.75	0.47	100.14	63.5	33.8	2.8				
SPaP (n = 5)	51.92	20.15	3.08	7.09	5.12	0.64	70.41	42.6	28.1	3.5				

Notes:

i. Values for olivine and plagioclase are given as average compositions, while for pyroxene as minimum and maximum compositions.

ii. Mineral chemistry data were performed on a JEOL JXA 8230 Superprobe at the University of Rio de Janeiro (Brazil) by using 15 KeV for analysis of olivine, pyroxene and plagioclase and 20 KeV for oxides, and a beam current of 20 nA. Corrections and calibrations were done according to the PROZA program (Bastin and Heijligers, 1990).

interpreted as resulting from melt mixing processes at shallow mantle depths (Fodor et al., 1998). However, it may also correspond to disequilibrium textures due to rapid decompression (Nelson and Montana, 1992), a feature that is predicted in monogenetic volcanoes.

4.4.2 MAJOR AND TRACE ELEMENT GEOCHEMISTRY

Even carefully preventing visible fragments of the peridotitic xenoliths usually hosted by the basalt lavas, it is possible that some disaggregated sub- to milimetric-sized olivine xenocrysts were powdered together with the whole-rock. This was critical and probably occurred in some samples of the SPaP eruptive center (SP-1, DCO-101 and -102, HD-31). As result, the samples had slightly inflated MgO (and Ni) contents, which led us to consider them carefully in our petrogenetic interpretations.

All oxide analyses were plotted after recalculating the values to free-LOI (loss on ignition) basis, although all studied samples can be taken as fresh because they had an LOI of less than 2 wt.%. Silica and total alkalis contents plot in the alkaline field on the TAS diagram (Fig. 4.2a) trending from nephelinites to basanites and alkali (olivine) basalts, whereas three samples of the SPaP eruptive center consisted of mostly primitive magmas with SiO₂<41.5 wt.% and MgO ~14.2–15.7 wt.%. As a whole, the MVF basalts represent mixtures of sodic to slightly potassic compositions (K₂O/Na₂O=0.26–0.63), except for the three samples from SPaP, which

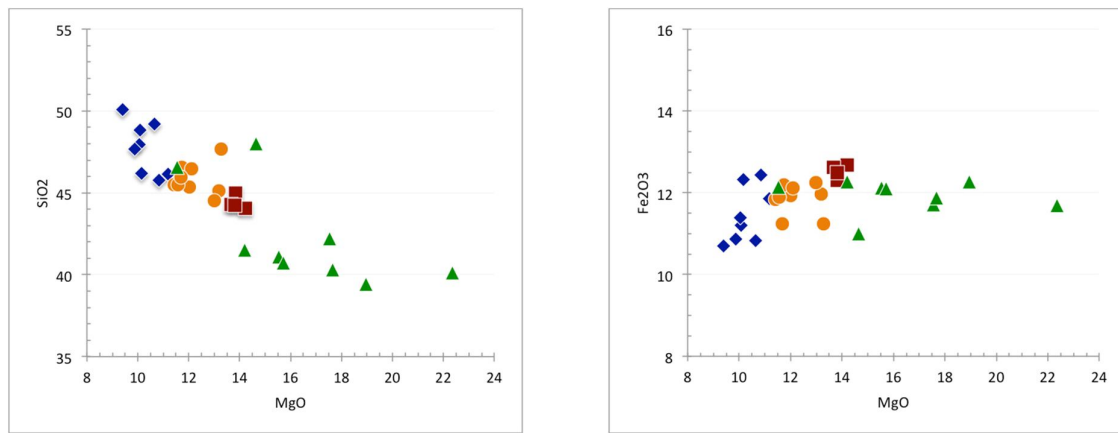
are all sodic ([Fig. 4.2b](#)). The Mg# ranged from 74 to 77 in the SPaP nephelinites and from 64 to 72 in the basanites and alkali basalts, with SPo having the highest and most variable SiO₂ (44.2–50.6 wt.%) contents and the lowest Mg# values. All samples were SiO₂-undersaturated rocks with variable %Ne_{norm} and %Ol_{norm} of, respectively, 5–12 and 14–22 for the basanites and the alkali olivine basalts of SPo, SeA and PiC, and 9–18 and 18–37 for nephelinites occurring in SPaP. Except for SeA, the other three eruptive centers also include olivine tholeiitic basalts with normative hypersthene >2.3.

In the Harker diagrams, it is evident that fractional crystallization of olivine and pyroxene (plus Fe oxides) affected the magmatic history of each volcanic center, as indicated by the decreasing of Ni, Cr, CaO and Fe₂O_{3T} as the MgO decreased ([Fig. 4.3](#)). This evidence is corroborated by the variability observed through the Fo content (88–77) and the Mg# (0.86–0.72) measured in the olivine and pyroxene crystals of SeA, PiC and SPaP. In contrast, the increasing Al₂O₃/CaO (not followed by Sr) suggests that plagioclase was preferentially accumulated instead of fractionating from the primary magmas, whereas Ba decreases jointly

Table 2. Major and trace element data for MVF eruptive centers

Volcanic center coordinates		Serrrote Preto - SPo Lat. 5°54'S/Long. 36°15'W							Serra Aguda-SeA Lat. 5°18'S/Long. 36°22'W					
Sample tag		HD-48	HD-51	DCO91	DCO92	DCO93	DCO95	DCO96	DCO97	DCO99	SA2	SA3	HD29	HD45
wt.%														
SiO ₂		48.63	48.4	45.8	49.71	45.45	45.7	50.2	47.7	47.14	44.81	43.96	44.09	43.68
TiO ₂		2.01	2.02	2.27	1.85	2.54	2.51	2.34	2.07	2.13	2.36	2.44	2.44	2.44
Al ₂ O ₃		12.95	13.58	12.61	14.48	13.28	12.69	14.85	13.29	13.74	11.66	11.18	11.69	11.49
Fe ₂ O ₃		10.71	11.11	12.44	10.63	12.14	11.74	10.29	11.33	10.75	12.26	12.65	12.56	12.33
MnO		0.14	0.16	0.17	0.14	0.16	0.16	0.12	0.16	0.15	0.18	0.19	0.18	0.18
MgO		10.52	10	10.85	9.33	10	11.08	7.34	10	9.77	13.77	14.18	13.6	13.63
CaO		9.3	9.14	9.7	8.47	9.83	10.06	7.53	9.42	10.17	9.46	9.63	9.97	9.69
Na ₂ O		2.93	2.95	3.93	3.47	2.79	3.11	3.76	3.62	3.08	3.18	3.15	2.77	3.03
K ₂ O		1.24	1.31	1.62	0.9	1.65	1.44	2.16	1.26	1.52	1.07	1.47	1.54	1.55
P ₂ O ₅		0.39	0.37	0.65	0.31	0.6	0.49	0.52	0.54	0.45	0.65	0.75	0.68	0.74
LOI		1.36	1.58	0.84	1.16	1.98	1.8	1.75	0.71	1.49	1.03	0.63	0.94	0.61
SUM		100.18	100.7	100.93	100.45	100.42	100.86	100.91	100.2	100.39	100.61	100.39	100.46	99.37
ppm														
Cr		418	335	349	na	na	342	157	335	na	650	746	593	582
Co		191	186	192	92	189	226	177	165	207	54	57	200	214
Ni		263	174	227	139	151	204	88	167	163	401	414	423	330
Pb		2.2	1.8	1.9	na	2.5	2.4	2.2	2.8	na	2.5	2.8	na	na
Rb		35	32	26	24.2	47	49.2	60.5	34.3	38.5	26.7	37.3	41	46
Sr		500	558	779	520	1104	704	725	631	615	726	778	779	848
Y		22	20.8	21.9	19.2	21.9	21.7	20.7	22.7	20.6	24.8	25.2	26	30
Zr		161	150	167	133	206	184	229	172	160	206	218	157	208
Nb		39	36.6	53.6	28.4	60.4	48.8	63.8	54.6	42.4	58.2	63.9	57	70
Ba		388	389	434	337	596	520	668	485	477	630	553	525	587
Hf		3.8	4.8	4.5	4.1	5.4	4.9	6.5	5.1	4.6	4.7	4.6	3.7	4.7
Ta		2.3	2.4	3.4	2	3.7	3.1	4.5	3	2.5	3.5	3.8	3.6	4.7
Th		4	3.7	4.3	3.2	5.8	4.7	7.2	10	4.1	5.3	6.8	6.2	6.9
U		1	1	1.1	0.8	1.4	1.1	1.8	2	0.9	1.3	1.6	1.7	2
La		20.7	26.9	36.3	22.2	41.1	37	46.4	52.7	30.5	43.9	49.9	42.5	55.5
Ce		43	52.7	69.2	44.5	82	74.1	89.9	94.9	60.8	83.6	91.1	83.4	105
Pr		5.2	6.5	7.8	5.6	9.6	8.9	10.6	10.1	7.3	9.7	10.9	9.6	12.2
Nd		24.9	27.2	34.1	23.2	38.6	36.4	43.2	39.4	29	38.4	42.6	37.3	49.3
Sm		6.3	5.9	7.2	5.6	8.1	7.2	8.9	7.1	6.3	8.1	8.6	8.4	10.1
Eu		2.01	1.9	2.3	1.7	2.6	2.4	2.7	2.3	2.1	2.5	2.6	2.46	3.06
Gd		5	5.9	6.7	5.3	7.3	6.9	7.7	6.8	6	7.5	7.9	6.2	8
Tb		0.8	0.9	0.9	0.8	1	1	1	1	0.9	1	1	1	1.2
Dy		4.5	4.7	4.4	4.2	5.1	4.8	5.1	5	4.5	5.6	5.9	5.5	6.2
Ho		0.8	0.9	0.8	0.8	0.8	0.9	0.8	0.9	0.9	1	1	1	1.1
Er		2	2	1.8	1.8	2	2	1.9	2.3	2.1	2.3	2	2.4	2.8
Tm		0.3	0.3	0.2	0.3	0.3	0.3	0.2	0.3	0.3	0.3	0.3	0.3	0.3
Yb		1.3	1.5	1.5	1.4	1.5	1.5	1.4	1.6	1.7	1.7	1.8	1.8	2
Lu		0.18	0.2	0.2	0.2	0.2	0.2	0.2	0.2	0.2	0.3	0.2	0.24	0.26

The chondrite-normalized rare earth element (REE) patterns are shown in Fig. 4.4, and all demonstrate enrichment in light rare earth (LRE) elements, as commonly observed in strongly silica-undersaturated basalts. The enrichment is more significant in the SPaP samples than in the other eruptive centers, the latter showing similar $(\text{La}/\text{Yb})_{\text{N}}$ ratios of 11–22 (together with two SPaP samples – SP-2 and SP-3 collected from the adjacent plug), in contrast to the values of 32–41 calculated for the other HD- and DCO-tagged samples of SPaP lava flows. No Eu anomaly is observed, reinforcing that plagioclase precipitation was not an important process in the course of crystallization. Primitive mantle-normalized incompatibility profiles show overall enrichment in large ion lithophile (LIL) elements (right side of Fig. 4.4) from Rb to Ce, together with a negative Pb spike and downward slope to the less incompatible elements – a typical feature of OIB magmas. There is a good resemblance between the ‘spidergrams’ of SPo, SeA and PiC and samples SP-1 and SP-2 from SPaP, the undeniable effects of fractional crystallization observed for the SPo samples. Again, the HD- and DCO-tagged lavas of the SPaP eruptive center differ from the others by showing a downward concavity on the left side of their incompatible profiles defined by high normalized-abundances from Ba to Ce (Rb is depleted relative to Ba), which exceeded 100 times the values of the primitive mantle of Sun and McDonough (1989).



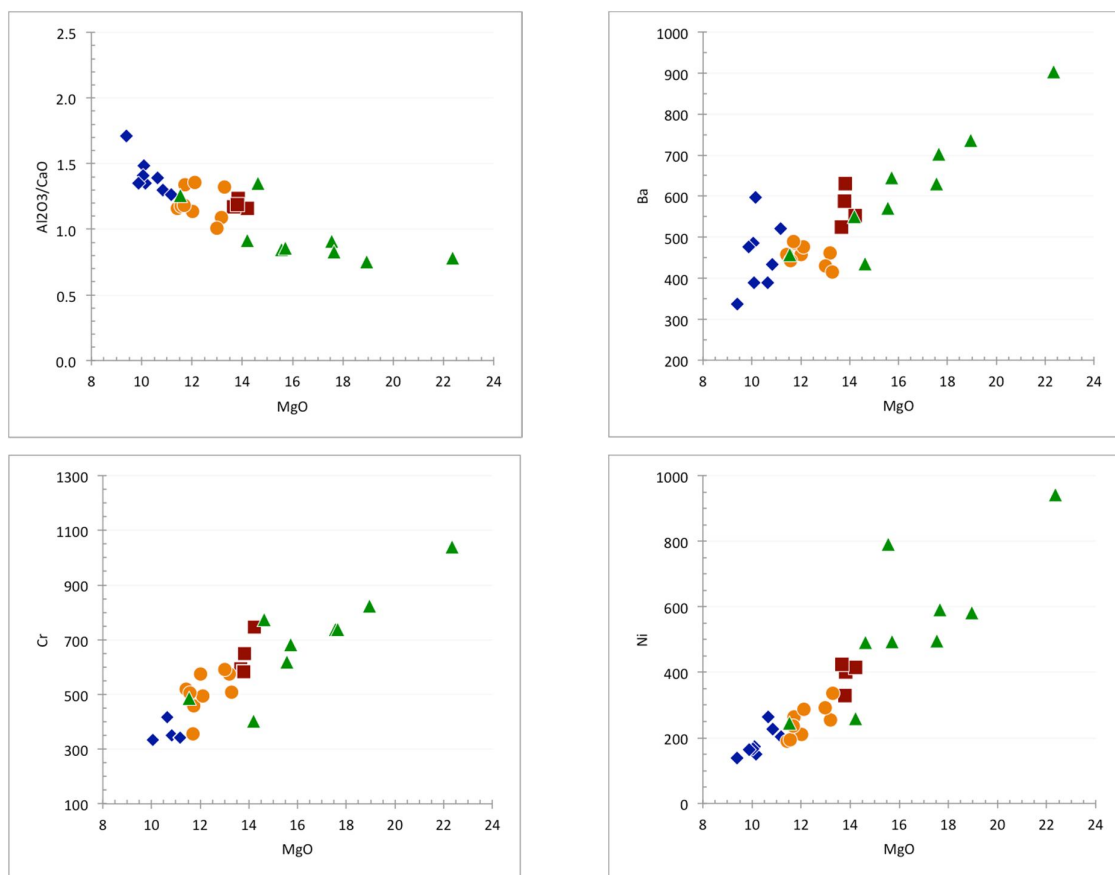
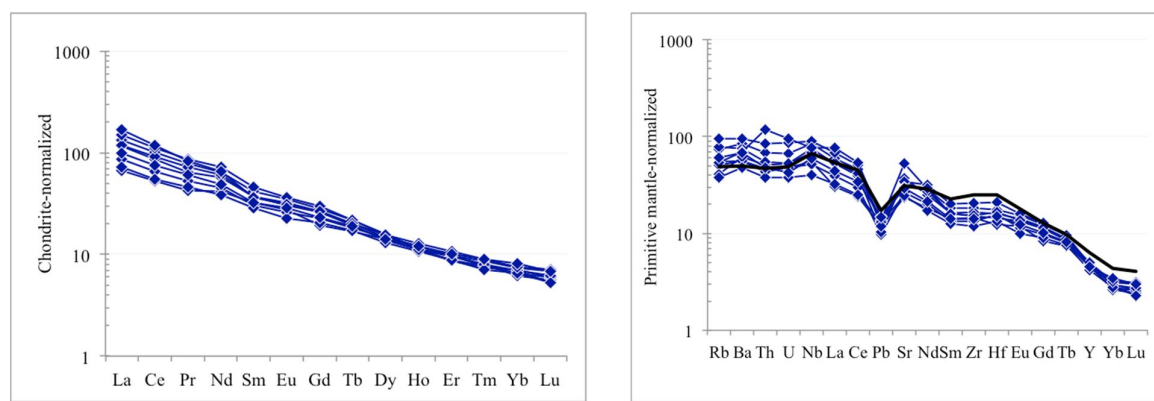


Figure 4.3. Variation diagrams of major elements against MgO. Symbols are as in Figure 4.2.



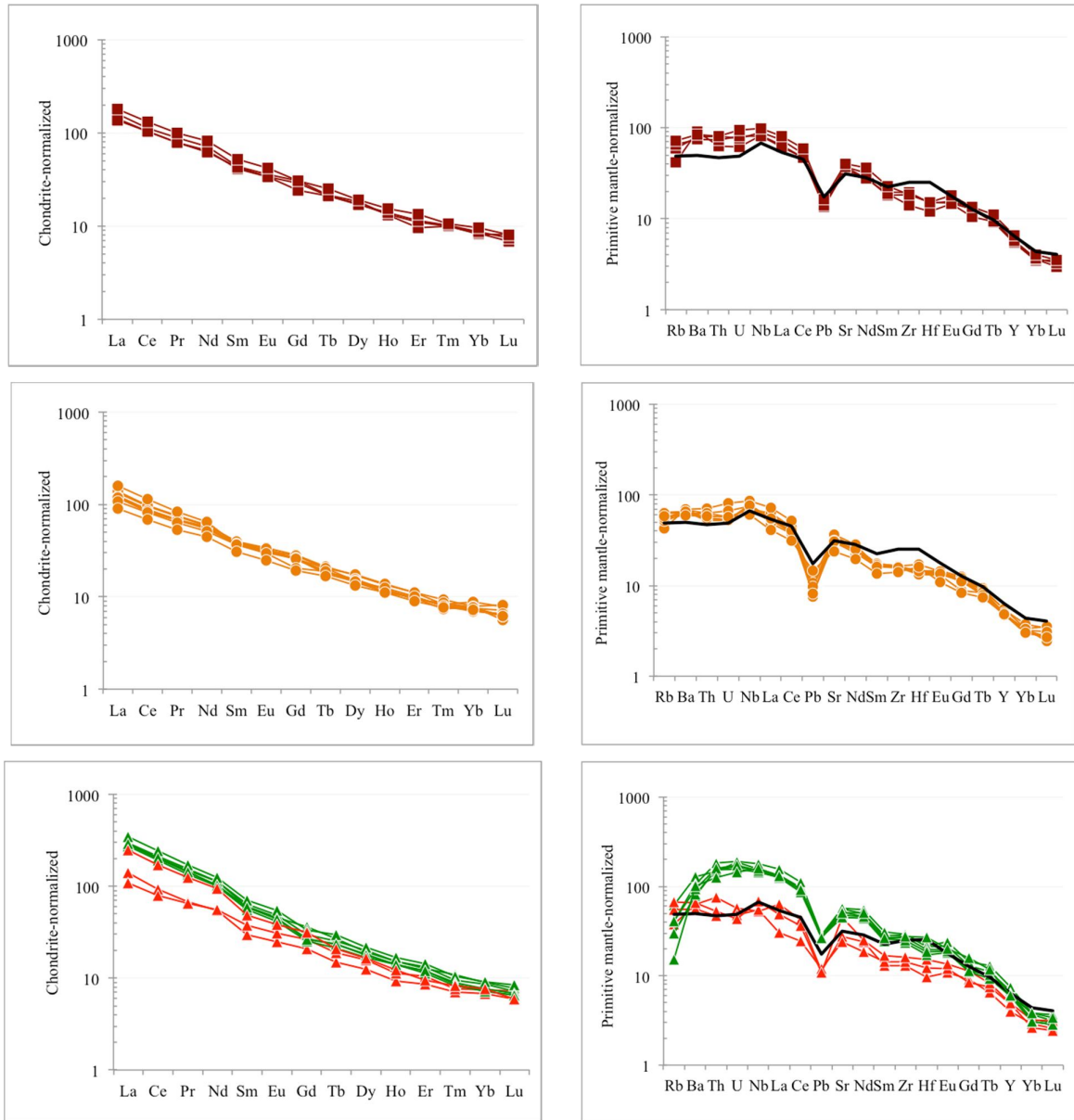


Figure 4.4. Profiles for the average abundances of (a) chondrite-normalized REE and (b) PM-normalized incompatible element patterns. Comparisons are made between the OIB average compositions presented by [Sun and McDonough \(1989\)](#). Normalization parameters are drawn from (a) [Boynton \(1984\)](#) and (b) [Sun and McDonough \(1989\)](#). Symbols are as in Figure 4.2.

4.4.3 SR-Nd-Pb ISOTOPE COMPOSITIONS

The isotope compositions of all samples are plotted in diagrams in the [Figure 4.5](#), but we focus on those from (a) to (d) in this section and discuss the overall results later in this paper. All results are plotted as present-day (measured) isotopic compositions because their ages are still unpublished results in [F.V. Silveira \(2006\)](#). Moreover, with present-day values, we can make more reliable comparison with modern mantle end-members, as illustrated.

Table 3. Sr, Nd, and Pb isotopic compositions of the MVF basalts

Volcanic center Sample tag	Measured (present day) isotopic compositions										
	$^{87}\text{Sr}/^{86}\text{Sr}$	$^{143}\text{Nd}/^{144}\text{Nd}$	$^{206}\text{Pb}/^{204}\text{Pb}$	$^{207}\text{Pb}/^{204}\text{Pb}$	$^{208}\text{Pb}/^{204}\text{Pb}$	$^{87}\text{Rb}/^{86}\text{Sr}$	$^{147}\text{Sm}/^{144}\text{Nd}$	$\epsilon(\text{Nd})_{t=0}$	$^{207}\text{Pb}/^{206}\text{Pb}$	$^{208}\text{Pb}/^{206}\text{Pb}$	$^{208}\text{Pb}^*/^{206}\text{Pb}^*$
Serrrote Preto-Spo											
HD-48	0.70461	0.512688	18.858	15.6	39.136	0.202	0.153	1.0	0.827	2.075	1.011
HD-51	0.70569	0.512519				0.166	0.132	-2.3			
DCO-91	0.70375	0.512757				0.097	0.127	2.3			
DCO-92	0.70600	0.512415				0.135	0.146	-4.4			
DCO-93	0.70576	0.512651				0.123	0.127	0.3			
DCO-95	0.70505	0.512603				0.202	0.119	-0.7			
DCO-96	0.70538	0.512647				0.241	0.125	0.2			
DCO-97	0.70471	0.512500				0.157	0.109	-2.7			
DCO-99	0.70502	0.512454				0.181	0.131	-3.6			
Serra Aguda-SeA											
SA-2	0.70465	0.512709	19.162	15.670	39.224	0.106	0.127	1.4	0.818	2.047	0.989
SA-3	0.70410	0.512721	19.343	15.701	39.375	0.139	0.122	1.6	0.812	2.036	0.986
HD-29	0.70472	0.512702	19.111	15.602	39.09	0.152	0.136	1.3	0.816	2.045	0.981
HD-45	0.70440	0.512599				0.157	0.124	-0.8			
Pico do Cabugi (Pic)											
PC-1	0.70430	0.512713	18.862	15.592	38.922	0.157	0.126	1.5	0.827	2.064	0.989
PC-2	0.70435	0.512707	18.846	15.592	38.9	0.157	0.136	1.4	0.827	2.064	0.988
PC-3	0.70431	0.512704	18.822	15.577	38.853	0.135	0.135	1.3	0.828	2.064	0.985
PC-4	0.70425	0.512702	18.829	15.577	38.854	0.127	0.128	1.3	0.827	2.064	0.985
PC-B2	0.70472	0.512599	18.764	15.608	39.154	0.183	0.131	-0.8	0.832	2.087	1.023
PC-B3	0.70480	0.512607	18.817	15.611	39.178	0.176	0.131	-0.6	0.830	2.082	1.020
HD-33	0.70437	0.512745				0.103	0.139	2.1			
HD-42	0.70553	0.512589				0.151	0.136	-1.0			
HD-46	0.70396	0.512652				0.214	0.112	0.3			
Serra Preta de Pedro Avelino (SPaP)											
SP-1	0.70382	0.512782	19.151	15.595	39.114	0.060	0.101	2.8	0.814	2.042	0.979
SP-2	0.70515	0.512389	18.359	15.572	38.728	0.119	0.107	-4.9	0.848	2.109	1.022
SP-3	0.70461	0.512671	18.726	15.596	38.775	0.129	0.133	0.7	0.833	2.071	0.987
DCO-101	0.70401	0.512748	19.173	15.540	39.080	0.054	0.112	2.2	0.811	2.038	0.973
DCO-102	0.70392	0.512808				0.058	0.109	3.3			
HD-31	0.70399	0.512834				0.068	0.111	3.8			
HD-41B	0.70390	0.512775	19.155	15.542	39.002	0.026	0.104	0.6	0.811	2.036	0.967
HD-43	0.70419	0.512669				0.096	0.112	0.6			
HD-44	0.70382	0.512695				0.063	0.112	1.1			
Minor eruptive centers*											
HD-30	0.70390	0.512866	19.192	15.556	39.108		0.103	4.5	0.811	2.038	0.974
HD-49	0.70576	0.512582					0.153	-1.1			
HD-50	0.70329	0.512854	19.148	15.533	38.715		0.127	4.2			
HD-52	0.70512	0.512197	18.224	15.483	38.251		0.125	-8.6	0.850	2.099	0.984
DCO-69	0.70368	0.512773	18.898	15.538	38.695		0.138	2.6	0.822	2.048	0.961
DCO-94	0.70561	0.512407	18.298	15.502	38.497		0.134	-4.5	0.847	2.104	1.003
DCO-98	0.70467	0.512665					0.128	0.5			
DCO-100	0.70430	0.512740	18.966	15.530	38.802		0.130	2.0	0.819	2.046	0.966
DCO-103	0.70418	0.512747	18.923	15.508	38.891		0.105	2.1	0.820	2.055	0.979
DKST	0.70431	0.512634				0.232	0.123	-0.1			

Except for part of the SPo and two minor eruptive centers, all other investigated basalts are conspicuously spread along the ‘mantle array’ as defined by Zindler and Hart (1986) (Fig. 4.5a). Most of them cluster on the depleted end of the array, displaying radiogenic Nd (higher than CHUR) and unradiogenic Sr (lower than BSE) isotopic ratios, the most enriched and depleted Sr-Nd-coupled compositions given by two minor eruptive centers (HD-52: 0.70512, 0.512197 and HD-50: 0.70329, 0.512854). The samples not enclosed within the array deviate towards more variable and slightly radiogenic Sr relative to chondritic to sub-chondritic Nd values. In binary diagrams including Pb isotopic ratios, the MVF basalts have relatively coherent behavior with slightly radiogenic $^{206}\text{Pb}/^{204}\text{Pb}$ ratios ranging between 18.73 and 19.34 combined with moderate $^{208}\text{Pb}/^{204}\text{Pb}$ (38.7–39.4) and $^{207}\text{Pb}/^{204}\text{Pb}$ (15.48–15.67) ratios (Fig. 4.5b-d). The samples all cluster above and parallel to the Northern Hemisphere Reference Line (NHRL) with both positive $\Delta 7/4$ (~9–16) and $\Delta 8/4$ (~23–70) values. The Sr-Nd isotopic inconsistency observed for a few samples of the SPo and for some minor eruptive centers relative to the whole group could not be confirmed in the modeling made using Pb data because only two of them had their Pb isotopic compositions determined. However, the subset of three samples plotted at the lower end of the Sr-Nd mantle array coherently plot as a separate group deviating towards more unradiogenic Pb values in the other diagrams (Fig. 4.5b-f), thus requiring the presence of an enriched component in the MVF mantle source.

4.5 DISCUSSION

4.5.1 FRACTIONAL CRYSTALLIZATION AND CRUSTAL ASSIMILATION

Before using the geochemical and isotopic dataset to constrain the origin of the mantle sources for the MVF basalts, we need to certify the primary nature of our samples. Except for the SPo samples that have Mg# ~0.61–0.68 (average Ni ~175 ppm), combined with large variation in silica contents, all other MVF basalts had low silica (≤ 50 wt.%) and high MgO (mostly >11 wt.%, to Mg# ≥ 0.68) contents, and the average Ni and Cr for each SeA, PiC and SPaP ranged

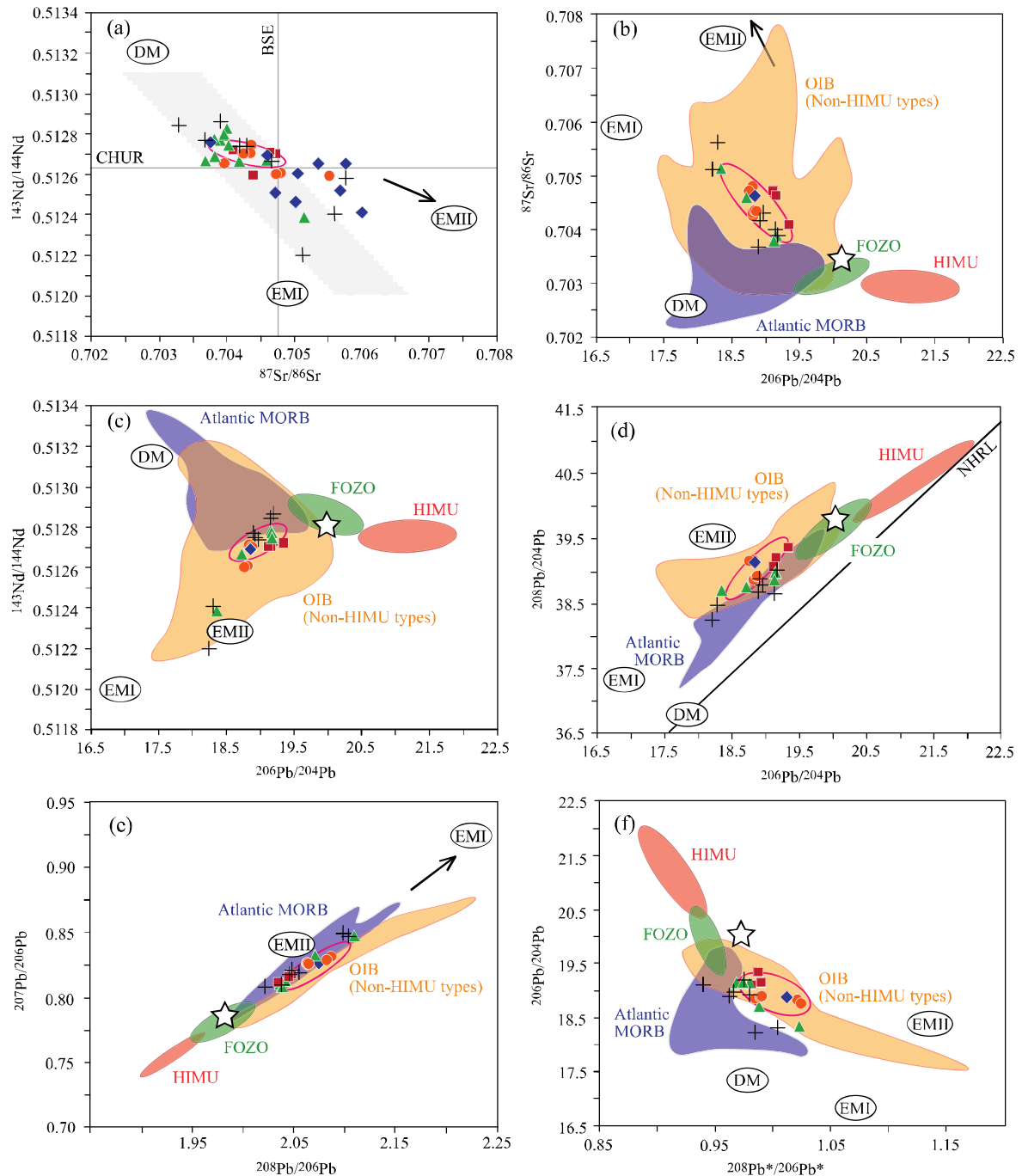


Figure 4.5. Isotopic companion plots used to compare the Sr, Nd and Pb signatures of the four MVF lava groups to the distinct mantle endmembers – HIMU, FOZO and EM (I and II). The sources are: HIMU and FOZO – Stracke et al. (2005), EMI-II estimated after Lustrino and Dallai (2006). Atlantic MORB and non-HIMU OIBs, as defined by Stracke et al. (2005), are also included for comparison (the fields for both Pacific and Indian MORB are not shown). The isotopic compositions of the CMDS FOZO-type olivine tholeiites (open star) and Fernando de Noronha lavas (pink ellipse) are shown for comparison. In (a) the shaded area is an approximation of the ‘mantle array’. All ratios are plotted as present-day values. Symbols are as in Figure 4.2, now including the ‘minor eruptive center’ group as crosses.

from 290–540 and 500–700 ppm, respectively, which satisfies the frequently used criteria for primitive (uncontaminated) magmas (Frei et al., 1978). Major variability in the elemental and isotopic compositions is observed for the subsets of the SPo and PiC samples, but the whole MVF was plotted along a unique tendency, indicating continuous fractionation of olivine and pyroxene, whereas plagioclase had a minor effect in the variability, as shown by the inverse correlation of $\text{Al}_2\text{O}_3/\text{CaO}$ and the random distribution of Sr (and Rb) with MgO. In contrast, Ba correlates positively with MgO, suggesting that although it was not identified as a modal phase, amphibole was likely present in the source.

A number of trace element ratios have been used to test crustal assimilation in mafic magmas ascending through the crust. For instance, Nb/U ratios can indicate chemical alteration by weathering or crustal assimilation because U is a highly incompatible element and accumulates into both lower and upper continental crusts. As a consequence, the average Nb/U ratios in these crustal reservoirs are significantly lower (e.g., Rudnick and Fountain, 1995) than the values typically found in oceanic (uncontaminated) basalts ($= 47 \pm 10$, Hofmann et al., 1986). Similarly, the correlations between ratios of highly incompatible and compatible (or lesser incompatible) elements, such as La/Sm, Ce/Pb and Pb/Nd (also $\text{P}_2\text{O}_5/\text{Nb}$) with the isotope ratios (not expected to vary through fractional crystallization) indicate role of crustal assimilation. Our results indicate that the Nb/U values found for the MVF fall within the range of oceanic lavas, although the SPaP samples display slightly lower values (~34), and the Ce/Pb values are overall >30 (a few samples ~20). These high values are consistent with the values reported for OIBs, especially those found in the HIMU (high U/Pb) endmember (Willbold and Stracke, 2006). When comparing Ce/Pb, $(\text{La}/\text{Sm})_N$ and $\text{P}_2\text{O}_5/\text{Nb}$ with $^{87}\text{Sr}/^{86}\text{Sr}$ ratios, no consistent trend towards crustal compositions was observed (Fig. 4.6a-c). Also, when the silica contents are plotted against the $^{87}\text{Sr}/^{86}\text{Sr}$ ratios, SeA shows no correlation, whereas SPo is dispersed, having two of the most radiogenic samples corresponding with the highest silica contents of ~50 wt.%. PiC shows a slight tendency to correlation (if excluding outliers), also followed by the two samples (SP-2 and SP-3) from SPaP (Fig. 4.6d). Therefore, although there is no compelling evidence towards large assimilation of crustal materials in the MVF magmas (as previously found by Fodor et al., 1998), there are samples that may record minor interactions of their parental magmas with crustal material. However, the geochemical and isotopic coherence of the ‘contaminated’ samples compared with other eruptive centers confirm that the chemical signature of the MVF basalts must reflect characteristics inherited from the mantle source(s) and melting-related processes.

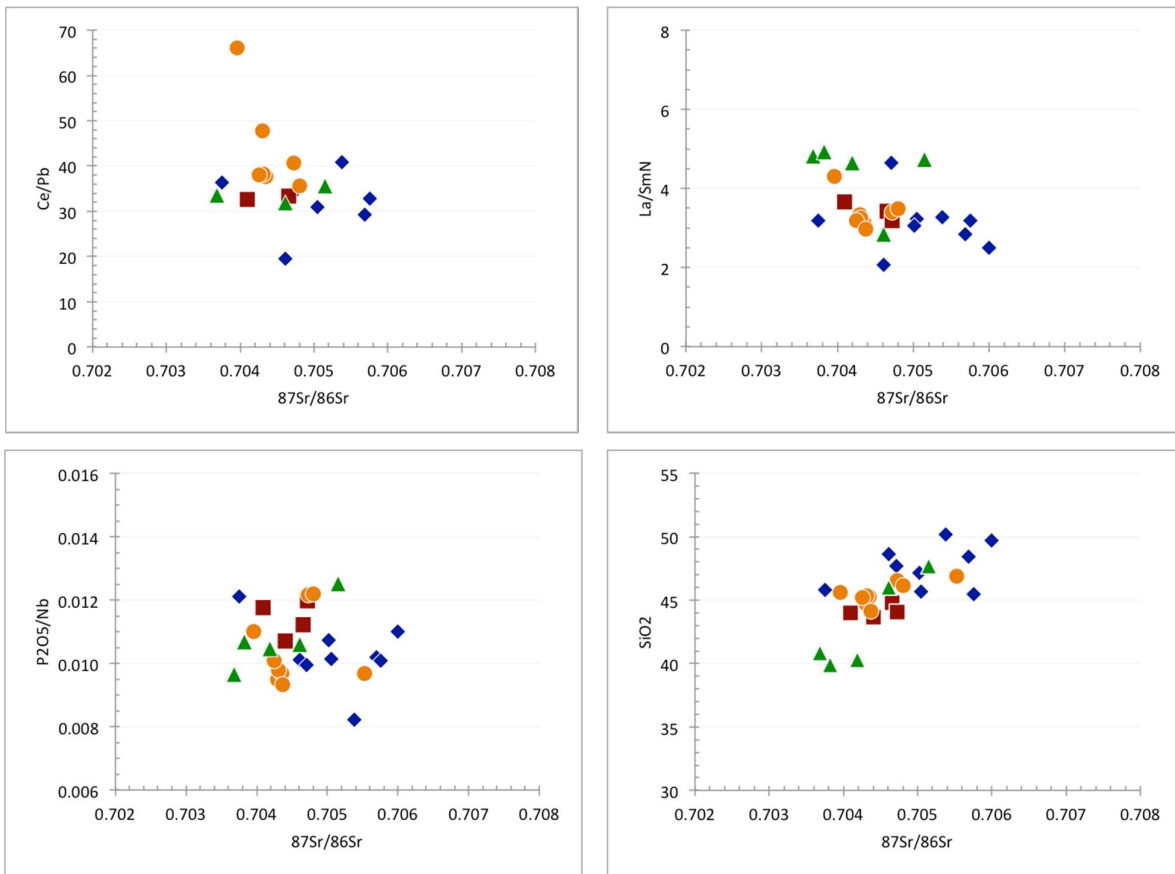


Figure 4.6. Plots of ratios between incompatible trace elements (and oxide – P_2O_5) against SiO_2 to qualitatively evaluate the extent of crustal contamination. Symbols are as in Figure 4.2.

4.5.2 ESTIMATION OF THE MELTING DEGREE AND MELT FRACTION

Except for the discrete correlation observed for the SeA basanites, the La/Sm ratios in the MVF basalts are not affected by fractionation because La is not a highly compatible element within any major fractionating mineral phase. Thus, we accept that the variation in the $(\text{La}/\text{Yb})_N$ ratios observed for each group can be better explained by small differences in melting degrees in a source containing residual garnet. The presence of garnet in the source of the MVF magmas can be corroborated by looking at the $(\text{Tb}/\text{Yb})_N$ ratio because Tb is difficult to fractionate in the absence of residual garnet (Fig. 4.7a). Thus, melts in equilibrium with garnet have higher Tb/Yb ratios (e.g., Wang et al., 2002), and the ratios are >2 in all studied samples.

The major difference regarding the REE patterns of our results is the higher $(\text{La}/\text{Yb})_N$ ratios of the SPaP subset compared with the others (Fig. 4.7b). Because La is more

strongly incompatible than Yb, smaller degrees of melting of (combined with major proportion of) a garnet-bearing source result in the more fractionated patterns found in the SPaP nephelinites. To minimize the effects of crystal fractionation and olivine accumulation, we selected only the 17 samples with MgO between 10 to 15 wt.% and Ni abundance from 200 to 500 ppm to constrain the partial melting degrees and the respective melt fractions on the $(\text{Dy}/\text{Yb})_N$ vs $(\text{La}/\text{Yb})_N$ diagram of Thirlwall et al., (1994). The covariance between these ratios along a mixing line formed by SPo, SeA and PiC alkali basalts and basanites define the role of ~5% of partial melting of spinel-facies lherzolite source ($\text{Dy}/\text{Yb}_N = 1.3$) and ~1% of partial melting of garnet-facies peridotite, with a melt fraction of 70:30 garnet:spinel. SPaP nephelinites, in turn, equilibrated from very low melting degrees (<0.1%) of garnet mantle sources with a major contribution (melt fraction 80:20) instead spinel-facies peridotite. The resulting melts segregate from depths close to 80–90 km for SPo, SeA and PiC, and ~120 km for SPaP based on the calculation of the equilibrium temperatures using the major oxide (SiO_2 and MgO) contents after Albarède (1992) and Scarrow and Cox (1995). The estimated temperatures of 1,350–1,400°C and ~1,470°C are consistent with the calculations of Herzber et al. (2007) for the melting temperatures of primary magmas with MgO contents of 10–14 wt.% (1,280–1,400°C) and 18–19 wt.% (~1,500°C). Because garnet is stable at temperatures above 1,100°C (Green and Ringwood, 1968), we argue that all MVF magmas were derived from sources with residual garnet in different proportions, and the SPaP magmas formed at deeper mantle regions.

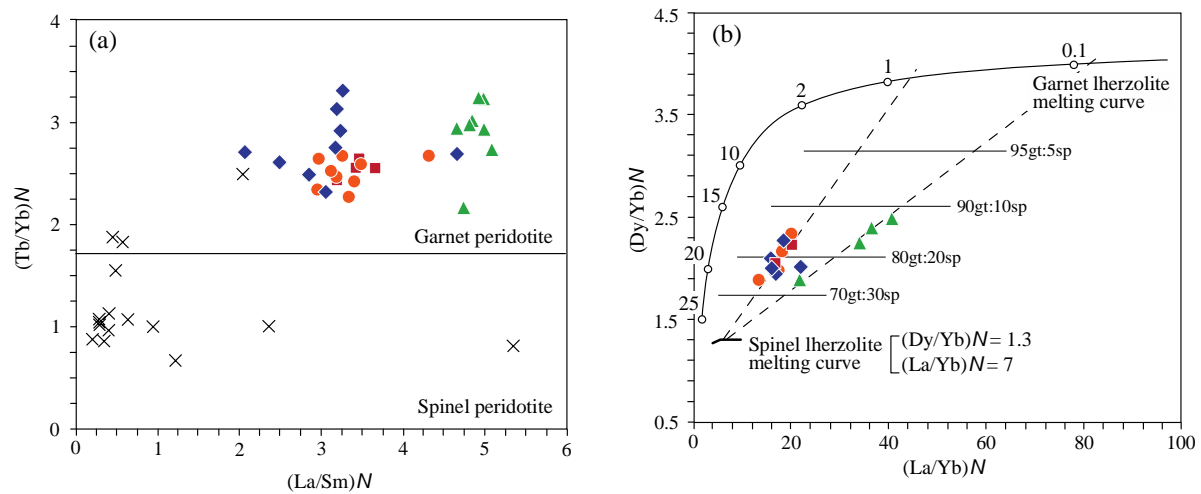


Figure 4.7. (a) Correlation between the normalized-La/Sm and Tb/Yb ratios showing that the MVF compositions are compatible with the melting of garnet-bearing mantle sources. Exes are the values found for spinel peridotite xenoliths hosted by these lavas (Rivalenti et al., 2007) and are shown for comparison. The horizontal line separates the two fields proposed by Wang et al. (2002) for the Basin and Range basalts. (b) Model of mixing curves between spinel and garnet lherzolite melts using normalized-Dy/Yb and La/Yb ratios to estimate rates of partial melting and magma sources for the MVF magmas. Symbols are as in Figure 4.2.

Primitive, mantle-normalized incompatible trace element patterns show generally coherent behavior throughout the basanites and alkali (and tholeiitic) basalts of the SPo, SeA and PiC eruptive centers. All centers show LIL (also Nb-Ta) enrichment, strong Pb (and K, not shown in Fig. 4.4) depletion and, to a minor extent, depletion in Sm relative to Nd. Excluding the samples in which we noted ‘inflation in MgO’, the SPaP nephelinites collected from the lava plateau (samples HD and DCO) are the most magnesian and have the most enriched incompatible trace element compositions of the MVF.

A decrease in the CaO/Al₂O₃ ratio from the nephelinites towards the basanites and alkali basalts is a first evidence to suggest melting from hydrated peridotite sources (e.g., Francis and Ludden, 1995). The role of hydrous mineral phases in the mantle sources can be evaluated from the correlation of the ratios between trace elements that are highly compatible with phlogopite and amphibole against those that are moderately compatible. Both Rb and Ba have partition coefficients for phlogopite that are higher than those found for amphibole (phl: $D_{Rb} \sim 6, D_{Ba} \sim 3$; amph: D_{Rb} and $D_{Ba} < 0.6$ at variable pressure conditions), whereas they compete for Sr (Adam et al., 1993; La Tourette et al., 1995); therefore, melts extracted from phlogopite are expected to have higher Rb/Sr and lower Ba/Rb values than those formed from amphibole-bearing peridotites. All MVF basalts have Rb/Sr < 0.1 and high and minimally variable Ba/Rb ratios ranging from 11 to 18. More extreme values were found in the SPaP subset (>23). However, one important depletion in Rb relative to Ba was observed for the SPaP nephelinites, whereas the ratio was normal for the SeA and PiC samples, suggesting that (minor volumes of) phlogopite may have coexisted deeply in the SPaP mantle source. Using the same argument and accepting that $D_K > K_{La}$ in K-rich amphiboles (exceeding 1, according Francis and Ludden, 1995), the resulting primitive melts from amphibole-bearing peridotites would have $(K/La)_N < 1$, a value that matches those found for our samples (Fig. 4.8a). Furthermore, because D_{Nb} and D_{Zr} are low in amphibole (~0.2–0.1 and ~0.35–0.25, respectively; e.g., Chazot et al., 1996), its presence does not hinder enrichment in Nb in the magma supply melted from such a source and would have no significant effect on the Zr and Hf contents. In contrast, these contents would be negatively impacted if large amounts of clinopyroxene also existed as a residual phase (e.g., Fujimaki et al., 1984), which might explain the slight depletion in Zr-Hf exhibited by the MVF basanites and alkali basalts relative to the typical OIB compositions (see back Fig. 4.4) but not by the SPaP nephelinites.

The presence of amphibole and minor phlogopite was also predicted to explain the variations in trace elements observed in the Fernando de Noronha lavas (Gerlach et al., 1987; Weaver, 1990), which have a number of compositional similarities with the MVF lavas (Fodor et

al., 1998; Rivalenti et al., 2007). Using the correlation between the Rb/Sr and $^{87}\text{Sr}/^{86}\text{Sr}$ ratios, the authors argued that the Fernando de Noronha compositions plotted transverse to mixing lines between clinopyroxene and phlogopite, with the analyses distributing towards radiogenic Sr and moderate to low Rb/Sr ratios (Fig. 4.8b). The MVF basalts plotted in a perfect array, indicating that K-rich amphibole and clinopyroxene existed as important residual phases equilibrated from 80–90 km to ~120 km deep into the lithospheric–asthenospheric mantle.

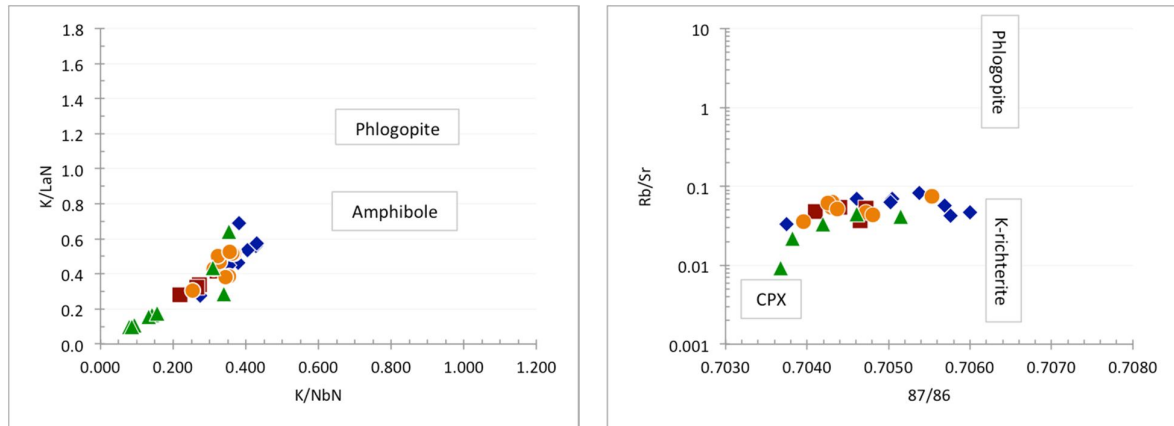


Figure 4.8. Correlation between (a) normalized-K/Nb and K/La and (b) Rb/Sr and $^{87}\text{Sr}/^{86}\text{Sr}$ ratios suggesting the preferential presence of amphibole (and clinopyroxene) instead of phlogopite as the hydrous residual phase in the MVF mantle sources. The arcuate array formed by the whole dataset in (b) suggests that a minor proportion of phlogopite was also present. Symbols are as in Figure 4.2.

4.5.3 THE ISOTOPE RESERVOIRS PROPOSED FOR THE MVF MAGMAS

Except for most of the SPo samples, nearly all of the MVF basalts have Sr-Nd isotope compositions plotted in the upper-left quadrant in the mantle array diagram (see back Fig. 5), which requires a depleted component in their mantle source(s). Moreover, all basalts provided very positive values for $\Delta 7/4$ and $\Delta 8/4$ for slightly to moderately radiogenic $^{206}\text{Pb}/^{204}\text{Pb}$ ratios, which suggests a component in the source having a high time-integrated (U+Th)/Pb ratio. Therefore, to evaluate models to test participation of mantle reservoirs with these isotope characteristics, we need to look carefully at the Pb isotopes.

In the concept of ‘mantle zoo’, a number of mantle domains resulting from distinct combinations of radiogenic isotope compositions can be envisaged, originally recognized from studies on OIB-type magmas. Such diversity deviated from the typical compositions found in mid-ocean ridge basalts because Pb isotope ratios in those basalts, and even in some MORB, are more radiogenic than the undifferentiated (primitive) mantle or bulk Earth (the “Pb paradox” of

Allégre et al., 1982; see also Murphy et al., 2002; Hart ad Gaetani, 2006; Hofmann, 2008). The modern HIMU endmember is part of this paradox and has been ascribed to a mantle reservoir having high U/Pb ratio (from μ parameter = $^{238}\text{U}/^{204}\text{Pb}$; Zindler and Hart, 1986), typically found in basalts from the St. Helena and Cook-Austral oceanic islands. Several works have suggested that the HIMU component is ubiquitous in the upper mantle, especially beneath the Atlantic Ocean and Europe (e.g., Hart et al., 1992; Hoenle et al., 1995), all consensually relating its origin to the recycling of oceanic crust that has undergone considerable dehydration in subduction zones (e.g., Stracke et al., 2003 and hereinafter references; also Hanyu et al., 2011; Kawabata et al., 2011). Recently, Stracke et al. (2005) reviewed a dataset of MORB and OIB isotope compositions by combining them to propose a pervasive presence of the FOZO component with slightly less radiogenic Pb isotope ratios than the classical HIMU, as it proposed by Zindler and Hart (1986). The authors distinguish FOZO from HIMU through lower $^{206}, ^{207}, ^{208}\text{Pb}/^{204}\text{Pb}$ but higher $^{208}\text{Pb}/^{206}\text{Pb}$ and $^{208}\text{Pb}^*/^{206}\text{Pb}^*$ ratios and argue that most of the isotopic compositions of the Atlantic and Pacific MORBs fall along a linear correlation between FOZO and a depleted component, with the Indian MORBs requiring involvement of a crust-like component that could be ancient sediments. As an additional conclusion, Stracke and colleagues also argue that the OIB magmas form mixing arrays originating from the MORB-FOZO array but diverging towards various isotopically enriched compositions, such as those of Zindler and Hart's EMI and EMII components.

Figure 4.5 shows that the MVF basalts plotted consistently as a group when the $^{87}\text{Sr}/^{86}\text{Sr}$ ratios are neglected because such ratios are variable due sensitivity to effects of crustal assimilation, which was already suggested for some of the SPo alkali basalts. This subset of four (or maybe five) samples of SPo and one minor eruptive center plotted away from the mantle array towards the most radiogenic Sr isotope values (≥ 0.7054) coupled with chondritic to sub-chondritic Nd values. Unfortunately, we have only one Pb isotope data point for them, which is sample HD-42, and it is coherent with the other 'uncontaminated' samples, with $^{206}\text{Pb}/^{204}\text{Pb} \sim 19.1$. All other samples, irrespective of the eruptive center, clustered along a mixed range between FOZO and a compositional field outlined by MORB-OIB (Fig. 4.5d-f). This mixing was previously demonstrated by Fodor et al. (1998), although the authors preferred HIMU instead of FOZO. Even considering that any studied sample provided $^{206}\text{Pb}/^{204}\text{Pb}$ (and derivative) ratios overlapping the FOZO field, as we have found for the Cretaceous olivine tholeiites that comprise the CMDS (values > 19.9 , for $T = 0$), we propose that the high U/Pb component needed to explain the Pb isotope signature of the MVF basalts might be better ascribed to FOZO than HIMU. However, the high variability in both Sr and Nd combined with the Pb isotope

compositions of these basalts necessarily requires an enriched component present in their mantle source, in close isotope similarity with the EMI and/or EMII-types found in OIB magmas. These two enriched endmembers require high and low time-integrated Rb/Sr and Sm/Nd ratios, respectively, to produce radiogenic Sr and unradiogenic Nd isotopic ratios, whereas EMI has lower uranogenic and thorogenic ratios than EMII (e.g., Lustrino and Dallai, 2003). A tendency towards EMI is depicted by the three disconnected samples from the whole sample grouping, but this is not true for their Nd compositions that are closer to EMII. Whatever this enriched component is, EMI or EMII, it is hard to assess looking only at our current isotopic dataset.

Weaver (1991) argued that some trace element ratios could be used to distinguish each one of the main OIB groups – HIMU and the two varieties of enriched mantle components (EMI and EMII). More recently, Willbold and Stracke (2006) re-evaluated the incompatible element systematics for the ‘mantle zoo’ components through several oceanic island basalts. They concluded that whereas the isotopic relationships may be explained by two general enriched components, which are EMI and EMII, the strong variance in terms of incompatible elements suggest there could be more than two EM sources. Despite the number of trace element ratios proposed to separate HIMU- from EM-derived magmas (e.g., K, Ba, Rb, Nb/La, Rb/Sr, Ce/Pb, U/Pb and Th/U) none were able to definitely distinguish between basalts originated from EMI and EMII sources. Our attempt to perform the same comparison (not shown) was unsuccessful, which led us to assume that the enriched component in the MVF basalts reflected complex chemical interactions in the source. A similar suggestion was made by Gerlach et al. (1987) when evaluating the trace element compositions of Fernando de Noronha lavas, the intake of (enriched) delaminated subcontinental lithosphere into the asthenosphere being envisaged as a possible mechanism to explain the deep origin for EM.

4.5.4 INSIGHTS ON THE CHEMICAL EVOLUTION OF THE SUBCONTINENTAL LITHOSPHERIC MANTLE IN THE NORTHEASTERN BORBOREMA PROVINCE

The mantle-derived magmatic events spanning from the Cretaceous to the Miocene make northeast Brazil a suitable area to investigate the chemical evolution of the lithospheric mantle. The magmatism started in the Early Cretaceous (~130 Ma) following the thinning and rifting of the lithosphere and emplacement of continental tholeiitic basalts (CDMS) that culminated with the opening of the Equatorial Atlantic. The CMDS consists mostly of evolved high-Ti tholeiites (MgO content <5 wt.%) and subordinate low-Ti tholeiites, the latter showing variable effects of

crustal assimilation on their geochemical and isotope signatures (Ngonge et al., submitted). Their Sr-Nd-Pb and trace element features show that the parental magmas of these two groups were segregated from enriched domains of the sub-continental lithospheric mantle. The Nb depletion and >1 Ga Nd model-ages of these tholeiites are consistent with an old, subduction-related metasomatic event inherited from the Proterozoic (Hollanda et al., 2003, 2006; Souza et al., 2007) and preserved in the lithospheric mantle beneath the region (Hollanda et al., 2006). In contrast, a distinct subset of dykes exposed to the south of the main swarm is formed by olivine tholeiites showing a peculiar Pb (combined with Sr-Nd) isotope signature attributed to FOZO. Ngonge et al. (submitted) have showed that such a FOZO source was deeper (~75 km), likely in the convective asthenosphere, than the enriched mantle domains that melted to generate the other tholeiites, roughly ~60 km in depth.

The involvement of FOZO component, however, can still be barely recognized in the MVF basalts, which results in a fundamental issue to reconcile the chemical history of the SCLM from the Cretaceous to the Cenozoic. If FOZO was an asthenospheric component in the Cretaceous, its imprint in the MVF magmas should be expected, which was estimated in this study to have segregated from depths of 80-90 km (for SPo, SeA and PiC) up to 120 km (for SPaP magmas). However, if asthenosphere remained convective from the Cretaceous to the Cenozoic, the chemical signatures in the MVF basalts should progress into a pure FOZO, which would mean the presence of a long-lived thermal anomaly (mantle plume) beneath northeast Brazil promoting continuous erosion of the lithospheric mantle in a nearly similar mechanism as predicted by Davies (1994) (e.g., also Tatsumi et al., 1991 for the Kenya rift). This is not true based on our results, which have shown that FOZO is rather a mixing endmember contributing to the MVF basalts rather than a sole mantle source, as seen for the CMDS olivine tholeiites. In addition, the acceptance of a long-lived thermal anomaly (the FOZO asthenosphere) as a mechanism to induce continuous melting and, therefore, uninterrupted magmatic activity, should either be attributed to an active mantle plume or persistence of plate-boundary efforts to favor progressive asthenospheric upwelling, both models consisting of non-realistic (and unsupported) hypotheses. For example, Luz et al. (2015) discarded a possible underplating of mafic magmas beneath the Borborema Province by showing consistent similarities in the gradient of primary and secondary seismic velocities (bulk Vp/Vs ratio) across that region. The authors modeled a crustal thickness of ~30–40 km and argued that minimal mafic underplating is a more reliable cause of the MOHO topography in that area. These results are in agreement with the statement of Knesel et al. (2011) based on a geochronological approach, from which no age progression was found between MVF basalts and equivalent rocks in Fernando de Noronha that could endorse a

pro-plume model. Thus, we propose that FOZO was originally asthenospheric during the Cretaceous and passively upraised during lithospheric thinning and ongoing rifting as a consequence of the major extensional efforts associated with the Atlantic Ocean opening. Such asthenosphere upwelled not only provided the amount of thermal energy needed to generate the CMDS magmas but also achieved depths shallow enough to decompress and melts itself and to generate the FOZO-type olivine tholeiites. As asthenosphere streamed into the resulting gaps were left as far as the lithosphere thinned, it became cooler and thermally and rheologically re-equilibrated as the rigid subcontinental lithospheric mantle. As a result, FOZO was preserved since the Cretaceous.

A recent review of global-scale seismological models reported by Fischer et al. (2010) showed that the lithosphere-asthenosphere boundary (LAB) for the region encompassing the Borborema Province is located at 80–90 km, in agreement with the predicted average depth of 81 ± 2 km estimated for Phanerozoic orogens (Rychert and Scherer, 2009). This estimate perfectly matches with our assessment of the melting temperature and depth for most of the MVF basalts studied here, which led us to identify the origin of these magmas at the LAB. The SPaP magmas, hence, were originated from deeper, asthenosphere-dominated domains.

The second issue is how to identify the origin of an EM endmember involved in the MVF petrogenesis, which has been identified through enrichment in LIL and LRE elements, variably radiogenic $^{87}\text{Sr}/^{86}\text{Sr}$ and unradiogenic $^{143}\text{Nd}/^{144}\text{Nd}$ combined with moderately radiogenic $^{206}\text{Pb}/^{204}\text{Pb}$ ratios. Such enriched compositions cannot be correlated with the evolved high-Ti and low-Ti Cretaceous tholeiite magmas because they contain clear Nb-depletion, which is absent in the Cenozoic basalts. These chemical differences suggest that the subduction-related lithospheric signature was not preserved, or it was localized at the shallowest depths beneath the northeastern Borborema Province and therefore not available to melt in the Cenozoic. In fact, looking at incompatible trace patterns found for the spinel-bearing peridotite xenoliths hosted in the MVF lavas, Nb is always depleted (Rivalenti et al., 2007) indicating that these lavas carried up fragments of ancient (Proterozoic) subduction-modified lithospheric mantle still preserved at shallow depths. Thus, the EM component in the MVF lavas represents a deep component derived from metasomatizing fluid-melts that have interacted with an OIB-type mantle to produce metasomatic minerals (as K-rich amphibole, mica) retaining highly incompatible trace elements (we recommend both the Menzies and Hawkesworth (1987) and Harlov and Austrheim (2013) for a wide review on this subject). According to the literature, the concentrations of metasomatic minerals in the mantle are expected to be low (a few fractions of a percent) and either small (<1%) or large (5–20%) melting degrees of such anomalously mantle domains would cause the

formation of alkaline magmatism. A good example of this statement was published by Roden et al. (1984) who claimed that St. Paul's rocks, a typical metasomatized massif presently located at the Equatorial mid-Atlantic ocean ridge, meet all of the requirements to be an alkali basalt source. Because the temperature of the asthenosphere is highly dependent on fluid-water content, the conditions required for its melting, as well as the fraction of melt produced from enriched(metasomatized) domains at and below the LAB, would be broadly achieved and fluctuated with time and space (Till et al., 2010). Assuming that there is no evidence for mantle plume activity or even passive asthenosphere upwelling related to lithospheric thinning processes (see comments above) at the Cenozoic in the northeastern Borborema Province, we are biased to accept that no major thermal anomaly was needed for generating the small-volume MVF eruptive centers, their formation being dependent on the permeability and chemical enrichment degree of the naturally adiabatic LAB-asthenosphere system in that region.

From these results, our understanding on the origin and even the nature of the EM-type endmember in the MVF basalts is still premature, and much remains to be learned. We have to acknowledge, however, that the chemical characteristics shared by MVF and Fernando de Noronha lavas allow us to reconcile these continental and oceanic areas into a common model of chemical evolution of the lithosphere-asthenosphere system. The passage of an ancient and cold continental lithosphere over a modern hotspot certainly impacts each one by allowing a number of chemical and physical interactions that are not easy to understand. The origin of both FOZO and EM beneath the South American continent, which are both pervasively found in several oceanic islands of the Atlantic Ocean requires consideration of the Proterozoic history of the West Gondwana (which includes the Borborema Province), a task that needs the integration of multidisciplinary information for a detailed investigation.

4.6 CONCLUSION

Cenozoic intraplate alkaline basalts comprise the MVF located at the northeastern tip of the South American continent (NE Brazil). The compositional variability observed between the studied eruptive centers is explained by the fractional crystallization of olivine and clinopyroxene, in addition to different proportions of residual mineralogy in the source. The source for the basanites and alkali basalts is estimated to be a garnet-bearing domain existing at the lithosphere-asthenosphere boundary (80–90 km deep), whereas the nephelinites are derived from the adiabatic asthenosphere with temperatures ~1,470°C. These rocks display incompatible

trace element patterns and Sr-Nd-Pb isotope compositions similar to FOZO and EM-type OIB magmas. The DM endmember must be present as a third component, but hidden by the more obvious features of FOZO and EM. This wide vertical mantle column was presumed to be invaded by metasomatic fluid-melts responsible for the pervasive EM signature recognized in the MVF lavas. Such an enrichment event is decoupled from the subduction-type enrichment identified in the shallower lithospheric mantle source of the Cretaceous tholeiites, which had erupted 80 m.y. before the alkaline lavas. Because there is not a large difference between the chemical signatures of basanites and alkali basalts compared with nephelinites we presume that an EM component is present as (K-rich) metasomatic domains existing within the convective asthenosphere (source for nephelinites) or as metasomatic veins that invaded the overlaid LAB (source for the other basalt suite). Since these two global mantle endmembers are also identified in the basalts of Fernando de Noronha Island, we argue that there is a source-correlation between the sub-continental and sub-oceanic mantle domains that requires further investigation.

ACKNOWLEDGMENTS

This article was written as part of the E.D. Ngonge's Ph.D. thesis. Ngonge was supported by CAPES. M.H.B.M. Hollanda and M.M. Pimentel are grateful for grants received from the Brazilian National Research Council (CNPq) during course of this research project. M.H.B.M. Hollanda has also appreciated the scholarship grant given by CNPq for her Ph.D. The analytical tests and field trips were performed under the auspices of CNPq through Project 473.638/2011-8.

REFERENCES

- Adam, J., Green, T.H., Sie, S.H. 1993. Proton microprobe determined partitioning of Rb, Sr, Ba, Y, Zr, Nb and Ta between experimentally produced amphiboles and silicate melts with variable F content. *Chemical Geology*, 109: 29-49.
- Agustín-Flores, J., Siebe, C., Guilbaud-N, M. 2011. Geology and geochemistry of Pelagatos, Cerro del Agua, and Dos Cerros monogenetic volcanoes in Sierra Chichinautzin Volcanic Field, south of Mexico City. *Journal of Volcanology and Geothermal Research*, 201(1-4): 143-1162.
- Albarède, F. 1992. How deep do common basaltic magmas form and differentiate? *Journal of Geophysical Research*, 97: 10,997–11,009.
- Baker, J.A., Menzies, M.A., Thirlwall, M.F., Macpherson, C.G. 1997. Petrogenesis of Quaternary intraplate volcanism, Sana'a, Yemen: implications for plume-lithosphere interaction and polybaric melt hybridization. *Journal of Petrology*, 38(10): 1,359-1,390.
- Bastin,G.F.,Heijligers, H.J.M. 1990. Progress in electron-probe microanalysis. *Materialwissenschaft und Werkstofftechnik*, 21: 216-221.
- Bezerra, F.H.R., Vita-Finzi, C. 2000. How active is a passive margin? Paleoseismicity in northeastern Brazil. *Geology*, 28: 591-594.
- Boivin, Pi., Thouret, J-C. 2014. The Volcanic Chaîne des Puys: a unique collection of simple and compound monogenetic edifices. In: Fort, M., André, M.-F. (Eds.), Landscapes and landforms of France, Springer: 81-91.
- Boynton, W.V. 1984. Geochemistry of the rare earth elements: meteorite studies. In P. Henderson (Ed.), Rare-Earth Element Geochemistry, Elsevier: 63-114.
- Castro, D.L., Bezerra, F.H.R., Sousa, M.O.I., Fuck, R.A. 2012. Influence of Neoproterozoic tectonic fabric on the origin of the Potiguar basin, northeastern Brazil and its link with West Africa based on gravity and magnetic data. *Journal of Geodynamics*, 54: 29-42.
- Chazot, G., Menzies, M.A., Harte, B. 1996. Determination of partition coefficients between apatite, clinopyroxene, amphibole, and melt in natural spinel lherzolites from Yemen: implications for wet melting of the lithospheric mantle. *Geochimica and Cosmochimica Acta*, 60: 423-437.
- Davies, G.F. 1994. Thermomechanical erosion of the lithosphere by mantle plumes. *Journal of Geophysical Research, Solid Earth*, 99(B8): 15,709-15,722.
- Fisher, K.M., Ford, H.A., Abt, D.L., Rychert, C. 2010. The lithosphere-asthenosphere boundary. *Annual Review of Earth and Planetary Sciences*, 38: 551-575.
- Fodor, R.V., Dobosi, G., Sial, A.N. 1995. Zoned clinopyroxenes in alkalic basalt: clues to fractionation and magma-mixing histories for seemingly primitive magmas. *Chemistry Erde*, 55: 133-148.
- Fodor, R.V., Mukasa, S.B. and Sial, A.N. 1998. Isotopic and trace-element indications of lithospheric and asthenospheric components in Tertiary alkalic basalts, northeastern Brazil. *Lithos*, 43: 197-217.
- Fodor, R.V., Sial, A.N., Gandhok, G. 2002. Petrology of spinel peridotite xenoliths from northeastern Brazil: lithosphere with a high geothermal gradient imparted by Fernando de Noronha plume. *Journal of South American Earth Sciences*, 15: 199-214.
- Françolin, J.B.L., Cobbold, P.R., Szatmari, P. 1994. Faulting in the Early Cretaceous Rio do Peixe basin (NE Brazil) and its significance for the opening of the Atlantic. *Journal of Structural Geology*, 16(5): 647-661.
- Frey, F.A., Green, D.H., Roy, S.D. 1978. Integrated models of basalt petrogenesis: a study of quartz tholeites to olivine melilites from South Eastern Australia utilizing geochemical and experimental petrological data. *Journal of Petrology*, 19(3): 463-513.

- Furman, T., Bryce, J.G., Karson, J., Iotti, A. 2004. East African Rift System (EARS) Plume Structure: insights from Quaternary mafic lavas of Turkana, Kenya. *Journal of Petrology*, 45: 1,069-1,088.
- Gerlach, D.C., Stormer, J.C., Muller, P.A. 1987. Isotope geochemistry of Fernando de Noronha. *Earth and Planetary Science Letters*, 85: 129-144.
- Gioia, S.M.C.L., Pimentel, M.M. 2000. The Sm-Nd isotopic method in the Geochronology Laboratory of the University of Brasília. *Anais da Academia Brasileira de Ciências*, 72: 219-245.
- Green, D.H., Ringwood, A.E. 1968. The stability fields of aluminous pyroxene peridotite and garnet peridotite and their relevance in upper mantle structure. *Earth and Planetary Science Letters*, 3: 151-160.
- Hanyu, T., Tatsumi, Y., Senda, R., Miyazaki, T., Chang, Q., Hihara, Y., Takahashi, T., Kawabata, H., Suzuki, K., Kimura, J.-I. 2011. Geochemical characteristics and origin of the HIMU reservoir: a possible mantle plume source in the lower mantle. *Geochemistry, Geophysics and Geosystems*, 12(2), doi: 10.1029/2010GC003252.
- Hart, S.R., Hauri, E.H., Oschmann, L.A., Whitehead, J.A. 1992. Mantle plumes and entrainment: isotopic evidence. *Science*, 256: 517-520.
- Hoernle, K., Zhang, Y.-S., Graham, D. 1995. Seismic and geochemical evidence for large-scale mantle upwelling beneath the eastern Atlantic and western and central Europe. *Nature*, 374: 34-38.
- Hofmann, A. The enduring lead paradox. *Nature Geosciences*, 1: 812-813.
- Hollanda, M.H.B.M. 2002. Evolução geodinâmica do manto litosférico continental no Domínio Seridó – Província Borborema (NE do Brasil). Ph.D. thesis, Universidade de Brasília, Brazil, 84 pp.
- Hollanda, M.H.B.M., Pimentel, M.M., Jardim de Sá, E.F. 2003. Paleoproterozoic subduction-related metasomatic signatures in the lithospheric mantle beneath NE Brazil: inferences from trace element and Sr–Nd–Pb isotopic compositions of Neoproterozoic high-K igneous rocks. *Journal of South American Earth Science*, 15(8): 885-900.
- Hollanda, M.H.B.M., Pimentel, M.M., Oliveira, D.C., Jardim de Sá, E. F. 2006. Lithosphere-asthenosphere interaction and the origin of Cretaceous tholeiitic magmatism in NE Brazil: Sr-Nd-Pb isotopic evidence. *Lithos*, 86: 34-49.
- Holmes, A. 1946. An estimate of the age of the Earth. *Nature*, 157: 680-684.
- Houtermans, F.G. 1946. Die isotopenhäufigkeiten im natürlichen blei und das alter des urans. *Naturwissenschaften*, 33: 185-186.
- Irvine, T.N., Baragar, W.R.A. 1971. A guide to the chemical classification of the common volcanic rocks. *Canadian Journal of Earth Sciences*, 8: 523-548.
- Keresztsuri, G., Németh, K. 2013. Monogenetic basaltic volcanoes: genetic classification, growth, geomorphology and degradation. Open access, <http://dx.doi.org/10.5772/51387>.
- King, S.D., Anderson, D.L. 1995. An alternative mechanism of flood basalt formation. *Earth and Planetary Letters*, 136: 269-279.
- King, S. D., Anderson, D.L. 1998. Edge-driven convection. *Earth and Planetary Science Letters*, 160: 289-296.
- Kiyosugi, K., Connor, C.B., Wetmore, P.H., Ferweda, B.P., Germa, A.M., Connor, L.J., Hintz, A.R. 2012. Relationship between dike and volcanic conduit distribution in a highly eroded monogenetic volcanic field: San Rafael, Utah, USA. *Geology*, 40(8): 695-698.
- Knesel, K.M., Souza, Z.S., Vasconcelos, P.M., Cohen, B.E., Silveira, F.V. 2011. Young volcanism in the Borborema Province, NE Brazil, shows no evidence for a trace of the Fernando de Noronha plume on the continent. *Earth and Planetary Science Letters*, 302: 38-50.
- LaTourrette, T., Hervig, R.L. 1995. Trace element partitioning between amphibole, phlogopite and basanite melt. *Earth and Planetary Science Letters*, 135: 13-30.

- Lustrino, M., Dallai, L. 2003. On the origin of EM-I end-member. *Neues Jahrbuch für Mineralogie – Abhandlungen (Journal of Mineralogy and Geochemistry)*, 179(1): 85-100.
- Luz, R.M.N., Julià, J., Nascimento, A.F. 2015. Bulk crustal properties of the Borborema Province, NE Brazil, from P-wave receiver functions: implications for model of intraplate Cenozoic uplift. *Tectonophysics*, 644/645: 81-91.
- Matos, R.M.D. 1992. The northeast Brazilian rift system. *Tectonics*, 11: 766-791.
- McGee, L.E., Smith, I.E.M., Millet, M.A., Handley, H.K., Lindsay, J.M. 2013. Asthenospheric control of melting processes in a monogenetic basaltic system: a case study of the Auckland Volcanic Field, New Zealand. *Journal of Petrology*, 54: 2,125-2,153.
- Murphy, D.T., Kamber, B.S., Collerson, K.D. 2002. A refined solution to the first terrestrial Pb-isotope paradox. *Journal of Petrology*, 44(1): 39-53.
- Nelson, S.T., Montana, A. 1992. Sieve-textured plagioclase in volcanic rocks produced by rapid decompression. *American Mineralogist*, 77: 1,242-1,249.
- Németh, K. 2010. Monogenetic volcanic fields: origin, sedimentary record, and relationship with polygenetic volcanism. In: Cañon-Tapia, E., Szakács, A. (Eds.), *What is a volcano?* Geological Society of America, Special Paper, 470: 43-66.
- Ngonge, E.D., Hollanda, M.H.B.M., Archanjo, C.J., Oliveira, D.C. Petrology of continental tholeiitic magmas forming a 350 km-long Mesozoic dyke swarm in NE Brazil: constraints of geochemical and isotopic data. *Lithos*, submitted.
- O'Reilly, S.Y., Zhang, M. 1995. Geochemical characteristics of lava field basalts from eastern Australia and inferred sources: connections with the subcontinental lithospheric mantle. *Contributions to Mineralogy and Petrology*, 121: 148-170.
- Perlingeiro, G., Vasconcelos, P.M., Knesel, K.M., Thiede, D.S., Cordani, U. 2013. $^{40}\text{Ar}/^{39}\text{Ar}$ geochronology of the Fernando de Noronha archipelago and implications for the origin of alkaline volcanism in the NE Brazil. *Journal of Volcanology and Geothermal Research*, 249: 140-154.
- Perry, F.V., Baldridge, W.S., DePaolo, D.J. 1987. Role of asthenosphere and lithosphere in the genesis of late Cenozoic basaltic rocks from the Rio Grande rift and adjacent regions of the southwestern United States. *Journal of Geophysical Research*, 92: 9,193-9,213.
- Rivalenti, G., Mazzucchelli, M., Girardi, V.A.V., Vannucci, R., Barbieri, M.A., Zanetti, A., Goldstein, S.L. 2000. Composition and processes of the mantle lithosphere in northeastern Brazil and Fernando de Noronha: evidence from mantle xenoliths. *Contribution to Mineralogy and Petrology*, 138: 308-325.
- Rivalenti, G., Zanetti, A., Girardi, V.A.V., Mazzucchelli, M., Tassinari, C.C.G., Bertotto, G.W. 2007. The effect of the Fernando de Noronha plume on the mantle lithosphere in north-eastern Brazil. *Lithos*, 94: 111-131.
- Roden, M.K., Hart, S.R., Frey, F.A., Melson, W.G. 1984. Sr, Nd and Pb isotopic and REE geochemistry of St. Paul's rocks: the metamorphic and metasomatic development of an alkali basalt mantle source. *Contributions to Mineralogy and Petrology*, 85: 376-390.
- Roeder and Emslie, 1970. Olivine-liquid equilibrium. *Contribution to mineralogy and petrology*, 29: 275-289.
- Rogers, N.W. 1993. The isotope and trace element geochemistry of basalts from the volcanic islands of the southern Red Sea. In: Prichard, H.M., Alabaster, T., Harris, N.B.W., Neary, C.R. (Eds.), *Magmatic Processes and Plate Tectonics*. Geological Society of London, Special Publication, 76: 455-467.
- Rychert, C.A., Shearer, P.M. 2009. A global view of the lithosphere-asthenosphere boundary. *Science*, 324: 495-498.
- Scarwood, J.H., Cox, K.G. 1995. Basalts generated by decompressive adiabatic melting of mantle plume – a case study from the Isle of Skye, NW Scotland. *Journal of Petrology*, 36: 3-22.
- Sénant, J., Popoff, M. 1991. Early Cretaceous extension in northeast Brazil related to the South Atlantic opening. *Tectonophysics*, 198: 35-46.

- Shaw, J.E., Baker, J.A., Menzies, M.A., Thirwall, M.F., Ibrahim, K.M. 2003. Petrogenesis of the largest intraplate volcanic field on the Arabian Plate (Jordan): a mixed lithosphere–asthenosphere source activated by lithospheric extension. *Journal of Petrology*, 44 (9): 1,657-1,679.
- Sial A.N., Long L.E., Pessoa D.A.R., Kawashita K. 1981. Potassium-argon ages and strontium isotope geochemistry of Mesozoic and Tertiary basaltic rocks, Northeastern Brazil. *Anais da Academia Brasileira de Ciências*, 53: 115-122.
- Silveira, F.V. 2006. Magmatismo cenozóico da porção central do Rio Grande do Norte, NE do Brasil. Ph.D. thesis, Universidade Federal do Rio Grande do Norte, Brazil, 220 pp.
- Stracke, A., Hofmann, A.W., Hart, S.R. 2005. FOZO, HIMU and the rest of the mantle zoo. *Geochemistry, Geophysics, Geosystems*, 6(5), doi: 10.1029/2004GC000824.
- Souza, Z.S., Martin, H., Peucat, J.-J., Jardim de Sá, E.F., Macedo, M.H.F. 2007. Calc-alkaline magmatism at the Archean-Proterozoic transition: the Caicó complex basement (NE Brazil). *Journal of Petrology*, 48: 2,149-2,185.
- Sun, S.S., McDonough, W.F. 1989. Chemical and isotopic systematic of oceanic basalts: implications for mantle composition and processes. In: Saunders, A.D., Norry, M.J. (Eds.), *Magmatism in the Ocean Basins*, Geological Society Special Publications, 42: 313–345.
- Tatsumi, Y., Kimura, N., Itaya, T., Koyaguchi, T., Suwa, K. 1991. Intermittent upwelling of asthenosphere beneath the Gregory rift, Kenya. *Geophysical Research Letters*, 18(6): 1,111-1,114.
- Till, C.B., Elkins-Tanton, T., Fischer, K.M. 2010. A mechanism for low-extent melts at the lithosphere–asthenosphere boundary. *Geochemistry, Geophysics, Geosystems*, 11(10), doi: 10.1029/2010GC003234.
- Thirwall, M.F., Upton, B.G.J., Jenkins, C. 1994. Interaction between continental lithosphere and the Iceland plume-Sr-Nd-Pb isotopic geochemistry of Tertiary basalts, NE Greenland. *Journal of Petrology*, 35: 839-879.
- Van Schmus, W.R., Oliveira, E.P., Silva Filho, A.F., Toteu, S.F., Penaye, J., Guimarães, I.P. 2008. Proterozoic links between the Borborema Province, NE Brazil, and the Central African Fold Belt. In: Pankhurst, R.J., Trow, R.A.J., Brito neves, B.B., de Wit, M.J. (Eds.), *West Gondwana, pre-Cenozoic correlations across the South Atlantic region*. Geological Society, London, Special Publication, 294: 69-99.
- Vauchez, A., Neves, S.P., Caby, R., Corsini, M., Egydio-Silva, M.E., Arthaud, M., Amaro, V. 1995. *Journal of South American Earth Sciences*, 8(3/4): 247-266.
- Viegas, L.G.F., Archanjo, C.J., Hollanda, M.H.B.M., Vauchez, A. 2014. Microfabrics and zircon U-Pb (SHRIMP) chronology of mylonites from the Patos shear zone (Borborema Province, NE Brazil). *Precambrian Research*, 243: 1-17.
- Weaver, B.L. 1990. Geochemistry of highly-undersaturated ocean island basalt suites from the South Atlantic Ocean: Fernando de Noronha and Trindade islands. *Contributions to Mineralogy and Petrology*, 105: 502-515.
- Weaver, B.L. 1991. The origin of ocean island end-member compositions: trace element and isotopic constraints. *Earth and Planetary Science Letters*, 104: 381-397.
- Willbold, M., Stracke, A. 2006. Trace element composition of mantle end-members: Implications for recycling of oceanic and upper and lower continental crust. *Geochemistry, Geophysics, Geosystems*, 7(4), doi: 10.1029/2005GC001005.
- Zindler, A., Hart, S.R. 1986. Chemical geodynamics. *Annual Review of Earth and Planetary Sciences*, 14: 493-571.

CAPÍTULO 5

GEOQUÍMICA ISOTÓPICA Re-Os DE XENÓLITOS PERIDOTÍTICOS

5.1 INTRODUÇÃO

A caracterização química e isotópica dos xenólitos peridotíticos hospedados nos basaltos alcalinos Macau é de importância fundamental para a discussão sobre a natureza composicional e idade do manto litosférico no domínio Seridó/Rio Grande do Norte. Tendo em vista as publicações existentes sobre petrologia dos xenólitos continentais, hospedados nos basaltos alcalinos cenozóicos do MVF (Fodor et al., 2002; Rivalenti et al., 2000, 2007) e dos xenólitos oceânicos hospedados nos basanitos da Formação São José do arquipélago de Fernando de Noronha (Rivalenti et al., 2000), esse projeto de pesquisa esteve focado na obtenção de dados Re-Os combinados à determinações da concentração dos elementos do grupo da platina (adiante tratados como PGE – *Platinum Group Element*: Irídio – Ir, Ósmio – Os, Rutênio – Ru, Platina – Pt, Paládio – Pd e Rênio – Re). O objetivo maior foi obter informações sobre a cronologia (idades modelo T_{RD}) de eventos de empobrecimento (fusão parcial) e enriquecimento (metassomatismo) de domínios do manto litosférico continental e oceânico para complementar as interpretações apresentadas nos capítulos anteriores. Os tratamentos feitos com os dados Re-Os e PGE, ilustrados através de gráficos de correlação, bem como interpretações decorrentes podem ser considerados ainda preliminares, de forma que não foram organizados na forma de artigo científico.

A seguir, apresentamosos dados de análises químicas obtidas em olivina, e geoquímica de elementos maiores e menores obtidos em rocha-total de 7 amostras de xenólitos continentais e em 3 amostras de xenólitos oceânicos, sendo que análises de elementos traços foram obtidas em apenas 4 e 2 amostras, respectivamente, dos xenólitos continentais e oceânicos. A obtenção desses resultados objetivou a caracterização simples do conjunto estudado, e não exatamente a discussão petrogenética desses xenólitos, a qual é apropriada e detalhadamente conduzida nos artigos acima listados de R. Fodor e G. Rivalenti, e respectivos colaboradores. O conjunto de dados isotópicos Re-Os e concentrações de PGE foi obtido a partir de 16 amostras, sendo 11 de

xenólitos continentais coletados de todos os quatro centros eruptivos comentados no Capítulo 4 (SPo, SeA, PiC e SPaP), e 5 de xenólitos oceânicos. Faz-se necessário informar que a amostragem em Fernando de Noronha não foi intencionalmente realizada para esse projeto, as amostras analizadas tendo sido gentilmente cedidas pelas professoras Leila Marques (Instituto de Geofísica, Astronomia e Meteorologia da USP) e Maria Helena Hollanda (esta orientadora).

É importante informar que os trabalhos que versam sobre os xenólitos do NE do Brasil adotam uma classificação texturalprévia que não é seguida nesse estudo, sendo reconhecidos tipos protogranulares – grãos com contatos curvilineares em geral com tamanhos médios de até 5 mm, e porfiroclásticos – aqueles com porfiroclastos em geral maiores que 3 mm, com contatos retos, envoltos em matriz neoblástica mais fina. Devido à nossa amostragem limitada, não foi possível obter material suficiente para confecção de lâminas delgadas e análises geoquímicas e isotópicas, de forma que prioritariamente optamos por preterir o estudo textural em detrimento ao isotópico.

5.2 PROCEDIMENTO ANALÍTICO PARA OBTENÇÃO DE DADOS Re-Os E ELEMENTOS DO GRUPO DA PLATINA

As análises isotópicas Re-Os e determinações das concentrações de elementos do grupo da platina (PGE) foram obtidas no Laboratório de Geoquímica Isotópica da Universidade de Maryland, College Park, em colaboração com o Dr. Richard Walker.

5.2.1 DIGESTÃO ÁCIDA DA AMOSTRA

A preparação da amostra consiste em descartar qualquer fragmento de lava ao redor do xenólito, usando uma serra de diamante para, a seguir, proceder com a pulverização em almofariz de ágata. Dois ou três grãos de olivina foram retirados de cada amostra para análise química em microssonda. A digestão é feita em tubo Carius colocando: (i) ~0,5 a ~1,5 g da amostra pulverizada, (ii) aproximadamente 3 mL de HCl e 6 mL de HNO₃ concentrados e (iii) *spike*Re-Os *espike* C (PGE). Os tubos são imersos em gelo para impedir a oxidação de Os. O conteúdo de cada tubo é agitado durante alguns minutos e depois selados e acondicionados em cápsulas de aço (*steel jacket*) para, a seguir, serem aquecidos em forno a 270°C durante 96 horas.

5.2.2 PREPARAÇÃO DA FRAÇÃO DE Os

Após a abertura dos tubos Carius, as amostras são transferidas para um tubo cilíndrico de centrifugação de volume 15 ml, e centrifugadas durante 10 minutos para separar a solução ácida da fase sólida (resíduo). O resíduo é descartado. A separação de Os da fase aquosa inicia com a adição de 2 ml de CCl_4 (tetracloreto de carbono), uma vez que a fase aquosa e o CCl_4 são imiscíveis, Os permanecendo retido no composto orgânico e os outros PGE mantém-se na fase aquosa. Os é extraído do composto orgânico (CCl_4) através da adição de 4 ml de HBr. Após aquecimento por aproximadamente 12 horas (80–85°C), essa solução é centrifugada e o resíduo orgânico é descartado. A solução (com HBr) é aquecida até a secura em chapa a ~80°C para a evaporação total de HBr. A micro-destilação de Os é feita embecker de teflon específico, adicionando-se 20 μl de HBr concentrado na parte estreita do becker e 40–45 μl de dicromato diretamente adicionado à amostra seca, colocada na fechadura do becker. O Os purificado é depositado em filamentos de platina, junto com $\text{Ba}(\text{OH})_2$ e então aquecido a ~830°C. As análises duplicatas de uma solução padrão de Os produziram uma precisão de $\pm 0,1\%$ (2σ) para as razões $^{187}\text{Os}/^{188}\text{Os}$. Os brancos analíticos foram inferiores a 1,6 pg, os quais são desprezíveis em comparação às concentrações de Os nos xenólitos de peridotito investigados.

5.2.3 PREPARAÇÃO DA FRAÇÃO DE RE

Os PGE (Ir, Ru, Pt, Pd e Re) foram extraídos da fase aquosa através da técnica de cromatografia de troca iônica, usando 2 mL de resina aniônica AG1X8 *Eichrom*. Após os procedimentos de lavagem da resina, Re–Ru foram eluídos na passagem de 12 ml de $\text{HNO}_3\text{6N}$ pela resina, enquanto Pt–Ir foram coletados com 13 ml de HNO_3 e Pd com 14 ml de HCl concentrado. Todas as frações foram aquecidas até a secura; às frações de Pt–Ir e Pd foram adicionadas algumas gotas de HCl e HNO_3 e novamente submetidas à secagem. As frações de Re–Ru foram purificadas em colunas secundárias e coletadas com 7 ml de $\text{HNO}_3\text{6N}$. Algumas gotas de HCl e HNO_3 foram adicionadas e novamente elevadas à secura. O passo final consistiu na adição de $\text{HNO}_3\text{5\%}$ para análise espectrométrica em espectrômetro tipo *Nu Plasma multicollector*. Cada PGE foi analisado em modo estático usando 2 ou 3 multiplicadores eletrônicos. Alíquotas diluídas do meteorito ferroso *South Byron – Dronino* foram analizadas como padrão secundário, resultando em correção de fracionamento em torno de 2%. Medidas efetuadas no

padrão *UB-N* produziram uma precisão em torno de 3%. Os brancos analíticos foram: 0,26 pg para Ir; 7,68 pg para Ru; 559 pg para Pt; 8,3 pg para Pd e 1,82 pg para Re. Todas as concentrações foram corrigidas para o branco.

5.3 RESULTADOS

5.3.1 COMENTÁRIOS GERAIS SOBRE QUÍMICA MINERAL E GEOQUÍMICA DE ROCHA TOTAL

Análises químicas foram realizadas em 66 grãos de olivina de xenólitos continentais e oceânicos. Os teores de forsterita (Fo) medidos em todo o conjunto foi bastante homogêneos, variando entre 88,2 e 91%, os quais são considerados valores tipicamente encontrados em peridotitos de composição moderadamente refratária (p.ex., Pearson et al., 2014). Essa faixa de valores foi igualmente reportada nos trabalhos de Fodor et al. (2002) e Rivalenti et al. (2000, 2007) os quais apresentam, além de olivina, dados de química mineral para ortopiroxênio, clinopiroxênio e espinélio dos xenólitos continentais. A partir dos resultados obtidos, Fodor e colaboradores mostram existir correlação positiva entre os teores de Fo em olivina e Mg# em ortopiroxênio, o mesmo comportamento também observado para, respectivamente, %CaO e Wo nesses minerais, sugerindo equilíbrio químico aparentemente independente da temperatura. Comportamento contrário é observado quando da comparação entre Mg# e Wo obtidos para clinopiroxênio, em geral com valores Mg# discretamente mais elevados e conteúdos de CaO (Wo) inversamente correlacionados a aqueles em olivina. Dados de termobarometria calculados a partir da composição química desses minerais apontam para temperaturas médias de equilíbrio entre 800° e 1280°C (Rivalenti et al., 2000, 2007; Fodor et al., 2002) e pressões entre 1,3 e 2,7 GPa (Rivalenti et al., 2000) para ambas as suites de xenólitos, continentais e oceânicos. O estudo de Fodor e colaboradores para os basaltos continentais mostra, no entanto, que temperaturas mais elevadas são principalmente obtidas nos tipos porfiroclásticos, enquanto que valores em média <1100°C são encontrados nos tipos protogranulares. Essa variação do par temperatura-pressão é consistente, segundo aqueles autores, com gradiente térmico local (continente) de ~12–15°C/km, sendo os xenólitos porfiroclásticos representantes de domínios mais profundos (quentes) em comparação a aqueles protogranulares.

Sete xenólitos continentais e três oceânicos foram estudados para determinar as composições de elementos maiores, enquanto quatro xenólitos continentais e apenas dois coletados dos basaltos oceânicos foram analisados para elementos traços (Tabela 5.1). Os resultados mostram relativa variação nos teores de MgO (34 – 42 wt.%), Al₂O₃ (2,11 – 5,48

wt.%), CaO (2,12 – 4,48 wt.%) e TiO₂ (0,15 – 0,57 wt.%). As correlações entre MgO *versus* SiO₂, Al₂O₃ e CaO, bem como MgO/Fe₂O_{3T} *versus* TiO₂ ilustradas na Figura 5.1 (a-d) mostram a Tabela 5.1 Dados de geoquímica elementar e isótopos Re-Os para os xenólitos peridotíticos

Amostra	MVF-1	MVF-2	MVF-3	MVF-4	MVF-5	MVF-6	MVF-7	MVF-8	MVF-9	MVF-10	MVF-11	FN-1	FN-2	FN-3	FN-4	FN-5
	xenólitos continentais											xenólitos oceânicos				
<i>wt.%</i>																
SiO ₂	43.12											43.29	43.57			43.28
TiO ₂	0.15											0.44	0.08			0.57
Al ₂ O ₃	4.25											4.13	2.11			5.36
Fe ₂ O ₃	9.29											10.71	9.13			10.05
MnO	0.15											0.17	0.15			0.17
MgO	38.76											35.35	42.00			34.53
CaO	3.00											4.48	2.12			4.38
Na ₂ O	0.28											0.57	0.16			0.66
K ₂ O	0.06											0.21	0.03			0.23
P ₂ O ₅	0.03											0.09	0.02			0.13
LOI	0.7											0.97	0.46			1.00
SUM	99.09											99.45	99.36			99.36
Mg#	90.2											87.9	91			88.3
<i>ppb</i>																
La	1.60											7.70	1.70			
Ce	2.90											15.60	2.70			
Nd	1.50											8.00	1.20			
Sm	0.33											1.60	0.19			
Eu	0.13											0.52	0.08			
Tb	0.08											0.22	0.03			
Pr	0.34											1.92	0.29			
Tm	0.05											0.08	0.02			
Gd	0.43											1.57	0.29			
Dy	0.53											1.24	0.25			
Er	0.32											0.55	0.16			
Ho	0.10											0.21	0.06			
Yb	0.32											0.46	0.18			
Lu	0.05											0.07	0.03			
¹⁸⁷ Re/ ¹⁸⁸ Os	0.4593	0.7923	0.6709	3.9091	0.4337	0.4862	0.5561	0.7988	0.8155	1.0300	1.1645	1.7400	3.1400	#####	0.9243	0.8586
erro (2σ-absoluto)	0.0046	0.0079	0.0067	0.0391	0.0043	0.0049	0.0056	0.0080	0.0082	0.0103	0.0116	0.0174	0.0314	0.4378	0.0092	0.0086
¹⁸⁷ Os/ ¹⁸⁸ Os	0.1267	0.1281	0.1275	0.4208	0.1227	0.1239	0.1259	0.1297	0.1257	0.1185	0.1277	0.1203	0.1267	0.1303	0.1219	0.1204
erro (2σ-absoluto)	0.0002	0.0002	0.0002	0.0006	0.0002	0.0002	0.0002	0.0002	0.0002	0.0002	0.0002	0.0002	0.0002	0.0001	0.0002	0.0002
γOs (t = 0)	-0.2	+0.9	+0.4	+231	-3.4	-2.4	-0.9	+2.1	-1.0	-6.7	+0.6	-5.3	-0.2	+2.6	-4.0	-5.2
T _{RD} (Ga)	0.06	-0.15	-0.06	-78.80	0.65	0.48	0.18	-0.31	0.21	1.27	-0.09	1.01	0.06	1.01	-0.48	0.77
conteúdo [Fo]	89.7	89.5	89.5	89.4	89.7	90.4	89.9	89.9	88.2	91.0	88.8	88.7	89.9	89.7	88.7	90.3

comparação das duas suites de xenólitos estudados com um valor médio para o manto primitivo (MP) supercondrírico (enriquecido, ou não-depletado) e subcondrírico (fortemente depletado). A grande variação composicional sugere que os xenólitos provavelmente originaram de domínios enriquecidos e empobrecidos existentes em ambos ossegmentos litosféricos continental e oceânico. Outra informação importante pode ser extraída da tendênciaàs correlações inversas entre MgO e os demais óxidos principalmente evidente nos xenólitos continentais e menos nos oceânicos, provavelmente devido à amostragem limitada. Esse comportamento, aliado à presença de clinopiroxênio modal, tem sido reportado como características de peridotitos residuais

(Takazawa et al., 2000), menos férteis, e foi igualmente observado por Rivalenti et al. (2007) a partir de variações compostionais observadas em cristais zonados de clinopiroxênio. No entanto, esses autores observaram o enriquecimento em Al, Ca, Ti e Na das bordas em relação ao

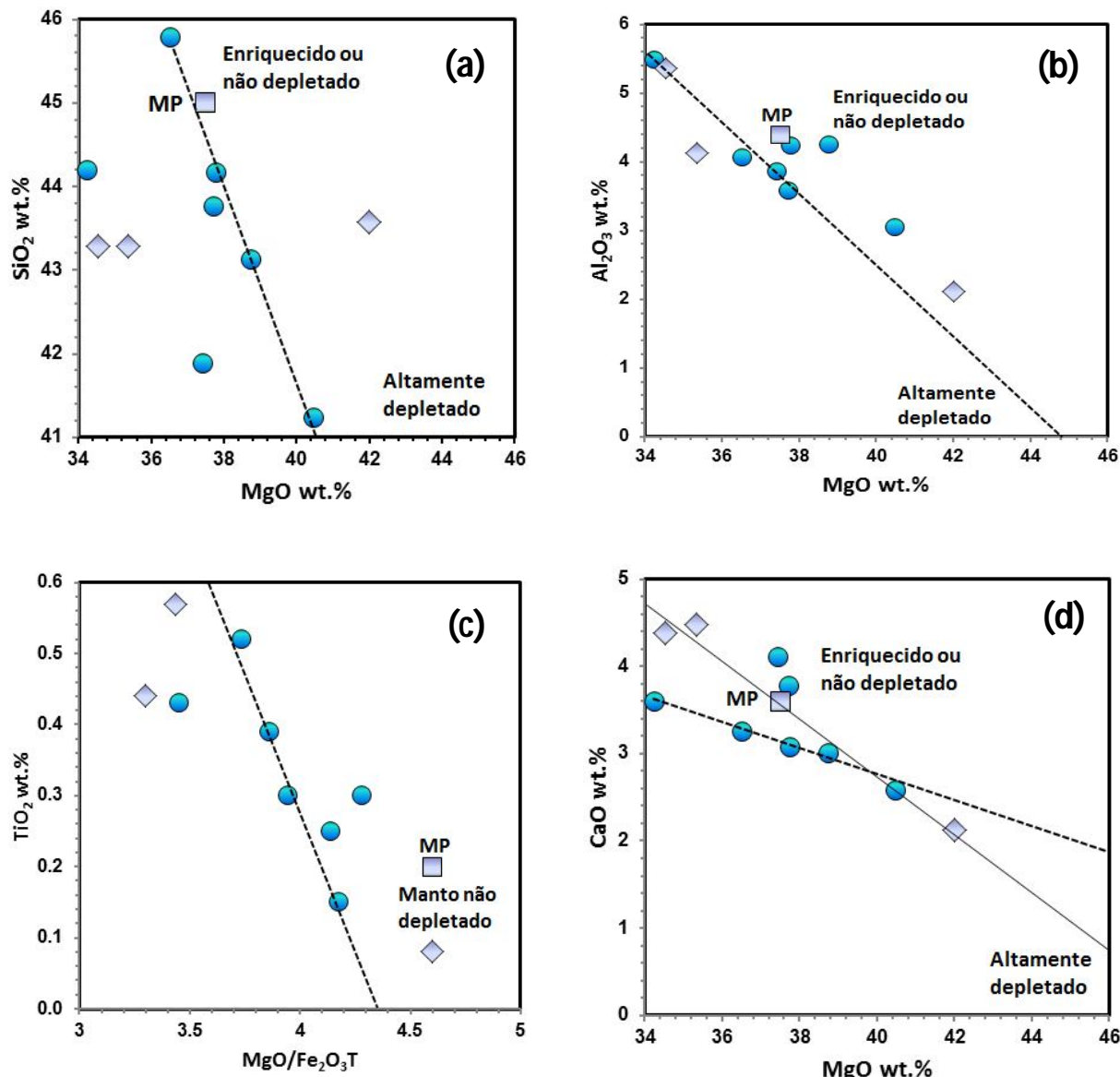


Figura 5.1. Óxidos vs MgO rocha total dos xenólitos de peridotitos de MVF e FN. MVF: círculos azuis; FN: losanges cinzas. PM = manto primitivo (valores de Sun and McDonough, 1989).

centro de cristais de clinopiroxênio dos xenólitos profiroclásticos sugerindo que os mesmos, comparativamente aos tipos protogranulares, seriam mais férteis. A refertilização de peridotitos residuais é discutida por Niu (1997) e Asimow (1999), os quais sugerem que a interação entre

tais peridotitos com líquidos basálticos explicaria as correlações inversas daqueles elementos com Mg.

Os padrões de elementos terras raras normalizadas para valores condrílicos (Boynton, 1984) também mostram a grande variação observada a partir dos dados de elementos maiores. As razões $(La/Yb)_N$ variam de 3.4 a 28, seguramente influenciada pelo maior fracionamento das terras raras leves em relação aos demais (Fig. 5.3), sendo La enriquecido entre 6–50 vezes em relação ao condrito. É evidente o padrão horizontalizado desde Sm (xenólitos continentais) ou Tb-Dy (ambos continentais e oceânicos) até Lu, cujas concentrações variam entre aproximadamente 0.7–3 vezes ao condrito, compatível com padrões de manto litosférico em fácies espinélio com ausência ou presença mínima de granada. O grau de enriquecimento em terras raras leves deve ser, no entanto, inferido com cautela. Rivalenti et al. (2007) discutem a validade em interpretar dados de elementos traços nos referidos xenólitos visto que mínima contaminação (<1%) decorrente da interação com líquidos basálticos poderiam influenciar significativamente as composições de elementos traços (avaliados a partir da análise em rocha total) e mesmo as composições isotópicas, enquanto pouco afetariam as concentrações de elementos maiores.

O modelo proposto por Rivalenti et al. (2007) baseado em modelagem numérica de dados químicos de clinopiroxênio da seção do manto litosférico amostrada pelos xenólitos continentais (aqui não comentados os dados de Fernando de Noronha) é compatível com a infiltração de agentes metassomáticos com assinatura isotópica tipo EMI, definida a partir da correlação entre razões isotópicas de Sr e Nd obtidas em clinopiroxênio. Esses autores sugerem que o grau de interação fluido:rocha teria sido maior nos domínios mais profundos amostrados pelos xenólitos porfioclásticos (950–1280°C), associando tais agentes aos magmas parentais dos basaltos alcalinos Macau. Embora Rivalenti et al. (2007) não apresentem composições isotópicas de Pb, a interpretação concorda com nossos resultados que apontam para a presença importante de um componente EMI na fonte dos basaltos alcalinos cenozóicos. O componente FOZO proposto (cf. Capítulo 4 desta tese) seria necessariamente buscado a partir de razões isotópicas de Pb.

A seção mais superior do manto litosférico continental, representada pelos xenólitos protogranulares, teria sofrido menor grau de interação (menor razão fluido:rocha) com EMI, segundo aqueles mesmos autores. As razões isotópicas Sr-Nd em clinopiroxênio desses xenólitos foram interpretadas por esses autores como sendo dominadas por mistura de componentes tipo DM+EMII. Tendo em vista o componente EMII não ter sido modelado para os xenólitos porfioclásticos, Rivalenti et al. (2007) atribuem a origem desse enriquecimento a eventos metassomáticos anteriores à geração dos basaltos alcalinos, correlacionando-o “[...*tentatively...*]”

à época de colocação dos diques Ceará-Mirim. Embora com abordagem mais qualitativa, Fodor et al. (2002) chegam a mesma conclusão que Rivalenti e colaboradores. A diferença entre os dois trabalhos sendo, fundamentalmente, a associação genética ou não com o *hotspot* (ou pluma) de Fernando de Noronha.

5.3.2 DADOS ISOTÓPICOS RE-Os E CONCENTRAÇÕES DE PGE

Os dados isotópicos Re-Os e concentrações de PGE para os xenólitos continentais e oceânicos estão listados na Tabela 5.1. Como comentários gerais, o padrão PGE de ambas as suites de xenólitos é definido por composições discretamente empobrecidas em relação ao manto primitivo (PUM, *Primitive Uniform Mantle*). Nos xenólitos continentais, à exceção de Ru e Re, os demais PGE se distribuem entre 0,4 e 1 vez ao condrito; Re é visivelmente mais enriquecido que os demais elementos, muito embora seja variável dentro de uma faixa de valores relativamente estreita (0,28–0,54 ppb, exceto a amostra MVF-4) quando comparável a Os (Fig. 5.4a). Os xenólitos oceânicos, por sua vez, mostram relativa constância de Os a Pd, sendo que em duas amostras Os é significantemente depletado (FN-3: 0,06 ppb e FN-4: 0,16 ppb) em relação aos demais elementos e aos teores obtidos nas outras amostras (1,21–2,9 ppb). Re, novamente, se destaca com valores mais elevados (1,06–1,72 ppb) que o manto primitivo (Fig. 5.4b). A larga variação de teores determinada para os xenólitos estudados, sobretudo para Re e Os, é consistente com a faixa de valores de 0,06 a 3,56 ppb para Os e 0,246 a 0,538 ppb para Re, estimada para manto com características tipicamente empobrecidas a tipicamente enriquecidas (fértil) em PGE (p.ex., Shirey e Walker, 1998).

Por simplificação, as comparações entre as composições isotópicas Re-Os das duas suites de xenólitos serão feitas a partir dos valores atuais das razões $^{187}\text{Os}/^{188}\text{Os}$ ($= \gamma\text{Os}$). Considerando que (1) a idade de extrusão das lavas tanto no continente (basaltos MVF) como no oceano (basaltos FN) não é superior a 25 Ma (Silveira, 2006; Perlingeiro et al., 2013) e (2) os baixos valores para $^{187}\text{Re}/^{188}\text{Os}$, a correção para idade seria mínima e, portanto, não influenciaria nas interpretações baseadas nos valores atuais. Por exemplo, para os xenólitos continentais com razões $^{187}\text{Re}/^{188}\text{Os}$ mais alta (3,91) e mais baixa (0,43), e respectivas razões $^{187}\text{Os}/^{188}\text{Os}$ atuais de 0,4207 e 0,1227, os valores calculados para 25 Ma seriam de 0,4191 e 0,1225. Apenas para um dos xenólitos oceânicos (FN-4) com razão $^{187}\text{Re}/^{188}\text{Os}$ de ~44 a composição isotópica de Os recalculada para a idade de extrusão magmática (~9 Ma; Perlingeiro et al., 2013) passaria de um valor discretamente mais radiogênico que o BSE (*Bulk Silicate Earth*) de 0,1303, para um valor também discretamente subcondrítico (~0,1243; $\gamma\text{Os} = -1,4$).

As razões $^{187}\text{Os}/^{188}\text{Os}$ dos xenólitos continentais variam dentro da faixa de valores atribuídos para o BSE, considerando as determinações de Meisel et al. (2001; 0,1296) e Walker et al. (2002; 0,1262), ou ainda em valores subcondríticos. Seis das onze amostras analizadas tiveram composições entre 0,1267 e 0,1297 (γOs entre -0,2 a +0,9), enquanto cinco forneceram valores mais baixos – MVF-5 (0,1227; $\gamma\text{Os} = -3,4$), MVF-6 (0,1239; $\gamma\text{Os} = -2,4$), MVF-7 (0,1259; $\gamma\text{Os} = -0,9$), MVF-9 (0,1257; $\gamma\text{Os} = -1$) e MVF-10 (0,1185; $\gamma\text{Os} = -6,7$). Mesmo considerando os valores negativos mais extremos, as composições isotópicas de Os dos xenólitos continentais perfeitamente se ajusta às composições atribuídas ao manto litosférico subcontinental ou abissais ($\gamma\text{Os} = -17$ a +1,6; p.ex., Shirey e Walker, 1998; Liu et al., 2015). O xenólito MVF-4 (coletado nos basaltos do centro PiC) exibe razão $^{187}\text{Os}/^{188}\text{Os}$ e $^{187}\text{Re}/^{188}\text{Os}$ muito mais elevadas (0,4208 e respectivo $\gamma\text{Os} = +231$; 3,91), num padrão consistente com enriquecimento anômalo de ^{187}Re quando comparado às demais amostras cujas razões $^{187}\text{Re}/^{188}\text{Os}$ variam de 0,43 a 1,03. Quando plotadas as razões $^{187}\text{Re}/^{188}\text{Os}$ versus $^{187}\text{Os}/^{188}\text{Os}$, não há ajustes possíveis para definir uma isócrona simples. À exceção do xenólito MVF-4, os demais xenólitos continentais mostram idades T_{RD} extremamente variáveis entre 1,3 e 0,1 Ga, sendo apenas uma idade modelo >1 Ga, enquanto as demais mostram distribuição desde 0,7 a 0,1 Ga. Valores negativos para a idade T_{RD} foram também calculados para parte desses xenólitos continentais.

As razões $^{187}\text{Os}/^{188}\text{Os}$ dos xenólitos oceânicos caem na faixa de valores menos radiogênicos que o BSE, facilmente observado a partir dos valores γOs negativos (-0,2 a -5,3), os quais estão associados à razões $^{187}\text{Re}/^{188}\text{Os}$ equivalentes àquelas dos xenólitos continentais. Apenas o xenólito FN-3 apresentou γOs positivo (+2,6), para uma razão $^{187}\text{Re}/^{188}\text{Os}$ de ~44 e concentração de Os mais baixa (0,06 ppb) entre todos os xenólitos estudados. Embora interpretado a partir de somente um resultado, a combinação desses valores sugere que domínios fortemente empobrecidos (baixa Os-ppb) do manto litosférico oceânico sofreram eventos de enriquecimento (alto ^{187}Re) relativamente recentes ($^{187}\text{Os}/^{188}\text{Os} \sim 0,13$), quando comparada à assinatura de Os do domínio continental. As idades T_{RD} calculadas mostram valores desde Neoproterozóico até o Cretáceo (1 a 0,06 Ga), à semelhança dos valores continentais.

5.4 COMENTÁRIOS PRELIMINARES SOBRE EXTRAÇÃO DE MAGMAS VERSUS METASSOMATISMO MANTO LITOSFÉRICO

O método Re-Os constitui-se em importante ferramenta para inferir a idade de processos de extração de magmas a partir do manto litosférico (Walker et al., 1989; Carlson e Irving 1994; Pearson, 1999; Peslier et al., 2000; Reisberg et al., 2005). A idade modelo é calculada assumindo que durante a fusão parcial do manto peridotítico fértil todo Re é retirado e transportado pelos magmas primários (Walker et al., 1989), dada a natureza incompatível deste elemento. Uma vez que Re é completamente removido (Handler et al., 1997), o material (peridotito) residual torna-se empobrecido mas mantém as proporções originais de Os. Como consequência, o manto litosférico refratário, pós-eventos de fusão parcial, deverá apresentar baixas razões $^{187}\text{Re}/^{188}\text{Os}$. A idade modelo de extração de Re desse peridotito (T_{RD}) representa, portanto, a idade do material residual e é calculada a partir de:

$$T_{RD} = 1 / \lambda \ln[(^{187}\text{Os}/^{188}\text{Os})_{mantle} - (^{187}\text{Os}/^{188}\text{Os})_{amostra} / (^{187}\text{Re}/^{186}\text{Os})_{mantle}] + 1,$$

onde as razões isotópicas do manto assumidas neste trabalho ($^{187}\text{Os}/^{188}\text{Os}$) = 1,06 e ($^{187}\text{Re}/^{186}\text{Os}$) = 3,3 (Walker et al., 1989). Peridotitos com teores de Fo elevados (≥ 90) são interpretados como resíduos de >25% de extração de magmas (Bernstein et al., 2007). Combinando a idade T_{RD} e teor de Fo dos xenólitos MVF-6 (Fo=90,4; $T_{RD} = 0,48\text{ Ga}$) e MVF-10 (Fo=91; $T_{RD} = 1,3 \text{ Ga}$) é possível, portanto, inferir que domínios do manto litosférico do domínio Rio Grande do Norte são fortemente refratários como resultado de extração de magmas desde o Meso- até Cambriano. A integração das composições desses dois xenólitos permite-nos comentar que o manto litosférico na região é heterogêneo quanto ao grau de fertilidade e idade, mas os dois parâmetros não estão necessariamente correlacionados. Por exemplo, o xenólito MVF-1 tem idade T_{RD} mais jovem (0,06 Ga) mas com Fo comparável (Fo = 89,7) ao xenólito MVF-5 cuja idade T_{RD} é 0,65 Ga. Além de amostrar domínios litosféricos antigos, os xenólitos continentais com idades T_{RD} entre 0,21–0,06 Ga representam domínios que sofreram eventos de fusão relativamente mais recente, provavelmente associados a magmatismo (diques) Ceará-Mirim e, talvez, ao vulcanismo Macau. Composições semelhantes são observadas nos xenólitos oceânicos, ou seja, manto litosférico antigo (Neoproterozóico a Cretáceo) e variavelmente refratário.

O comportamento químico de Re e Os durante processos de interação fluido:rocha pode variar substancialmente (Becker et al., 2001). Segundo esses autores, se a interação for discreta (baixa razão fluido:rocha), a refertilização elevaria a concentração de Re (altas razões $^{187}\text{Re}/^{188}\text{Os}$), bem como de outros elementos incompatíveis, mas pouco influenciaria a razão $^{187}\text{Os}/^{188}\text{Os}$. Razões fluido:rocha muito elevadas poderiam, ao contrário, introduzir ^{187}Os

adicional especialmente se o evento metassomático é antigo. Obviamente, alta ou baixa razão fluido:rocha diminuiriam, em proporções distintas, as idades modelo T_{RD} . Esse comportamento é observado em vários xenólitos continentais e em um dos xenólitos oceânicos através dos valores negativos da idade T_{RD} (-0,48 a -0,06 Ga), um forte indicativo para inferir adição de Re e, portanto, metassomatismo no manto litosférico subcontinental do nordeste do Brasil.

CAPÍTULO 6

CONSIDERAÇÕES FINAIS

O extremo nordeste da Província Borborema, mencionado como domínio Rio Grande do Norte ou Seridó, foi palco de inúmeros eventos de acresção crustal do Arqueano ao Paleoproterozóico (Dantas et al., 1998, 2004; Souza et al., 2007), com comprovado retrabalhamento da litosfera no Neoproterozóico. Essa mesma região foi submetida a afinamento litosférico e rifteamento crustal relacionados à abertura do oceano Atlântico Equatorial, durante o Cretáceo. Como consequência desse contexto tectônico, a região alojou um extensivo enxame de diques máficos, de natureza toleítica, regionalmente conhecido como Enxame de Diques Ceará-Mirim (p.ex., Bellieni et al., 1992; Archanjo et al., 2000, 2002; Hollanda et al., 2006). Já no Cenozóico, do Oligoceno ao Mioceno, a mesma região foi re-aquecida em decorrência de novo evento magmático representado por vulcões de pequeno volume alimentados pela erupção de magmas de natureza alcalina – o vulcanismo Macau (p.ex., Fodor et al., 1998; Knesel et al., 2011). Uma particularidade dos basaltos Macau é a presença de xenólitos peridotíticos, especialmente de fácies espinélio, que representam fragmentos do manto litosférico subcontinental abaixo da Província Borborema (Rivalenti et al., 2000, 2007; Fodor et al., 2002).

É inegável que, como reflexo de inúmeros processos tectônicos e magmáticos superpostos, a composição do manto litosférico tenha sido modificada ao longo da história geológica do domínio Rio Grande do Norte. Por exemplo, acresção juvenil e/ou retrabalhamento de crosta arqueana relacionadaa margens convergentes foi o cenário do Paleoproterozóico (dominante Riaciano) nesse setor da Província Borborema. A gênese do magmatismo calcio-alcalino que hoje é representado pelo embasamento gnáissico regional (Complexo Caicó) é atribuída à fusão do manto litosférico metassomatizado em zonas de subducção, como visto pelo enriquecimento em elementos incompatíveis e depleção em elementos tais como Nb-Ta, Ti e Zr (Souza et al., 2007). Após longo período de relativa quiescência tectônica e magmática (não há registro geológico de idade mesoproterozóica), essa região foi retrabalhada no Neoproterozóico (Ediacarano) em resposta à orogenia Brasiliiana. A intrusão de expressivo volume de magmas granitóides em associação espacial com magmas máficos de afinidade alcalina potássica (granitos *sensu lato* e K-dioritos), entre 600 e 520 Ma e com ε_{Nd} negativos e idades T_{DM} paleoproterozóicas (entre 2.2 e 1.8 Ga), atestam que a reciclagem do sistema crosta-manto foi mais importante no Neoproterozóico que acresção crustal juvenil (Jardim de Sá, 1994;

Hollanda et al., 2003). Ainda, anomalias negativas de Nb, Ti e Zr, como observados para os gnaisses paleoproterozóicos, confirma a derivação dos magmas K-dioríticos a partir de domínios do manto litosférico modificados por um componente de subducção. O mecanismo para fusão parcial desse manto antigo durante o Neoproterozóico ainda não é claro. Ganade-Araújo et al. (2014) discutem a existência de uma extensa zona de subducção relacionada ao fechamento do oceano Goiás-Pharusiano e aglutinação do Gondwana Ocidental, entre 650–610 Ma. Fusão do manto litosférico, nesse contexto, seria favorecida pelo amplo rebaixamento da temperatura do *solidus* peridotítico, o domínio Rio Grande do Norte posicionado na região distal (*backarc*) em relação ao *front* de subducção/colisão. Delaminação de parte da litosfera espessada num amplo contexto de convergência (subducção/colisão) neoproterozóica é igualmente possível ao final do Brasiliano. Qualquer que tenha sido o mecanismo para promover a fusão do manto litosférico subcontinental abaixo do domínio Rio Grande do Norte, e consequente geração dos magmas máficos K-dioríticos, certamente afetou as características químicas do manto. Tendo sido esse manto já enriquecido em elementos incompatíveis no Paleoproterozóico, e com razões $^{87}\text{Sr}/^{86}\text{Sr}$ elevadas e valores εNd fortemente negativos, as evidências de um enriquecimento neoproterozóico superposto seriam dificilmente reconhecidas.

É provável que, no Cretáceo, a assinatura do metassomatismo paleoproterozóico tenha sido em parte ‘diluída’ após a extração dos magmas parentais dos K-dioritos e, possivelmente, pela superposição de enriquecimento no Neoproterozóico. Dada a complexidade em isolar os efeitos de dois ou mais eventos superpostos, preferimos conservadoramente considerar que esses magmas toleíticos (os *evolved high-Ti tholeiites* e *low-Ti tholeiites*) foram extraídos de domínios do manto litosférico subcontinental extensivamente modificado no “Proterozóico”. Idades modelo T_{DM} desses diques entre 1,5–1,0 Ga foram interpretadas por Hollanda et al. (2006) como prováveis idades de mistura devido superposição de eventos metassomáticos cronologicamente distintos, coexistindo no manto litosférico.

Investigar o sistema crosta-manto litosférico exige também reconhecer a participação e a natureza química da astenosfera. Em contextos de subducção em margens convergentes é esperado que delaminação litosférica e/ou eclogitização de crosta/litosfera oceânica subductada modifiquem o manto convectivo e mesmo domínios mais profundos. No Cretáceo, identificamos a presença ativa da astenosfera como fonte para os toleitos ‘mais primitivos’ (*olivine tholeiites*), segregados a partir de profundidade em torno de 75 km. Os dados isotópicos de Pb, modelados de acordo com a revisão apresentada por Stracke et al. (2005), indicam que esse componente astenosférico teria composições moderadamente radiogênicas em Pb, assemelhando-se a FOZO. A presença de um componente radiogênico em Pb já havia sido aventada em trabalhos anteriores

sobre os toleitos Ceará-Mirim, levando à correlações com a pluma de St. Helena. Nesta tese, a hipótese de participação da pluma de St. Helena é preterida frente às semelhanças com FOZO. Há, no entanto, uma tendência a assumir origem comum para FOZO e HIMU com forte participação de crosta oceânica antiga subductada (ver revisão em Starcke et al., 2005). Nesse caso, é imediata a correlação das composições reconhecidas localmente nos olivina toleitos com reciclagem de crosta oceânica, consumida durante eventos de subducção proterozóicos. Uma contribuição adicional para a discussão, no caso específico do Cretáceo na Província Borborema, poderia vir da modelagem quantitativa das composições isotópicas e de elementos traços dos olivina toleitos a partir de composições (teóricas ou aproximadas) de crosta oceânica com idades distintas (1 ou 2 Ga). O cenário tectônico no Cretáceo, portanto, comporta afinamento da litosfera continental e consequente ascenção da astenosfera FOZO, a fusão do manto litosférico induzida pelo calor da astenosfera ascendente, a qual por si só sofreria fusão em graus (e volumes) variáveis a depender da profundidade final atingida.

É fato que as composições isotópicas dos basaltos alcalinos Macau não apontam para *endmembers* puros, como visto para os olivina toleitos (FOZO) e mesmo para as demais suítes toleíticas derivadas claramente do manto litosférico subcontinental, enriquecido. Ao contrário, as composições isotópicas se distribuem quase linearmente entre um componente (moderadamente) radiogênico em Pb (com baixas razões Rb/Sr e Sm/Nd) e um componente enriquecido. Para explicar esse comportamento, sugerimos que, a partir do Cretáceo, a astenosfera FOZO teria se re-equilibrado termalmente e reologicamente substituindo o manto litosférico afinado, de acordo com modelos já aventados de substituição de manto litosférico delaminado ou termalmente erodido por manto convectivo juvenil (p.ex., Xu, 2001; Zheng et al., 2001; Wu et al., 2003; Gao et al., 2004). No entanto, a ausência de anomalias negativas de Nb-Ta e Ti nesses basaltos, aliada à estimativas de profundidade de segregação entre 80–90 km (até 120 km no caso dos magmas nefeliníticos do centro eruptivo SPaP), significativamente maiores que aquelas dos magmas toleíticos, é evidência conclusiva para a não correlação com uma fonte enriquecida por subducção, como identificada para os diques toleíticos. As similaridades compostionais entre os basaltos Macau e as lavas de Fernando de Noronha leva-nos a acreditar que a fonte tipo-EM teria sido relacionada a fluidos metassomáticos profundos, provavelmente capturados quando da passagem do continente sobre aquele *hotspot*, durante o Cenozóico. Como continuidade, estudos futuros deverão abordar a modelagem desse componente EM a partir de amostras do arquipélago de São Pedro–São Paulo, localizado na dorsal Atlântica equatorial. Em um trabalho pioneiro sobre geoquímica elementar e isotópica (Sr-Nd-Pb) dos peridotitos e veios honblendíticos do arquipélago, Roden et al. (1984) discutem a potencialidade dessas rochas como fonte para

geração de magmas alcalinos, sem dúvida, uma alternativa a ser explorada em futuras abordagens sobre o vulcanismo Macau e Fernando de Noronha.

Por fim, o estudo Re-Os nos xenólitos peridotíticos hospedados nos basaltos alcalinos nos trouxe informações sobre a história química do manto litosférico no domínio Rio Grande do Norte. Embora as interpretações dos dados ainda tenham caráter preliminar, e devam ser melhor analisados e discutidos antes de sua publicação, está claro que os xenólitos confirmam a recorrência de múltiplos eventos de extração de magmas (fusão parcial) a partir do manto litosférico subcontinental na região. As idades modelo T_{RD} se distribuem do Mesoproterozóico (1,3 Ga) até o final do Cretáceo (~60 Ma), mas com concentração maior de idades no Neoproterozóico e Cretáceo inferior. Idades mais jovens, cenozoicas, não foram calculadas a partir dos dados isotópicos Re-Os, o que confirma a não cogeneticidade entre os basaltos hospedeiros e xenólitos, cada um representando produtos de diferentes profundidades do manto subcontinental.

REFERÊNCIAS

- ARCHANJO, C.J., TRINDADI, R.I., MACEDO, J.W.P. AND ARAUJO, M.G. Magmatic fabric of a basaltic dyke swarm associated with Mesozoic rifting in NE Brazil. *Journal of South American Earth Science*, 13 (3), 179-189. 2000.
- ARCHANJO, C.J., ARAÚJO, M.G.S., LAUNEAU, P. Fabric of the Rio Ceará-Mirim mafic dyke swarm (Northeastern Brazil) determined by anisotropy of magnetic susceptibility and image analysis. *Journal of Geophysical Research*, 107(B3), 2046: 1-13. 2002.
- ASIMOW, P.D. A model that reconciles major- and trace-element data from abyssal peridotites. *Earth and Planetary Science Letters*, 169, 303–319. 1999.
- BELLINI, G., MACEDO, M.H.F., PETRINI, R., PICCIRILO, E.M., CAVAZZINI, G., COMIN-CHIARAMONTI, P., ERNESTO, M., MACEDO, J.W.P., MARTINS, G., MELFI, A.J., PACCA, I.G. and DE MIN, A. Evidence of magmatic activity related to Middle Jurassic and Lower Cretaceous rifting from northeastern Brazil (Ceará-Mirim: K/Ar age, paleomagnetism, petrology and Sr-Nd isotope characteristics. *Chemical Geology*, 97, 9-32. 1992.
- BOYNTON, W.V. Geochemistry of the rare earth elements: meteorite studies. In P. Henderson (Ed.), *Rare-Earth Element Geochemistry*, Elsevier: 63-114. 1984.
- BERNSTEIN, S., KELEMEN, P.B., HANGHØJ, K. Consistent olivine Mg# in cratonic mantle reflects Archean mantle melting to the exhaustion of orthopyroxene. *Geology* 35, 459–462. 2007.
- CARLSON, R.W., IRVING, A.J. Depletion and enrichment history of subcontinental lithospheric mantle: an Os, Sr, Nd and Pb isotopic study of ultramafic xenoliths from the Northwestern Wyoming craton. *Earth and Planetary Science Letters*, 126, 457-472. 1994
- DANTAS, E.L., HACKSPACHER, P.C., VAN SCHMUS, W.R., AND BRITO NEVES, B.B. Archean accretion in the São José do Campestre massif, Borborema Province, Northeast Brazil. *Revista Brasileira de Geociências*, vol. 28 (2), 221-228. 1998.
- DANTAS, E. L., VAN SCHMUS, W. R., HACKSPACHER, P. C., FETTER, A. H., BRITO NEVES, B. B., CORDANI, U., NUTMAN, A. P., WILLIAMS, I. S. The 3.4 e 3.5 Ga São José de Campestre massif, NE Brazil: remnants of the oldest crust in South America. *Precambrian Research*, 130(1-4), 113-137. 2004.
- FODOR, R.V., MUKASA, S.B. AND SIAL, A.N. Isotopic and trace-element indications of lithospheric and asthenospheric components in Tertiary alkalic basalts, northeastern Brazil. *Lithos*, 43, 197-217. 1998.
- FODOR, R.V., SIAL, A.N. and GANDHOK, G. Petrology of spinel peridotite xenoliths from northeastern Brazil: lithosphere with a high geothermal gradient imparted by Fernando de Noronha plume. *Journal of South American EarthScience*, 15, 199-214. 2002.
- GANADE DE ARAUJO, C.E., CORDANI, U.G., WEINBERG, R.F., BASEI, M.A.S., Armstrong, R., Sato, K. Tracing Neoproterozoic subduction in the Borborema Province (NE-Brazil): Clues from U-Pb geochronology and Sr-Nd-Hf-O isotopes on granitoids and migmatites. *Lithos*, 202-203, 167-189. 2014.
- GAO, S., RUDNICK, R.L., YUAN, H.L. Recycling lower continental crust in the North China craton. *Nature*, 432, 892-897. 2004.
- HANDLER, M.R., BENNETT, V.C., ESAT, T.M. The persistence of off-cratonic lithospheric mantle: Os isotopic systematics of variably metasomatised southeast Australian xenoliths. *Earth and Planetary Science Letters*, 151, 61–75. 1997.
- HOLLANDA, M.H.B.M., PIMENTEL, M.M., OLIVEIRA, D.C. AND JARDIM DE SÁ, E. F. Lithosphere-asthenosphere interaction and the origin of Cretaceous tholeiitic magmatism in NE Brazil: Sr-Nd-Pb isotopic evidence. *Lithos*, 86, 34-49. 2006.
- HOLLANDA, M.H.B.M., PIMENTEL, M.M., JARDIM DE SÁ, E.F. Paleoproterozoic subduction-related metasomatic signatures in the lithospheric mantle beneath NE Brazil: inferences from trace element and Sr-Nd-Pb

isotopic compositions of Neoproterozoic high-K igneous rocks. *Journal of South American Earth Science*, 15(8): 885-900. 2003.

JARDIM DE SÁ, E.F. A Faixa Seridó (Província Borborema, NE do Brasil) e seu significado geodinâmico na Cadeia Brasiliiana/Pan-Africana. Universidade de Brasília, Brasília, Tese de Doutorado, n 3, 803 p. e anexos. 1994.

KNESEL, K.M., SOUZA, Z.S., VASCONCELOS, P.M., COHEN, B.E., SILVEIRA, F.V. Young volcanism in The Borborema Province, NE Brazil, shows no evidence for a trace of the Fernando de Noronha plume on the continent. *Earth and Planetary Science Letters*, 302: 38-50. 2011.

LIU, J., RUDNICK, R.L., WALKER, R.J., XU, W-L., GAO, S., WU, F-Y. Big insights from tiny peridotites: Evidence for persistence of Precambrian lithosphere beneath the eastern North China Craton. *Tectonophysics*, 650, 104-112. 2015.

MEISEL, T., WALKER, R.J., IRVING, A.J., LORAND, J.-P. Osmium isotopic compositions of mantle xenoliths: a global perspective. *Geochimica et Cosmochimica Acta* 65, 1311–1323. 2001.

NIU, Y., LANGMUIR, C.H., KINZLER, R.J. The origin of abyssal peridotites: a new perspective. *Earth and Planetary Science Letters*, 152, 251–265. 1997.

PEARSON, D.G. The age of continental roots. *Lithos*, 48, 171-194. 1999.

PESLIER, A.H., REISBERG, L., LUDDEN, J., FRANCIS, D. Os isotopic systematics in mantle xenoliths; age constraints on the Canadian Cordillera lithosphere. *Chemical Geology*, 166, 85-101. 2000.

PERLINGEIRO, G., VASCONCELOS, P.M., KNESEL, K.M., THIEDE, D.S., CORDANI, U.G. $^{40}\text{Ar}/^{39}\text{Ar}$ geochronology of the Fernando de Noronha Archipelago and implications for the origin of alkaline volcanism in the NE Brazil. *Journal of Volcanology and Geothermal Research*, vol. 249, 140-154. 2013.

REISBERG, L., ZHI, X., LORAND, J.P., WAGNER, C., PENG, Z., ZIMMERMANN, C. Re-Os and S systematics of spinel peridotite xenoliths from east central China: Evidence for contrasting effects of melt percolation. *Earth and Planetary Science Letters*, 239, 286 – 308. 2005.

RIVALENTI, G., MAZZUCHELLI, M., GIRARDI, V.A.V., VANNUCCI, R., BARBIERI, M.A., ZANETTI, A. & GOLDSTEIN, S.L. Composition and processes of the mantle lithosphere in northeastern Brazil and Fernando de Noronha: evidence from mantle xenoliths. *Contribution to Mineralogy and Petrology*, 138, 308-325. 2000.

RIVALENTI, G., ZANETTI, A., GIRARDI, V.A.V., MAZZUCHELLI, TASSINARI, C.C.G. AND BERTOTTO, G.W. The effect of the Fernando de Noronha plume on the mantle lithosphere in north-eastern Brazil. *Lithos*, 94, 111-131. 2007.

RODEN, M.F., FREY, F.A. AND CLAGUE, D.A. Geochemistry of the tholeiitic and alkali lavas from the Koolau Range, Oahu, Hawaii: implications for Hawaiian volcanism. *Earth and Planetary Science Letters*, 69, 141-158. 1984.

SHIREY, S.B., WALKER, R.J. Re-Os isotopes in cosmochemistry and high-temperature geochemistry. *Annual Reviews of Earth and Planetary Science*, 26, 423–500. 1998.

SOUZA, Z.S., MARTIN, H., PEUCAT, J.J., JARDIM DE SÁ, E.F., MACEDO, M.H.F. Calc-Alkaline Magmatism at the Archean-Proterozoic Transition: the Caico Complex Basement (NE Brazil). *Journal of Petrology*, vol. 48, 2149-2185. 2007.

SUN, S.-S and McDONOUGH, W.F. Chemical and isotopic systematics of oceanic basalts: implications for mantle composition and processes. In: Saunders, M.J. Magmatism in the ocean basins. Londres. *Geological Society Special Publication* 42: 313-345, 1989.

TAKAZAWA, E., FREY, F.A., SHIMIZU, N. AND OBATA, M. Whole rock compositional variations in an upper mantle peridotite (Horoman, Hokkaido, Japan): Are they consistent with a partial melting process? *Geochimica et Cosmochimica Acta*, vol. 64, 695-716. 2000.

SILVEIRA, F.V. *Magmatismo Cenozóico da porção central do Rio Grande do Norte, NE do Brasil*. Tese de doutorado, Universidade Federal do Rio Grande do Norte, 220p. 2006.

STRACKE, A., HOFMANN, A.W., HART, S.R. FOZO, HIMU, and the rest of the mantle zoo. *Geochemistry, Geophysics, Geosystems*, 6(5), Q05007, doi: 10.1029/2004GC000824. 2005.

WALKER, R.J., PRICHARD, H.M., ISHIWATARI, A., PIMENTEL, M.M. The osmium isotope composition of convecting upper mantle deduced from ophiolite chromites. *Geochimica et Cosmochimica Acta* 66, 329-345. 2002.

WALKER R. J., CARLSON R. W., SHIREY S. B. AND BOYD F. R. Os, Sr, Nd, and Pb isotope systematics of southern African peridotite xenoliths: implications for the chemical evolution of subcontinental mantle. *Geochimica et Cosmochimica Acta*, 53(7), 1583-1595. 1989.

WU, F.Y., WALKER, R.J., REN, X.W., SUN, D.Y., ZHOU, X.H. Osmium isotope constraints on the age on the age of the lithospheric mantle beneath northeastern China. *Chemical Geology*, 196, 107-129. 2003.

XU, Y.G. Thermo-tectonic destruction of the Archean lithospheric keel beneath the Sino-Korean Craton in China: evidence, timing and mechanism. *Physics and Chemistry of the Earth (A)*, 26, 747-757. 2001.

ZHENG, J.P., O'REILLY, S.Y., GRIFFIN, W.L., LU, F.X., ZHANG, M. & PEARSON, N.J. Relict refractory mantle beneath the eastern North China block: significance for lithosphere evolution. *Lithos*, 57, 43-66. 2001.

Appendix A1. Olivine compositions of olivine tholeites (manuscript on the Petrology of the CMDS

Sample name	SiO ₂	TiO ₂	Al ₂ O ₃	Cr ₂ O ₃	FeO	MnO	MgO	NiO	CaO	K ₂ O	Na ₂ O	V ₂ O ₃	Total	Fo	Fa
<i>Olivine chemical compositions</i>															
DCO125.1center	38.984	0.000	0.041	0.070	16.908	0.193	43.184	0.343	0.236	0.008	0.013	0.021	100.000	82	18
rim	37.769	0.012	0.017	0.038	21.729	0.304	39.647	0.192	0.281	0.000	0.001	0.011	100.000	76	24
DCO125.2center	36.558	0.000	0.004	0.031	30.142	0.512	32.221	0.092	0.411	0.000	0.018	0.000	99.989	65	35
rim	36.524	0.000	0.000	0.000	31.172	0.517	31.259	0.147	0.343	0.002	0.035	0.000	99.998	63	37
DCO125.3center	37.053	0.000	0.000	0.050	27.982	0.383	34.000	0.109	0.404	0.000	0.012	0.000	99.992	68	32
rim	36.153	0.023	0.000	0.029	33.476	0.500	29.342	0.113	0.300	0.000	0.065	0.000	100.000	60	40
DCO125.4center	37.252	0.040	0.022	0.001	26.842	0.371	34.909	0.158	0.335	0.020	0.029	0.022	100.000	69	31
rim	36.839	0.025	0.000	0.007	29.451	0.438	32.831	0.093	0.292	0.000	0.018	0.007	100.000	66	34
DCO136.1center	36.504	0.002	0.000	0.081	31.766	0.402	30.821	0.117	0.276	0.021	0.011	0.000	100.000	63	37
rim	35.872	0.001	0.000	0.034	34.798	0.411	28.593	0.071	0.151	0.026	0.043	0.000	100.000	59	41
DCO136.2center	35.823	0.030	0.000	0.009	35.167	0.433	28.083	0.145	0.241	0.013	0.026	0.022	99.991	58	42
rim	36.290	0.021	0.000	0.001	33.578	0.437	29.235	0.128	0.218	0.009	0.048	0.035	100.000	61	39
DCO136.3center	36.678	0.032	0.016	0.000	31.487	0.385	31.089	0.117	0.181	0.015	0.000	0.000	100.000	63	37
rim	36.301	0.027	0.002	0.000	31.881	0.388	31.054	0.155	0.139	0.012	0.039	0.003	100.000	64	36
DCO137.1center	35.727	0.000	0.014	0.000	36.273	0.460	27.111	0.164	0.242	0.001	0.000	0.001	99.993	57	43
rim	35.700	0.048	0.000	0.000	36.252	0.390	27.283	0.088	0.186	0.013	0.036	0.000	99.996	58	42
DCO137.2center	35.746	0.016	0.005	0.000	36.612	0.462	26.756	0.115	0.262	0.008	0.000	0.016	99.998	55	45
rim	35.400	0.015	0.000	0.046	36.733	0.468	27.021	0.080	0.162	0.028	0.031	0.014	99.998	56	44
DCO137.3center	35.342	0.000	0.000	0.001	37.458	0.406	26.459	0.090	0.244	0.000	0.000	0.000	100.000	55	45
rim	35.836	0.003	0.000	0.000	36.376	0.485	27.028	0.047	0.205	0.007	0.004	0.010	100.000	56	45
DCO137.4center	36.599	0.000	0.000	0.000	31.918	0.345	30.716	0.137	0.275	0.007	0.000	0.003	100.000	63	37
rim	35.938	0.032	0.000	0.004	34.573	0.483	28.607	0.109	0.252	0.000	0.002	0.000	100.000	59	41
DCO137.5center	36.098	0.005	0.000	0.033	33.734	0.343	29.291	0.137	0.301	0.000	0.000	0.049	99.991	60	40
rim	35.655	0.000	0.000	0.017	36.333	0.484	27.191	0.082	0.203	0.000	0.030	0.005	99.999	56	44
DCO137.rim	35.331	0.004	0.017	0.022	37.460	0.442	26.395	0.059	0.243	0.012	0.000	0.015	100.000	56	44
DCO137:rim	36.139	0.000	0.006	0.066	33.785	0.393	29.262	0.081	0.229	0.000	0.015	0.020	99.996	60	40

Detection limits for oxide analysis were:

	Na	Mg	Si	Al	K	Ca	Ti	Cr	Fe	Mn	Ni	V	Total
Minimum	0.00	26.40	35.33	0.00	0.00	0.01	0.00	0.00	16.91	0.19	0.05	0.00	99.99
Maximum	0.07	43.18	38.98	0.04	0.03	0.41	0.05	0.08	37.46	0.52	0.34	0.05	100.00
Average	0.02	31.05	36.46	0.01	0.01	0.23	0.01	0.02	31.65	0.40	0.13	0.01	100.00
Error	0.02	4.35	0.88	0.01	0.01	0.10	0.01	0.02	5.20	0.09	0.07	0.01	0.00

ANEXO 1. COMPOSIÇÕES DE OLIVINA DE XENÓLITOS OCEÂNICOS - FERNANDO DE NORONHA

	FN1				FN2				FN4			
	1	2	1	2	1	2	1	2	1	2	1	2
SiO ₂	40.79	40.66	40.92	40.9	40.85	40.650	40.99	41.12	41	40.86	41.28	41.09
TiO ₂	0.0122	0.0244			0.012		0.0244		0.0672	0.0122	0.0122	0.0306
Al ₂ O ₃	0.0304	0.0015	0.0102	0.0145	0.0175	0.019	0.0313	0.0113	0.0298	0.0218	0.0357	0.0405
Cr ₂ O ₃	0.0577	0.0162			0.002		0.038		0.0308	0.0217	0.0217	0.0508
FeO	10.68	10.76	10.98	10.53	10.9	11.230	10.4	10.67	9.62	9.6	9.65	9.62
MnO	0.1632	0.1779	0.1253	0.1686	0.1192	0.174	0.1716	0.1479	0.1241	0.1437	0.1632	0.1355
MgO	47.75	48.14	48.57	48.42	48.33	47.670	48.4	48.49	49.03	48.94	48.89	49.12
NiO	0.3837	0.4022	0.417	0.3999	0.3807	0.386	0.41	0.4221	0.4019	0.4027	0.3944	0.4129
CaO	0.0357	0.0366	0.063	0.0148	0.0408	0.087	0.0423	0.0478	0.0958	0.0853	0.0518	0.0699
TOTAL	99.85	100.27	101.13	100.46	100.65	100.280	100.47	100.95	100.36	100.08	100.54	100.61
Fo	88.7002	88.6944	88.6318	88.9714	88.6603	88.1670	89.0840	88.8767	89.9695	89.9530	89.8328	89.9678
Fa	11.1276	11.1194	11.2383	10.8526	11.2155	11.6498	10.7566	10.9693	9.9012	9.8969	9.9669	9.9091
SiO ₂	41.02	40.7	40.79	40.68	40.91	41.31	41.05	40.96	40.77	41.05	41.33	40.83
TiO ₂	0.003		0.0035	0.0142	0.0122		0.0397			0.0214		0.0458
Al ₂ O ₃	0.0088	0.021		0.0054	0.0018		0.0162	0.0151		0.0206	0.0338	0.0119
Cr ₂ O ₃	0.0271	0.0235	0.009	0.0198	0.0036		0.0307	0.0362	0.0163		0.0362	0.0244
FeO	9.77	9.86	11.78	11.88	11.73	11.37	9.82	9.8	9.99	10.33	9.79	10.04
MnO	0.1496	0.1305	0.1865	0.1789	0.163	0.1573	0.1589	0.1298	0.1329	0.1511	0.1159	0.1341
MgO	48.35	48.86	47.51	47.42	48.06	47.42	49.12	48.68	48.39	48.78	48.47	48.62
NiO	0.4055	0.4126	0.4224	0.3706	0.4127	0.3927	0.4284	0.3888	0.3701	0.395	0.3774	0.3805
CaO	0.0232	0.0511	0.0437	0.0642	0.0535	0.0132	0.0279	0.0387	0.0415	0.0406	0.0635	0.0544
TOTAL	99.67	100.36	100.66	100.75	101.12	100.32	100.89	100.14	99.93	100.56	99.88	100.42
Fo	89.6794	89.7098	87.6193	87.5150	87.8099	87.9995	89.7690	89.7319	89.4971	89.2429	89.7145	89.4478
Fa	10.1640	10.1541	12.1854	12.2975	12.0209	11.8347	10.0660	10.1321	10.3633	10.6001	10.1637	10.4019

ANEXO 1. COMPOSIÇÕES DE OLIVINA DE XENÓLITOS OCEÂNICOS - FERNANDO DE NORONHA

	FN5									
	1	2	1	2	1	2	1	2	1	2
SiO ₂	41.25	40.89	41.19	41.36	41.26	41.13	41.21	41	41.41	41.38
TiO ₂	0.0092	0.0733				0.0122	0.0856			0.0214
Al ₂ O ₃		0.0174			0.0101	0.0053	0.0065		0.0228	0.0196
Cr ₂ O ₃	0.0091	0.0326	0.0199	0.0018		0.0218	0.04		0.0018	
FeO	9.75	9.82	10.02	9.88	9.81	9.87	9.81	9.88	9.82	9.99
MnO	0.1474	0.1353	0.1378	0.1698	0.1337	0.1225	0.1277	0.1711	0.1565	0.1635
MgO	48.62	48.76	48.7	48.71	48.76	48.86	48.65	48.75	48.6	48.69
NiO	0.4132	0.4197	0.3952	0.4247	0.3962	0.424	0.4113	0.3995	0.3971	0.4008
CaO	0.0041	0.001	0.0426	0.0301	0.0474	0.0507	0.0686	0.0035	0.032	0.0005
TOTAL	100.21	100.15	100.5	100.58	100.43	100.51	100.41	100.21	100.48	100.7
Fo	89.7505	89.7234	89.5247	89.6260	89.7341	89.7080	89.7190	89.6324	89.6731	89.5264
Fa	10.0950	10.1352	10.3314	10.1965	10.1261	10.1642	10.1473	10.1889	10.1629	10.3028

Anexo 1B. Composições de forsterita em olivina nos xenólitos continentais

Os números: 1 e 2 representam pontos de análise em um grão

	MVF-1			
	1	2	1	2
SiO ₂	40.74	40.73	40.79	40.86
TiO ₂			0.0429	0.0369
Al ₂ O ₃	0.0079	0.0317	0.0097	0.0048
Cr ₂ O ₃	0.0109	0.0509		0.0456
FeO	10	10	9.85	9.96
MnO	0.1443	0.132	0.149	0.154
MgO	49.58	49.19	49.45	49.39
NiO	0.4161	0.4111	0.4175	0.4471
CaO	0.0273		0.0477	0.0291
TOTAL	100.93	100.55	100.79	100.95
Fo	89.7037	89.6419	89.8121	89.6957
Fa	10.1480	10.2214	10.0342	10.1454

	MVF-2											
	1	2	1	2	1	2	1	2	1	2	1	2
SiO ₂	40.96	40.82	40.93	40.76	40.66	40.74	40.88	40.84	40.81	40.81	40.86	40.89
TiO ₂			0.0123	0.0276	0.0461				0.0215	0.0123	0.037	
Al ₂ O ₃	0.0012		0.0064	0.018	0.0041	0.0116	0.005	0.0033	0.0286	0.0189		0.0142
Cr ₂ O ₃	0.0055				0.0018	0.0164	0.0055	0.0529		0.042	0.0073	
FeO	10.3	10.33	10.19	9.93	9.77	9.91	10.06	9.99	10.29	10.02	10.06	10.01
MnO	0.1543	0.1157	0.134	0.1234	0.1298	0.1213	0.1966	0.1652	0.1493	0.1292	0.1257	0.1504
MgO	48.32	47.91	48.14	48.5	48.32	48.15	48.31	48.64	48.26	48.34	48.53	48.07
NiO	0.3589	0.38	0.3953	0.4038	0.3718	0.3731	0.3765	0.3987	0.4211	0.4118	0.3622	0.3761
CaO	0.0325	0.0307	0.0125	0.0144		0.04	0.0307	0.0408	0.0129	0.02	0.0003	
TOTAL	100.14	99.59	99.83	99.77	99.31	99.36	99.86	100.13	99.99	99.82	99.99	99.52
Fo	89.1763	89.1022	89.2612	89.5830	89.6914	89.5359	89.3567	89.5152	89.1782	89.4630	89.4662	89.3994
Fa	10.6620	10.7756	10.5976	10.2875	10.1718	10.3360	10.4368	10.3121	10.6651	10.4012	10.4022	10.4417

	MVF-3				
	1	2	1	2	1
SiO ₂	40.86	40.72	40.95	40.6	40.73
TiO ₂				0.0092	0.0184
Al ₂ O ₃	0.0392	0.0507	0.0193	0.033	0.0156
Cr ₂ O ₃	0.0091	0.0419	0.0055	0.031	0.0455
FeO	10.04	10.1	10.02	10.11	10.02
MnO	0.1117	0.1282	0.149	0.1539	0.1319
MgO	49.08	48.8	48.95	49.31	48.8
NiO	0.3614	0.383	0.4022	0.4028	0.3961
CaO	0.0648	0.0635	0.0772	0.0887	0.073
TOTAL	100.58	100.31	100.59	100.74	100.24
Fo	89.603251	89.479182	89.562174	89.543782	89.549408
Fa	10.280902	10.38728	10.282955	10.297454	10.313092

	MVF-4						
	1	2	1	2	1	2	1
SiO ₂	40.75	41.06	40.81	40.71	40.92	40.78	40.58
TiO ₂	0.0062	0	0.0369		0.0523		
Al ₂ O ₃	0.0182	0.033	0.0103	0.0082	0.0209	0.0122	0.0204
Cr ₂ O ₃	0.0328	0.0018	0.0055	0.0548	0.031	0.0401	
FeO	10.08	10	10.28	9.85	10.2	10.19	10.05
MnO	0.1267	0.1319	0.1592	0.1179	0.1461	0.1539	0.1067
MgO	48.38	48.33	48.48	48.31	48.34	48.14	48.39
NiO	0.3839	0.3793	0.3747	0.4014	0.3832	0.3499	0.3645
CaO	0.0182	0.0529	0.0618	0.0379	0.0624	0.0429	0.0629
TOTAL	99.83	100.01	100.22	99.5	100.18	99.72	99.58
Fo	89.4175	89.4771	89.2220	89.6260	89.2803	89.2425	89.4660
Fa	10.4495	10.3842	10.6116	10.2497	10.5664	10.5954	10.4219

	MVF-5									
	1	2	1	2	1	2	1	2	1	2
SiO ₂	40.56	40.59	40.92	40.78	40.65	40.71	40.82	40.78	40.45	40.64
TiO ₂	0.0122			0.0582	0.0337			0.0245		0.0245
Al ₂ O ₃	0.022	0.0418	0.0286	0.0389	0.0381	0.0267	0.023	0.0132	0.0245	0.0222
Cr ₂ O ₃	0.0454	0.0255	0.0146		0.02	0.0255		0.0237	0.0582	0.0182
FeO	9.96	10.39	10.32	10.16	10.13	10.14	10.18	10.07	10.16	10.12
MnO	0.1102	0.1414	0.0849	0.1419	0.1521	0.1829	0.1342	0.125	0.1373	0.1381
MgO	48.91	48.83	48.97	48.91	49.09	48.9	48.79	48.86	48.82	48.78
NiO	0.4041	0.3825	0.3787	0.3874	0.3832	0.397	0.3773	0.3703	0.3912	0.4292
CaO	0.0636	0.0775	0.0906	0.0916	0.0832	0.0758	0.0957	0.0587	0.0638	0.0806
TOTAL	100.13	100.5	100.85	100.62	100.58	100.47	100.44	100.34	100.13	100.27
Fo	89.6459	89.2068	89.3505	89.4325	89.4852	89.4109	89.3981	89.5213	89.4194	89.4477
Fa	10.2393	10.6465	10.5615	10.4201	10.3573	10.3991	10.4622	10.3486	10.4377	10.4085

	MVF-6							
	1	2	1	2	1	2	1	2
SiO ₂	40.51	40.67	40.72	41.14	41.29	40.91	40.78	40.6
TiO ₂		0.04			0.1137	0.0307		
Al ₂ O ₃	0.0311	0.0051	0.004	0.0052	0.0174	0.0325	0.0129	0.0225
Cr ₂ O ₃	0.0073	0.0219	0.0383		0.0949	0.0274	0.0037	0.0164
FeO	9.84	9.92	9.83	9.83	9.48	9.56	9.23	9.26
MnO	0.1061	0.1261	0.173	0.1381	0.1547	0.1692	0.1335	0.1303
MgO	49.15	49.34	48.97	49.42	49.47	49.56	49.05	49.51
NiO	0.4344	0.4138	0.4175	0.3967	0.3803	0.4062	0.3885	0.3781
CaO	0.0351	0.0113	0.0527	0.0253	0.0465	0.0446	0.0791	0.0731
TOTAL	100.12	100.55	100.22	100.96	101.05	100.75	99.71	100
Fo	89.8054	89.7488	89.7185	89.8349	90.1501	90.0792	90.3267	90.3832
Fa	10.0845	10.1209	10.1014	10.0225	9.6897	9.7461	9.5336	9.4817

	MVF-7	
	2	1
SiO ₂	40.66	40.47
TiO ₂	0.0491	0.0215
Al ₂ O ₃	0.0048	0.0162
Cr ₂ O ₃	0.0018	0.0055
FeO	9.67	9.76
MnO	0.1377	0.1386
MgO	48.98	49.41
NiO	0.4137	0.4197
CaO	0.0159	0.0162
TOTAL	99.93	100.27
Fo	89.9012	89.8968
Fa	9.9552	9.9600

	MVF-8											
	1	2	1	2	1	2	1	2	1	2	1	2
SiO ₂	41.13	41.13	40.98	40.67	40.82	40.89	40.96	41.04	40.78	40.98		
TiO ₂			0.0062	0.0245	0.0307					0.0583		
Al ₂ O ₃	0.0158	0.0122	0.0089		0.0169	0.0055	0.0279	0.0244	0.0025	0.0107		
Cr ₂ O ₃	0.0219	0.0127	0.0364	0.0091		0.0218	0.0364	0.0018				
FeO	10.22	10.33	10.48	10.49	10.45	10.22	10.32	10.3	10.38	10.37		
MnO	0.155	0.1387	0.1319	0.1526	0.1334	0.124	0.1171	0.1573	0.1281	0.1584		
MgO	47.94	48.35	47.81	47.85	48.31	48.33	48	48.31	48.16	48.52		
NiO	0.3746	0.3779	0.3524	0.3927	0.4043	0.3878	0.3921	0.3893	0.3882	0.391		
CaO	0.0399	0.009	0.0243	0.0043	0.0181	0.0228	0.208	0.0105	0.0291	0.0127		
TOTAL	99.9	100.36	99.85	99.6	100.19	100	99.9	100.25	99.94	100.46		
Fo	89.1735	89.1691	88.9272	88.9068	89.0555	89.2805	89.1284	89.1714	89.0947	89.1479		
Fa	10.6627	10.6855	10.9334	10.9322	10.8048	10.5893	10.7481	10.6636	10.7706	10.6868		

	MVF-9											
	1	2	1	2	1	2	1	2	1	2	1	2
SiO ₂	40.58	40.55	40.35	40.38	40.2	40.390	40.44	40.34	40.2	40.42	40.52	40.68
TiO ₂	0.0122				0.0701	0.052	0.0122	0.0183		0.1131		0.0122
Al ₂ O ₃			0.0113		0.0057	0.012			0.006	0.016		0.0019
Cr ₂ O ₃	0.045	0.047	0.0234	0.01	0.0361		0.0127		0.0487	0.0018		0.0325
FeO	11.74	11.61	11.69	11.68	11.58	11.420	11.49	11.49	11.53	11.2	11.42	11.66
MnO	0.1877	0.1512	0.1762	0.1645	0.1682	0.143	0.1907	0.1955	0.1484	0.1776	0.1794	0.1668
MgO	47.59	47.91	47.94	47.96	47.7	47.930	47.96	47.74	48.07	47.73	47.94	47.63
NiO	0.3676	0.3888	0.3633	0.352	0.3727	0.421	0.3838	0.373	0.371	0.3611	0.4012	0.3757
CaO	0.0178	0.0219	0.0369	0.0226			0.0027	0.0123	0.0515	0.0256	0.0357	0.0219
TOTAL	100.55	100.68	100.6	100.58	100.15	100.370	100.5	100.17	100.42	100.04	100.5	100.58
Fo	87.6726	87.8956	87.8072	87.8313	87.8604	88.0797	87.9791	87.9259	88.0058	88.2045	88.0485	87.7734
Fa	12.1309	11.9468	12.0095	11.9975	11.9636	11.7710	11.8222	11.8695	11.8398	11.6090	11.7644	12.0520

	MVF-10											
	1	2	1	2	1	2	1	2	1	2	1	2
SiO ₂	41.34	41.02	41.18	41.04	41.5	41	41.27	41.13	40.89	41.03		
TiO ₂	0.0492	0.0555					0.0124	0.0154	0.0247			
Al ₂ O ₃	0.0048		0.0383	0.0145	0.0151	0.0224	0.0104	0.0113	0.0133	0.0049		
Cr ₂ O ₃	0.0292			0.0219			0.0422	0.0183			0.0037	
FeO	8.6	8.84	8.95	8.81	8.55	8.86	8.78	8.77	8.83	8.83		
MnO	0.1114	0.1232	0.1361	0.1347	0.1224	0.1176	0.1405	0.13	0.1445	0.1511		
MgO	49.45	49.48	49.08	49.51	49.26	49.45	49.65	49.2	49.3	49.13		
NiO	0.3781	0.3619	0.408	0.4083	0.3908	0.4071	0.3628	0.3772	0.4103	0.3658		
CaO	0.0321	0.0153	0.0382	0.0211	0.0532	0.0286	0.0374	0.0096	0.0135	0.0129		
TOTAL	99.99	99.9	99.83	99.98	99.9	99.88	100.31	99.67	99.62	99.53		
Fo	91.006	90.7752	90.5915	90.7974	91.0113	90.7568	90.8435	90.7869	90.7338	90.6985		
Fa	8.8773	9.09637	9.26582	9.06223	8.86024	9.12063	9.01047	9.07686	9.1151	9.14307		

	MVF-11			
	1	2	1	2
SiO ₂	40.96	41	40.72	40.45
TiO ₂		0.0399	0.0062	
Al ₂ O ₃	0.0175	0.0013	0.0072	0.0146
Cr ₂ O ₃	0.0455	0.0109		
FeO	10.58	10.65	10.78	10.44
MnO	0.1318	0.1531	0.1627	0.1568
MgO	47.71	47.74	48.13	47.62
NiO	0.3913	0.389	0.3949	0.3977
CaO	0.0302	0.0128	0.0274	0.0131
TOTAL	99.87	99.99	100.23	99.09
Fo	88.8139	88.7353	88.6881	88.9017
Fa	11.0468	11.1030	11.1416	10.9320